FABRICATION AND EVALUATION OF PROTOTYPES OF BIOARTIFICIAL GRAFTS FOR CUTANEOUS WOUND HEALING APPLICATION

A THESIS PRESENTED BY

R Deepa

TO

SREE CHITRA TIRUNAL INSTITUTE FOR MEDICAL SCIENCES AND TECHNOLOGY, TRIVANDRUM, INDIA

IN PARTIAL FULFILMENT OF THE REQUIREMENTS

FOR THE AWARD OF

DOCTOR OF PHILOSOPHY

2014

DECLARATION

I, **R Deepa**, hereby certify that I had personally carried out the work depicted in the thesis entitled, *"**Fabrication and evaluation of prototypes of bioartificial grafts for cutaneous wound healing application**"*, except where due acknowledgment has been made in the text. No part of the thesis has been submitted for the award of any other degree or diploma prior to this date.

Trivandrum
20-11-2014

R Deepa
Reg.No: PhD/2009/12
Roll No: 5965

SREE CHITRA TIRUNAL INSTITUTE FOR MEDICAL SCIENCES AND TECHNOLOGY, TRIVANDRUM – 695011, INDIA

(An Institute of National Importance under Govt of India)

Phone – (91)0471-2520248 Fax-(91)0471-2341814

CERTIFICATE

This is to certify that **Ms R Deepa** in the division of Experimental Pathology of this Institute has fulfilled the requirements prescribed for the Ph. D. degree of the Sree Chitra Tirunal Institute for Medical Sciences and Technology, Trivandrum. The thesis entitled, "***Fabrication and evaluation of prototypes of bioartificial grafts for cutaneous wound healing application***" was carried out under my direct supervision. No part of the thesis was submitted for the award of any degree or diploma prior to this date.

*Clearance was obtained from the Institutional Ethics Committee/ Institutional Animal Ethics Committee for carrying out the study.

Trivandrum
20-11-2014

Dr. T V Anilkumar, MVSc, PhD
(Research Supervisor)

Scientist F, Experimental Pathology
BMT wing, SCTIMST, Trivandrum.

The thesis entitled

Fabrication and evaluation of prototypes of bio artificial grafts for cutaneous wound healing application

Submitted by

R Deepa

for the degree of

Doctor of Philosophy

Of

SREE CHITRA TIRUNAL INSTITUTE
FOR MEDICAL SCIENCES AND TECHNOLOGY,
TRIVANDRUM - 695011

Is evaluated and approved by

……. ……..

Dr. T V Anilkumar Examiner

(Research Supervisor)

Dedicated to my family, teachers & friends...

ACKNOWLEDGEMENT

*I would like to express my sincere gratitude and humble respect to my guide **Dr. T V Anilkumar**, for his valuable guidance and continuous encouragement throughout the course of this thesis. I thank him for the great effort he has put into training me in the scientific field.*

*I am extremely grateful to my doctoral advisory committee, **Dr. Mira Mohanty, Dr. T V Kumary, Dr. T.V Kumary, and Dr. Anoopkumar T** for their timely suggestions, support, ideas and comments in each stage of the work.*

*I also thank the **Director,** SCTIMST and the **Head**, BMT Wing, SCTIMST for all the facilities provided during the course of my work. I am thankful to the **Registrar**, the **Deputy Registrar**, the **Dean**, the **Associate Dean** (Ph. D.), staffs of academic division and staffs of accounts, library, Computer division, Stores and purchase- BMT Wing for their timely help.*

*I am indebted to the **Council of Scientific and Industrial Research**, Govt. of India for the individual fellowship and project funding provided during the doctoral programme as well as **Indian Council of Medical Research**, Govt.of India for funding international trave.l*

*I would like to thank **Dr. Sharma**, **Mr. Willi Paul, Dr. Rekha** and **Ms. Jasmine** for the various help they have rendered to me. I express my sincere gratitude to **Mr**. **Rajan**, **Mr. Ramesh Babu** and staff of Precision fabrication facility for building the burn making device for animal surgeries. I thank **Mr. Manoj, Mr. Sunil** and all members, DLAS for their help with animal experiments, **Dr. Jayasree, Ms. Arya Saraswathi** and **Mr**. **Shaiju**, Biophotonics and imaging laboratory for helping me in optical imaging of wound samples, **Dr. H K Varma** and **Mr. Nishad**, SEM for their help with SEM analysis, **Dr. Prabha D Nair** and all members of DTERT for their help, **Dr. Anilkumar PR** for the ELISA reading and other members of TIC for helping me with tissue culture. I also thank **Dr. Sabareswaran**, **Ms**. **Sulekha**, **Dr. Arya** and members of histopathology lab for cryosectioning facility.*

*I express my sincere thanks to **Dr. Sulfikar**, and **Dr. Albin** Trivandrum Medical College, for*

exposing me to intricacies of skin grafting and wound management. On a personal note I would like to thank ***Dr. Finosh, Ms. Neena, Ms. Rakhi, Ms. Sunitha, Ms. Thasneem, Ms. Priya, Ms. Caroline, Ms. Rethikala, Ms. Swapna, Ms. Anupriya, Mr. Bejoy, Dr. Linda, Dr. Anwar*** *and* ***Dr. Renjith P Nair*** *for their friendship, help and support. I also thank my colleagues past and present,* ***Ms. Vineetha VP, Mr. Thulseedharan, Mr. Jaseer Muhamed, Ms. Medha Murali, Dr. Akhila Rajan, Ms. Geetha CS*** *and* ***Ms. Reshma*** *for their constant support and encouragement.*

I have no words to thank the endless sacrifices and prayers received from ***my family*** *which provided me with all the success. I also wish to extend my sincere gratitude to my* ***parents*** *and* ***in laws*** *for their constant encouragement, love and support. Last but not the least, with great pleasure I thank my husband* ***Dr. Vinod S Nair****, for the relentless support and my daughter* ***Vedika****, for her lovely smiles which enabled me to complete this thesis happen with satisfaction.*

Above all, I bow before ***The Almighty*** *for being there with me forever and always, showering me with innumerable blessings and helping me tide over every difficult situation in life.*

Deepa Revi

Contents

Page No

List of Figures

List of tables

List of abbreviations

ASMA	alpha smooth muscle actin
CDS	cholecyst derived scaffold
cm	centimeter
CSIS	commercial small intestine submucosa marketed by Cook Surgisis
DAPI	4',6-diamidino-2-phenylindole
DED	de-epithelialized dermis
DMEM	Dulbecco's Modified Eagle's Medium
DPX	distrene with butyl phthalate in xylene
ECM	extracellular matrix
EDTA	Ethylenediaminetetraacetic acid
FITC	fluoresceinisothiocyanate
GAG	glucosaminoglycan
g	grams
H and E	hematoxylin and eosin
HBSS	Hanks balanced salt solution
HFCDS	homologous fibroblast loaded cholecyst derived scaffolds
HFLC	homologous fibroblast loaded chitosan graft
HRP	horse radish peroxidase
IHC	Immunohistochemistry
JDS	jejunum derived scaffold
kg	kilogram
mg	milligram
ml	milliliter
mm	millimeter
MTT	(3-(4,5-dimethylthiazol-2-yl)-2,5)-diphenyltetrazolium
nm	nano meter
NCC	non cellular chitosan graft
PBS	phosphate buffered saline
PCNA	proliferating cell nuclear antigen
rpm	rotations per minute
OW	open wound
TSC	trisodium citrate
UDS	urinary bladder derived scaffold
WVTR	water vapor transmission rate
ºC	degree Celsius
µ	microns

SYNOPSIS

Fabrication and evaluation of prototypes of bioartificial grafts for cutaneous wound healing application

Artificial skin grafts of xenogenic origin have been used for therapeutic management of massive skin loss. These grafts can be classified into two: acellular grafts and cell loaded grafts. Extracellular matrices isolated from small intestine of mammalian organs and tissues have been widely used in wound healing applications. Similar scaffolds prepared from other tubular organs like urinary bladder have also been used in wound healing applications. However, many complications are associated with the use of such scaffolds as grafts for cutaneous wound healing. Hence, there is a quest for better biological scaffolds for regenerative medical applications in general and wound healing application in particular.

Cholecyst derived scaffold recovered from extracellular matrix of porcine gall bladder has variable application in the field of regenerative medicine. The present thesis centers on the hypothesis that the cholecyst derived scaffold has excellent wound healing property. This thesis is divided into different chapters. The first chapter is the introduction which defines the topic and objective of the study. The major objectives of the study are:

- To fabricate bioartificial graft for wound healing application from cholecyst, small intestine and urinary bladder and evaluate their properties as skin grafts.

- To study the wound healing potential of the fabricated grafts *invivo* in rabbit full thickness skin excision wound.
- To fabricate candidate tissue constructs by seeding different types of cells on cholecyst-derived extracellular matrix scaffolds.
- To study the wound healing potential of cell-loaded cholecyst derived scaffold and cholecyst derived scaffold without any cells *in vivo* in rabbit full thickness burn wounds.

The second chapter is the review of literature which gives insights into the various advancements and developments in the field of skin tissue engineering for cutaneous wound healing applications with a brief overview on structure and function of skin and the patho-biology of cutaneous wound healing. The third (Materials and Method), fourth (Results) and fifth (Discussion) chapters are divided into four different sections. Each of the objectives is dealt with in the sections.

The first section is about the fabrication of prototypes of grafts using cholecyst, jejunum and urinary bladder and their evaluation *in vitro* to assess their suitability as bioartificial grafts. The fabricated grafts were termed cholecyst derived scaffold, jejunum derived scaffold and urinary bladder derived scaffold based on the organ of origin. The physical properties such as moisture content, flexural rigidity, water vapor transmission rate, suture retention strength and biochemical constituents such as collagen, elastin, sulphated glucosaminoglycans and nuclear remnants of the different scaffolds were compared with the commercially popular small intestine submucosa, marketed by Cook

Surgsis® Biodesign™. The cholecyst derived scaffold had similar physical properties of commercial prototypes but had higher contents of biomolecules such as elastin and sulphated glucosaminoglycans compared to the reference material. Hence, cholecyst derived scaffold was deemed to have the potential for inducing cutaneous wound healing.

The second section deals with *in vivo* experiment by using rabbit full thickness excision wound model. To determine the wound healing potential of the scaffold, full thickness excision wound were created on rabbit dorsum which was treated with the prototypes of the scaffold. At the end of each experimental period (3, 7, 14 and 30 days), the rabbits were euthanized and samples were collected from the wound site for histomorphology and histomorphometry evaluations. In each instance, wound healing histomorphological parameters such as re-epithelialization, collagen deposition, neo-vascularization, cell proliferation, mesenchymal cell infiltration and myofibroblast response were quantified for all the grafts using histomorphometry. The observations suggested that cholecyst derived scaffold induced higher early cell proliferation and myofibroblast response and hence, has several advantages in wound healing application.

The third section presents details about fabrication of bioartificial grafts by seeding cells on to the extracellular matrix scaffolds. The scaffolds used were cholecyst derived scaffold, jejunum derived scaffold and urinary bladder derived scaffold. The cells used were HaCaT cells (representing major cells of epidermis of skin) and dermal fibroblasts (representing major cells of dermis of skin). The morphology of fabricated tissue

constructs was studied using microscopy and growth of cells on the scaffolds was evaluated using proliferation assay. Both HaCaT cells and dermal fibroblasts grew well on the cholecyst derived scaffold, retaining their characteristic morphology. The homologous rabbit dermal fibroblast loaded on cholecyst derived scaffold was chosen for treating full thickness burn wound in rabbit model.

In fourth section, a prototype of cell loaded bioartificial graft (homologous rabbit dermal fibroblast loaded on porcine cholecyst derived scaffold) was used for treating acute full thickness burn wound on rabbit dorsum. To determine the wound healing potential of cell seeded cholecyst derived scaffold, a total of three full thickness burn wounds were created on rabbit dorsum using a fabricated burn device. The wounds were treated with cell loaded cholecyst derived scaffold or CDS without viable cells. One wound was left untreated and this was the open control. At the end of the experimental period (3, 7, 14 and 30 days), 3 rabbits were euthanized and samples were collected from the wound site for histomorphology and histomorphometry evaluations. In each instance, wound healing histomorphological parameters such as re-epithelialization, neo-epidermal thickness, collagen deposition, neo-vascularization, cell proliferation, and myofibroblast response were quantified for all the grafts using histomorphometry. The cell loaded cholecyst derived scaffold induced better wound healing of the burn wound compared to non cell loaded cholecyst derived scaffoldas demonstrated by increased collagen deposition during 14^{th} day thicker neo-epidermis and high cell proliferation.

The sixth chapter is the summary and conclusion. A brief note on future prospects and limitation of the study is also recorded. In conclusion, cholecyst derived scaffold was found to be a potential biomaterial for wound healing application. When used as a graft on full thickness excision wound, the cholecyst derived scaffold induced higher cell proliferation and wound contraction compared to others *in vivo.* Homologous rabbit dermal fibroblast loaded cholecyst derived scaffold healed full thickness burn wound with higher epidermal thickness compared to non cell loaded cholecyst derived scaffold as grafts. Evaluation of various wound healing parameters through histomorphometry can be used to assess and predict the wound healing outcome after *in vivo* experiments.

Chapter 1

Introduction

Graft assisted healing is an important strategy for managing complicated skin wounds in clinical practice. Full thickness skin wounds more than 4 cm in diameter, benefits from this strategy *(Metcalfe and Ferguson, 2007).* Skin grafting is recommended frequently while treating third degree burns, venous ulcers, pressure ulcers or diabetic ulcers. Other surgeries that need skin grafts include infected wounds, cosmetic alterations, reconstructive surgeries and in skin cancer surgery where there has been extensive skin loss *(Thione et al., 2011).* In any instance, the objective of using skin grafts or assisted healing is induction of accelerated healing response and restoration of complete skin structurally and functionally *(Adams and Ramsey, 2005).*

The use of autologous graft is the gold standard in clinical skin grafting *(Andreassi et al., 2005).* Allografting is another alternative *(Supp and Boyce, 2005).* However, the major disadvantage associated with both autografts and allografts is donor site morbidity. Extensive pain and wound contracture accompanied with the tissue harvest and transplantation of allograft and autograft are serious limitations *(Namazi, 2014).* Hence, various bioartificial grafts and skin substitutes of both xenogenic and synthetic origin are considered for wound healing applications. However, none of the currently available bioartificial grafts or skin substitutes is able to restore the complete structure and function of lost skin.

In this context, tissue engineering offers unlimited opportunities for fabricating bioartificial skin grafts and skin substitutes. It is argued that the rapidly emerging field

of tissue engineering holds the key for the fabrication of a structurally complete skin construct *in vitro* that can act as a functionally complete skin after *in vivo* application *(Priya et al., 2008).* The basic principle behind tissue engineering is propagation and growth of cells on appropriate scaffold with added growth factors that provide clues for cell proliferation and differentiation in the scaffold. An ideal scaffold forms a substrate for cell attachment and provides signals in the form of growth factors for the cell proliferation, growth and differentiation for optimal functioning of the cells seeded on to it *(Metcalfe and Ferguson, 2007).* Various synthetic polymer scaffolds and scaffolds of biological origin are used for the fabrication of bioartificial grafts but the former lack bio-inductive properties *(Badylak, 2007).*

Natural extracellular matrix (ECM) extracted from animal organs/tissue satisfies all the basic requirement of an ideal scaffold. They have several growth factors that provide biological signals to the cells grown over it; in addition of being a natural substrate for cell attachment, proliferation, growth and differentiation. Hence, they are called natures ideal scaffold materials *(Badylak et al., 2009).* Scaffolds derived from porcine small intestinal submucosa and urinary bladders are extensively used for tissue engineering applications. They are also used as xenografts clinically in various wound healing application *(Badylak et al., 2009).* Porcine cholecyst (gall bladder) has tissue architecture similar to small intestine and urinary bladder and forms a source organ for isolation of ECM for tissue engineering application and scaffold preparation *(Burugapalli et al., 2007).* However, its use for wound healing has not yet been studied. Against this background, the present thesis hypothesizes that scaffolds prepared from

porcine cholecyst has wound healing potential both as xenografts and for fabricating bioartificial skin graft. To test the hypothesis, several prototypes of potential bioartificial grafts were fabricated and the wound healing properties of these potential grafts were evaluated.

1.1 Objectives of the study

The major objectives of the study were the following

1. To fabricate bioartificial graft for wound healing application from cholecyst, small intestine and urinary bladder and evaluate their properties as skin grafts.
2. To study the wound healing potential of the fabricated grafts *in vivo* in rabbit full thickness skin excision wound.
3. To fabricate candidate tissue constructs by seeding different types of cells on cholecyst derived scaffold.
4. To study the wound healing potential of cell-loaded cholecyst derived scaffold and cholecyst derived scaffold without any cells *in vivo* in rabbit full thickness burn wounds.

Chapter 2

Review of Literature

Over the past decades, there have been significant advances in the field of tissue engineered skin replacements. Several clinical products have germinated mainly due to the better understanding of the structure and function of skin as well as the cellular mechanisms during the process of wound healing *(Horch et al., 2005).* This review explains briefly the structure and function of skin and the patho-biology of cutaneous wound healing. Furthermore, this review also gives insights into the various developments in the field of skin tissue engineering for cutaneous wound healing applications.

2.1 General structure of skin

Skin is the largest and most variable organ in the human body. It occupies two square meters of the surface area and accounts for 8% of total mass of the body. Its thickness varies at different parts ranging from 0.05mm (least thick in the eyelids) to 5 mm (most thick in the soles). Its complexity is such that it has more than 8 different types of cells and 3 distinct layers *(McLafferty et al., 2012).*

2.1.1 Epidermis

The epidermis is the outermost layer of skin and lodges cells such as keratinocytes, melanocytes, Merkel cells in the basal layer and the Langerhans cells in the upper layers. The epidermis is devoid of blood vessels and it is possible to rub of the cells from it without bleeding *(Sassolas, 2010).*

2.1.1.1 Stratum basale

It is the bottom most layer in the epidermis which maintains the basal stem cells. During development, the stem cells divide and one daughter cell enters the cycling pool progressing into outer layers of the epidermis, while the other daughter cell remains in the basal layer as stem cell. The basal layer is mitotically active. Alterations in the proliferative mechanisms such as wounding and exposure to carcinogens stimulate these stem cells to divide. Other cells of stratum basale include melanocytes and merkel cells. Basal layer communicates with the dermis via the basement membrane. Basal layer contains normal housekeeping organelles and keratin filaments organized into fine bundles around the nucleus, desmosome and hemidesmosomes *(Dreno, 2009).*

2.1.1.2 Stratum spinosum

The polygonal cells in this layer have increased focal junctions or desmosomes. The cell in this layer contains tonofilaments (tension filament) and prekeratin (tension resisting protein). During the histology processing, due to shrinkage of artifacts, the cells in this layer show spiny appearance in the desmosomes. This is also called as the nodes of Bizzozero. Golgi apparatus in these cells secret lamellar bodies. Large keratin bundles are organized concentrically around nucleus and inserted peripherally into the desmosome forming supportive mesh in the cells. Langerhans cells are mostly present in this layer *(Lawton, 2006a).*

2.1.1.3 Stratum granulosum

The cells in this layer have a granular appearance due to the presence of basophilic keratohyalin granules which expel lipid contents into the intercellular spaces. The granules contain proteins like profilaggrin, keratin intermediate filament, loricrin, involucrin etc. Profilaggrin gets converted to filaggrin which serves as a matrix protein that promote aggregation and disulfide bonding of keratin filaments, so it is also called filament aggregation proteins. The lamellar granules contain glycoproteins, glycolipids, sterols, several acid hyaluronidase, lipase, protease, phosphatase, glycosidase etc. The cell in this layer is mostly squamous and is usually 3 to 5 cell layers thick *(Nicol, 2005).*

2.1.1.4 Stratum lucidum

This layer is only present in thick skin where it helps reduce friction and shear forces between the stratum corneum and stratum granulosum. Here, the cells are densely packed with eleidin, an intermediate stage in the production of keratin. The glabrous (non hairy skin) is characterized by thick epidermis (divided into several well-marked layers, including a compact stratum corneum) by the presence of encapsulated sense organs within the dermis and by a lack of hair follicles and sebaceous glands. Hair-bearing skin, on the other hand, has both hair follicles and sebaceous glands but lacks encapsulated sense organs *(Dreno, 2009).*

2.1.1.5 Stratum corneum

This layer is responsible for maintaining the integrity and hydration of the skin. Corneocytes are flattened polyhedral cells with neither nucleus nor cytoplasmic organelles. These cells are therefore biologically dead. This layer occurs as a result of

the final phase of keratinocyte differentiation and is filled with keratin and other products such as lipids, fatty acids and ceramides. The stratum corneum consists of 30 layers of dead scaly keratinized cells. Those at the surface flake off as tiny scales called danders. Dandruff is composed of clumps of danders struck together by oil from scalp. The cell envelope of corneocytes broadens and its cytoplasm is replaced by keratin tonofibrils produced by the keratohyalin granules. Cells are struck together by lipid derived from membrane coating granules *(Lawton, 2006b).*

2.1.2 Basement membrane

Basement membrane has two regions. Lamina lucida faces towards the epidermis side and the lamina densa faces towards the dermis side. The basal layer cells are attached to basement membrane zone proteins through hemidesmosomes. The basement membrane zone proteins also give various signals controlling the proliferation, migration, and differentiation of keratinocytes. Major constituents in the basement membrane of skin are collagen IV, laminin, collagen VII etc *(McLafferty et al., 2012).*

2.1.3 Dermis

Dermis is the tough, supportive connective tissue matrix containing specialized structures present immediately below the basement membrane and is intimately connected to the epidermis. Almost 70% of dermis is collagen which imparts toughness and strength to the structure *(McLafferty et al., 2012).* Elastin is loosely arranged in all direction in the dermis and is responsible for the elasticity of the skin. They are

numerous near the hair and sweat glands and least in the papillary layer. The ground substance in the matrix is glucosaminoglycans (GAG). The dermis contains fibroblasts (which synthesize collagen, elastin, other connective tissue and GAG), dermal dendrocytes (cells with immune function), mast cells, macrophages and lymphocytes. The thickness of dermis ranges from 0.03- 3mm. The dermis has 2 layers - Papillary dermis and Reticular dermis *(Lawton, 2006c).*

2.1.3.1 Papillary dermis

Papillary layer constitutes the superficial 20% of the dermis and is composed of areolar connective tissue with thin loosely arranged collagen and elastic fibers. It houses the mechanoreceptors, Meissner's corpuscles. Papillary dermis has fingerlike projections that extend into the overlying epidermis interdigitating into epidermal rete ridges and rete pegs. This set up increases surface area for exchange of gases, nutrients, and waste products between the dermal layers. The avascular epidermis depends on the diffusion of these materials from dermis. The interdigitation also strengthens the dermal-epidermal relationship *(McLafferty et al., 2012).*

2.1.3.2 Reticular dermis

This layer constitutes 80% of the dermis and has coarse and horizontally running collagen fibers, reticular fibers and elastin fibers which form networks giving strength and resilience. The dermis of the skin lodges cells like fibroblasts, mast cells, blood vessels and various sensory receptors *(Nicol, 2005).*

2.1.4 Epidermal appendages

These are intra-dermal epithelial structures lined with epithelial cells which have the potential for cell division and differentiation. These are important source of epithelial cells during injury, which accomplish re-epithelialization when the overlying epidermis be removed or destroyed in situations such as partial thickness burns, abrasions, or split-thickness skin graft harvesting. The epidermal appendages include sebaceous gland, sweat gland and hair follicles *(Lawton, 2006d).*

2.1.5 Innervations of the skin

The skin is richly innervated and the highest densities of nerves are found in the hands face and genital region. All the cell bodies are in the dorsal root ganglia. Both myelinated and non-myelinated fibers are found. The cells produce neuro-peptide (E.g. substance P). Merkel cells of the epidermis detect light touch. Meissner's corpuscles in the dermis also detect light touch. Pacinian corpuscles detect pressure. Pain is transmitted through naked nerve endings located in the basal layer of the epidermis. Krause bulbs detect cold. Ruffini (bulbous) corpuscles detect heat *(McLafferty et al., 2012).* (See Appendix I histology of skin)

2.2 Functions of skin

Skin provides mechanical and protective barrier against microorganism and the environment. Skin excretes waste products and has a role in the thermoregulation of the body. It can also synthesize Vitamin D in the presence of sunlight. The dermis and basal

layer of epidermis are provided with various tactile and mechanoreceptors which provide afferent sensory signals to the brain, aiding in various sensations *(Subramanyan et al., 2007).*

2.3 Cutaneous wound healing

Skin, the most exposed organ in the body, is prone to injury. The process of repair of the injury occurs through wound healing. The cellular and molecular mechanisms occurring in the patho-biology of acute wound healing are extremely important for understanding the advances in the wound repair *(Shah et al., 2012).* Wound healing is a complex process with three sequential but overlapping phases. These are the inflammatory phase, proliferative phase and remodeling phase *(Li et al., 2007).*

2.3.1 Inflammatory phase

Injury to skin causes clotting of blood and platelet aggregation primarily to arrest the bleeding at the injured site. This is followed by the inflammatory phase. During this phase, the migration of leucocytes including neutrophils and macrophages occurs to the site of injury. There is a release of growth factors as well as 'the mediators of inflammation' at the wound site. The main function of inflammatory stages is to ward off any infection and induce the proliferation of cells. This is done by the release of degrading enzymes, phagocytosis and killing of microorganisms by the polymorphonuclear cells and macrophages that are recruited into the wound site. Macrophages have major regulatory role in the progression of wound healing process

and they control the next phages of wound healing *(Sindrilaru and Scharffetter-Kochanek, 2013).*

2.3.2 Proliferative phase

The proliferative phase also called the regeneration phase results in the laying down of ECM and building up of damaged tissue. The fibroblasts and endothelial cells are activated and they migrate using the fibrin-fibronectin clot matrix into the wound site from the undamaged normal dermis. Process like angiogenesis, fibroplasia, granulation tissue formation, ECM deposition, re-epithelialization and wound contraction occurs during this stage. Angiogenesis results in the formation of new blood vessels to provide oxygenation and nutrition at the healing site. Granulation tissue formation helps in the healing of the wound by the ingrowths of proliferating cells like fibroblasts, macrophages and endothelial cells into the tissue deficient area. The proliferating fibroblasts increases the cell density and population in the dermis (fibroplasias) and they start to secret various structural proteins like collagen, elastin, GAG, nidogen, fibronectin etc which helps in the deposition of ECM proteins *(Heng, 2011)*. The epidermal cells also start to divide, migrate over the granulation tissue and secrete various growth factors and cytokines for inducing wound closure by the process of re-epithelialization. Some of the activated fibroblast converts into a myofibroblast that facilitate wound contraction. The growth factors and proteases secreted by the macrophages are also sequestrated into the healing matrix and stimulate cells as they move into the wound. The activities of protease restricted at the leading edge of

migrating cells are critical for ingrowths of regenerating tissue into the wound and promote healing *(Ireton et al., 2013).*

2.3.3 Remodeling phase

The last phase called the remodeling phase results in the maturation of the laid up ECM and attempts the reversion of granulation tissue to the original status before wounding. The type III collagen is degraded and replaced by stronger type I collagen. Another important feature of remodeling phase is the removal of myofibroblasts, from the healed site through the process of apoptosis *(Diegelmann and Evans, 2004).*

2.4 Skin grafts

Skin grafts are used routinely to close difficult skin defects that cannot heal by itself *(Ratner, 1998).* The skin grafts of biologic origin are divided into autografts, allografts and xenografts *(Halim et al., 2010).*

2.4.1 Autografts

A section of skin harvested from the patient's own body and grafted back to the patients wound site is termed as an autograft. Practically, there is minimal immunological rejection or other associated adverse effect as the material is recognized as self by the host immune response. Disadvantages associated with autografts are reduced donor availability and donor morbidity. Split-thickness skin autograft consists of epidermis and upper part of dermis of variable thickness. The remaining lower portion of dermis is left behind the donor site to help in the healing process. The donor site thus heals by

secondary epithelialization from the wound edges and keratinocytes within the adnexa of the deeper dermis. On the other hand, full thickness skin autograft consists of the epidermis and the entire dermis. These are mainly used in reconstruction of wounds in head, neck, hands, and regions around genitals and breast where, the wounds that are more probable to cause harmful aesthetics and functional impairment due to scarring and wound contracture *(Achora et al., 2014).*

2.4.2 Allografts

A section of skin harvested from another person of the same species is called allografts *(Darwish, 2011).* These can act as skin substitutes and provide a temporary coverage to the wound. However, allogeneic grafts are more prone to immune rejection and less effective compared to autografts *(Rinker and Vyas, 2014).* Human amniotic membrane used in 1910, and still occasionally used as epidermal barrier to induce healing is an example of epithelial allograft *(Nordback et al., 2012).* Another example for dermal allografts is de-epithelialized dermis (DED) obtained from human cadavers. Preparation of DED varies with the process involved for the removal of cells and long term preservation. The various processes during its preparation procedures include gamma irradiation, solvent dehydration, cryopreservation, lyophilization and treatment with glycerol and combination of detergents and acid washes of the cadaveric dermis. The DED acts as a scaffold for the in growth of host fibroblasts and endothelial cells and thus causes wound repair *(Han et al., 2007).* Advent of tissue engineering has given rise to cellular dermal allografts by addition of allogeneic fibroblasts alone or in combination with keratinocytes on collagen based matrices *(Horch et al., 2005).*

Composite allografts contain both the epidermal and the dermal components of skin. Here, a combination of bovine type I collagen gel or non porous collagen sponge and living neonatal fibroblasts acts as the dermal component whereas a cornified epidermal layer composed of neonatal keratinocytes forms the epidermal component of skin.

2.4.3 Xenografts

Tissue pieces harvested from one species and implanted into another species are called xenografts *(Darwish, 2011).* Animal derived materials are readily available commercially for skin repair. The main issue associated with xenografts is the potential transmission of diseases and infection. But, this can be controlled by a process of rigorous screening for zoonotic disease in donor animals before harvest of the tissue. Another issue is the immune rejection due to xeno-antigens. This can be solved by removal of epithelial cells from the skin. Processed bovine/porcine dermis and porcine small intestinal submucosa are examples of xenografts currently used for wound healing application *(He et al., 2003).*

2.5 Skin regeneration

Tissue engineered skin substitute provides a logical therapeutic option to acute and chronic wounds. Tissue engineered skin substitutes were developed as an adjunct or an alternative to the use of patients own skin which still remains the golden standard *(Andreassi et al., 2005).* Tissue engineering/regenerative medicine strategies require interaction and integration of scaffold with tissue and cells in the surrounding niche

through incorporation of appropriate physical and cellular signals usually in the form of growth factors. The important aspect of skin tissue engineering is delivering cells and growth factors through appropriate scaffolds for the repair and regeneration of skin *(Howard et al., 2008).*

2.5.1 Delivering cells for skin regeneration

2.5.1.1 Cell suspensions and sprays

The development in the field of skin tissue culture followed different ways. The cells were delivered into the target wound site in the form of suspensions or sprays. Initially epithelial cells were mixed with serum, blood suspension or saline and layered on wounds as suspension for aiding wound healing. Later non-cultured keratinocytes from biopsies were suspended in fibrin matrix to heal complicated wounds. They were also seeded directly on to the diabetic wound to induce healing. The delivering of cells into the wound site directly in the form of cell spraying has many advantages. It requires a fewer cells to treat larger areas thus reducing the application time and cell number. This technique also reduces blister formation. This method also ensures the maintenance of proper keratinocyte phenotype and higher tendency of cell adherence to the wound during cell delivery *(Horch et al., 2005).*

2.5.1.2 Cultivated autografts

Fragments of skin tissue remains viable and can be transported to donor or tissue culture site using medium. *In vitro,* skin produced cell outgrowth when cultured in suitable

media. Earlier, it was reported that skin remained viable even in ascitic fluid. However, the first breakthrough was obtained when the epidermal cells were cultivated *in vitro* from skin biopsies. A biopsy of 2.5 cm^2 approximately was required for producing keratinocyte sheets to cover 70% total burn surface area in an adult within 3 weeks *(Gallico et al., 1984).* This still remains a landmark in the history of tissue engineering of skin. Furthermore, cultured autologous epidermal sheets were used to treat burn wounds. Eventually, the major disadvantages reported were fragility and low mechanical strength of the sheets, chances of blister formation and infection, lack of adherence and absence of the important dermal component. Another major disadvantage was these cultured autologous epidermal sheets were not immediately available for burn victim and required a 3 week generation time. Subsequently, to overcome this problem, various experience with the use of cultured allogeneic keratinocytes for treatment of burns, acute as well as chronic wounds were studied *(Fohn and Bannasch, 2007).*

2.5.1.3 Allogeneic cells

The most commonly used source for isolation of allogeneic keratinocytes is neonatal foreskin which are more mitotically active and responsive compared to adult skin *(Zhang and Michniak-Kohn, 2012).* With the technique of epidermal cell isolation and expansion freely gaining popularity, attempts were also made to treat wounds using keratinocytes derived from epidermis of cadaveric skin. Cryopreserved allografts gave similar results to freshly prepared allografts thus enabling mass production, wide

availability of 'off shelf grafts' for skin regeneration. In recent times *in vitro* culture development has been characterized by principally 3 culture ideas - multilayered epithelial transplants, composite multilayered dermal epidermal analogs and pre-confluent cell grafting. However, these preparations had very low mechanical strength and hence were relatively fragile. To overcome this, a membrane delivery system called scaffold to provide mechanical support for cultured keratinocytes or other cells in early post-transplantation periods was used *(Horch et al., 2005).*

2.5.2 Membrane delivery system or scaffolds

Tissue engineering of skin is based on the interaction between the cells and matrix (scaffolds) and this has lead to significant advances in the field of wound healing which uses scaffolds for the delivery of cells *(Metcalfe and Ferguson, 2007).* Scaffold or matrix can be divided into two, based on the presence or absence of viable cells in them. Acellular matrix does not contain any viable cells but only the scaffold that acts as a regeneration template. The mechanism of action of acellular scaffold is by helping in the attachment, infiltration and proliferation of host cells and inducing favorable healing response. Cellular matrices have viable cells cultured on them at the time of grafting. Various scaffolds are used extensively used in skin tissue engineering applications *(Ringe and Sittinger, 2014).* Based on the source of material used, scaffolds can be broadly divided into - biologic scaffolds, polymer or alloplastic (synthetic) scaffolds and mixed (or hybrid) scaffolds *(Badylak et al., 2009).*

2.5.2.1 Biologic scaffolds

Collagen is the most abundant protein in the ECM. Its structural and functional characteristics similar to native ECM stimulated the use of collagen matrices for various wound healing applications in variety of forms such as gels, sheet, lattice, mesh or sponge. However, the various disadvantages of collagen based matrices are contraction of collagen lattice, decreased synthesis of collagen, poor bio-stability and low mechanical properties**.** Modification of collagen by cross linking or combining with other natural ECM molecules (such as GAG and/or chitosan) or synthetic polymers (such as polycaprolactone and/or polygalactic acid) may overcome this problem to some extent. Various commercially available cell loaded collagenous matrices are available *(Chan and Leong, 2008).*

For example Orcel, used in burn wounds, is a bilayered cellular matrix made of type 1 collagen sponge with allogeneic skin cells cultured on two separate sides. The donor dermal fibroblasts are cultured within the porous sponge side of the collagen matrix while keratinocytes, from the same donor, are cultured on the coated, non-porous side of the collagen matrix. In Apligraft, suspension of dermal fibroblasts is seeded in bovine type I collagen solution while the keratinocytes are layered over it and raised into air liquid interface *(Lindblad, 2002).*

Chitosan is the most widely used biopolymer for wound healing application after collagen because of its biodegradability, haemostatic activity, and antibacterial properties. Chitosan is also known to induce collagen synthesis and have the capacity to

incorporate growth factors like fibroblast growth factor due to its electrostatic property and thus speed up wound healing rate. Chitosan materials can be easily fabricated into different structures such as gels, solutions, matrix and sponges under various process conditions. Their main disadvantages include unsatisfactory mechanical properties, severe shrinkage, and deformation after drying. This can be overcome by crosslinking treatments or combining with other biomaterials like alginate, collagen etc *(Francesko and Tzanov, 2011).*

Other biologic materials such as fibrin *(Currie et al., 2001),* gelatin, elastin and alginate in various forms (sheets, suspensions, gel, membrane, sponge or film) or in combination with collagen or chitosan are also used in skin tissue engineering. GAG such as hyaluronic acid and chondroitin 6 sulphate act as excellent scaffold material for seeding keratinocytes and fibroblast *(Metcalfe and Ferguson, 2007).* For example micro perforated sheets made of hyaluronic acid cultured with keratinocytes (Laserskin) or fibroblasts (Hyalograft 3D) acts as allogeneic cell loaded grafts while hyaluronic acid in combination with a biodegradable polymer acts as non cellular graft *(Pajardi et al., 2014).* Elastin, GAG, alginates, hydroxyapatites and polypeptides like fibronectin are also used as scaffolds to deliver skin cells to wound or to coat polymers scaffold for wound healing application *(Blais et al., 2013).*The main disadvantage of biologic scaffolds is their low mechanical strength which lead to the use of synthetic polymer scaffolds.

2.5.2.2 Synthetic or alloplastic scaffolds

The biologic matrices have been highly successful and are extensively used and its use will be broadened in future. However, their disadvantages like low mechanical strength, shrinkage, contraction, difficulty in handling, and risks of immunological rejection, prompted the use of synthetic polymers which have higher mechanical properties and more flexible fabrication ability than biopolymers *(Weigel et al., 2006).* Synthetic polymers possess higher batch to batch uniformity, are less expensive and can be tailor made to the required physical properties, but they have limited cellular recognition and tissue compatibility.

Polyurethane (Tegaderm), the most extensively used material in wound dressing act as an acellular matrix. It is semi-permeable i.e. they are impermeable to bacteria and water but permeable to moist and gas. It has limited adherence to wound and cells. However, the biocompatibility and inertness of the polymer can be improved by coating it with collagen or collagen derived peptides *(Ridha et al., 2008).* Synthetic polymers used in sutures and wound dressing are also extensively investigated as matrix materials for dermal regeneration. These include polycaprolactone, poly (l-lactide), copolymer poly (ethyleneglycolterephthalate)-poly (butylenes terephthalate) etc. Polyglycolic acid/polylactic acid (Polyglactin) is used to culture human neonatal fibroblasts in Dermagraft (Advanced Tissue Sciences) for treating diabetic foot ulcers (Shevchenko et al., 2010). However, their main problem is hydrophobicity and lack of biological

signals, resulting in limited cell attachment and proliferation. This can be overcome by combining biologic material with polymer resulting in hybrid scaffolds *(Metcalfe and Ferguson, 2007).*

2.5.2.3 Mixed or hybrid scaffolds

Hybrid scaffolds contain both synthetic and biologic material in combination. The presence of synthetic polymer imparts adequate mechanical strength while ECM component provides the bio-mimetic nature that helps in cell recognition, attachment and proliferation *(Badylak, 2007).* Most of the composite or bilayered skin grafts and skin substitutes are fabricated using hybrid scaffolds *(Metcalfe and Ferguson, 2007).*

The most important breakthrough was achieved when a bilayered acellular skin substitute with an inner matrix of pore size 40 microns composed of bovine collagens and GAG mimicking dermis was layered with an outer sialastic coating mimicking epidermal analog. The porous GAG-collagen (dermal analog) facilitates in growth of cells like fibroblasts and endothelial from the wound providing adequate ECM synthesis and vasculature. The collagen GAG-dermal matrix can also be applied to wound as a single layered product, without the silastic epidermal analog to acts as a dermal substitute *(Shores et al., 2007).* The various advantages of this composite graft are that it controls moisture loss, prevents bacterial entry and acts as a template to generate a neo-dermis. Silicone layer is peeled off and the epidermal layer may be provided after vascularization. The risk associated with the application of this bilayer is development of seroma and hematoma *(Yao et al., 2013).*

Another example for composite hybrid acellular graft is Biobrane. Here, collagen peptides are coated beneath a 3D interwoven nylon filament. The collagen peptide helps in attaching the graft firmly to the wound by binding with the fibrin secreted from the wound *(Felder et al., 2012).* A protective epidermal cover is provided by layering it with silicone which forms the outer layer. The proliferation of cells between the nylon matrixes provide further adherence of graft in the wound. Small pores are present to make the graft semi-permeable that allow transudates to escape. The wound heals as host fibroblasts and capillaries invade the wound and repair the dermal defect, allowing re-epithelialization from wound margin by adnexal keratinocytes *(Whitaker et al., 2008).* As skin regeneration takes place, the graft separates from the wound, allowing easy removal. The advantages of Biobrane are firm adherence to wounds, a semi-permeable barrier to evaporative losses, and permeability to topical antibiotics; however, it requires a vascularized wound base *(Pham et al., 2007).* Biobrane is indicated for clean, superficial partial-thickness burns not involving chemicals or petroleum-based products, for temporary coverage of freshly excised deep partial- or full-thickness wounds and to cover donor site for split thickness skin graft. In collagen coated polygalactin mesh with a semi-permeable nylon mesh cultured with fibroblasts *(Alrubaiy and Al-Rubaiy, 2009),* fetal fibroblasts are allowed to proliferate in the polygalactin mesh for 17 days and these synthesis ECM components such as collagen, fibronectin, proteoglycans, growth factors etc. This is followed by cryopreservation which allows the availability of growth factors and proteins without any cellular activity. List of commonly used bioartificial grafts is given in Table 1.

Table 1 Commonly used bioartificial grafts

Product	Component	Features (Advantages and Disadvantages)
Biobrane	Silicone Nylon mesh collagen	Can be easily peeled off; good for donor sites and superficial partial-thickness burns within 6 hrs; shortens time in hospital; low cost, Temporary coverage
Transcyte	Silicone, Nylon mesh collagen + fibroblast	Readily available; easier to remove than allograft; good for partial-thickness burns; stimulates epithelialization; less scarring; improves healing rate, Temporary coverage; cost 16 times more than Biobrane
Apligraf	Neonatal keratinocyte collagen + fibroblast	Immediate availability; 1 step procedure; easy to handle; hastens healing in deep and chronic wounds; improves cosmetic and functional outcomes, Temporary coverage; limited viability; most expensive.
Dermagraft	Polyglycolic A polygalactin fibroblast	Readily available; living dermal structure; used for chronic lesions, foot ulcers, Temporary coverage; only 1 main application
Integra	Silicone collagen GAG	Immediate permanent wound coverage; allows migration of patient's own endothelial cells and fibroblasts; greater elasticity; avoids risk of infection, complete wound excision; 2 step procedure; relatively expensive compared to cadaveric allografts; learning curve is steep.
Alloderm	Cadaveric human dermis	Immediate permanent wound coverage; good for being a template for dermal regeneration; good take rates, Allograft supply; little barrier function; no virus screening; 2 step procedure; most expensive
Epicel	Cultured keratinocyte	Covers large areas; permanent; immediate permanent wound coverage; minimal risk of disease transmission 3 – 5 wks to produce 1.8 m2 from 2 cm2; fragile; expensive because of quality control; spontaneous blistering; susceptible to infection and contractures

2.6 Wound healing application of ECM scaffold

ECM is a complex interdigitating meshwork of proteins and polysaccharides produced by the cells into the spaces between them. In short the non-cellular material around cells is called ECM. The ECM is diversely arranged in various tissues. For example in the epidermis of skin the ECM is scanty and forms the basement membrane *(Heisenberg and Fassler, 2012).* Whereas in the dermis of the skin, the ECM forms the bulk of the tissue and carries the mechanical stress to which the tissue is subjected. The ECM is composed of structural proteins like collagen and elastin; GAG like hyaluronan, chondroitin sulfate, keratin sulfate and heparin sulfate; linker or adhesive proteins like laminin, fibronectin, nidogen and various other proteoglycans and glycoproteins. The most abundant protein (~25 % of all the whole-body proteins), collagen plays an important role in cell differentiation, polarity, movement and role in tissue and organ development. Collagen contributes to the stability and structural integrity of skin. The next abundant protein, elastin contributes to the stretching ability of the skin. The GAGs in dermis can for porous hydrated gels and resist bulk compressive force in skin. The linker proteins in skin have various binding domains that attach to growth factors and other cells to bring about various functional activities. The cells of the skin such as keratinocytes and melanocytes (in epidermis) and fibroblasts, endothelial cells and macrophages (in dermis) interact with each other through transmembrane receptors like integrin and dystroglycan by signal transduction with the intimate involvement of ECM *(Glim et al., 2014).* Custom made by the resident cells in different tissues and organs

including skin, the ECM is thus continuously interacting with the surrounding environment and cells. The ECM hence supports cell adhesion, growth, proliferation and differentiation. ECM is also biocompatible, non immunogenic, non toxic and biodegradable. The ECM also has bio-inductive property because of the ability to degrade *in vivo*. Degradation products release various bioactive molecules which can modulate and accelerate wound healing activity by assisting in angiogenesis, cell proliferation, cell migration and differentiation. The mechanical properties of the ECM depend on the fiber alignment of collagen in the source organ and rate of degradation. However these functions can be engineered to impart sufficient strength to the ECM scaffold *(Badylak et al., 2009).*

The ECM has all the bio-components essential for the support of proliferation, migration and differentiation of cells. They are rich in GAG, laminin, fibronectin and natural fibrous proteins like collagen and elastin on which the cells attach and grow *(Kleinman et al., 2003).* ECM is even known to aid angiogenesis, an important requirement in the healing of any damaged organ by regulating the migration, proliferation and sustenance of endothelial cells *(Raines, 2000).*They also house cryptic peptides and bio-active molecules including growth factors. Even the degradation products of ECM release bioactive products mimicking growth factors *(Reing et al., 2009).* The growth factors like vascular endothelial growth factor, fibroblast growth factor, platelet derived growth factor, Transformation derived growth factor beta are required for the healing of both acute and chronic wounds. Hence ECM, termed as

natures ideal scaffold material *(Badylak et al., 2009),* has the potential to aid in wound healing.

2.6.1 ECM from human dermis

ECM derived from human dermis has a porous and fibrillar structure. The decellularised and lyophilized form of cadaveric human dermis marketed as AlloDerm has been used as allografts in burn wound reconstruction and hernia repair. Another cross linked form of human dermis (marketed as Graft Jacket) is used in the treatment of diabetic ulcers in human subjects. The natural human dermis without any cross linking (Axis dermis) is used in sustaining prolapse of pelvic organs *(Badylak et al., 2009).*

2.6.2 ECM from porcine urinary bladder

ECM derived from porcine urinary bladder is also used as scaffold in regenerative medicine. The urinary bladder derived matrix is reported to heal complex wound *(Sasse et al., 2013)* and aid in esophageal reconstruction *(Nieponice et al., 2014).* It is also shown to induce skeletal myogenesis *(Sicari et al., 2014)* and is also used in the repair and reconstruction of ladder preventing lower leg amputation *(Fleming et al., 2014).* It is also used in burn wound care *(Mitchell and Gallagher, 2012),* gynecology *(Merguerian et al., 2000)* and hair repair *(Hitzig, 2012).*

2.6.3 ECM from porcine small intestinal

The ECM derived from porcine small intestinal submucosa (marketed as Oasis and Surgisis Cook) has bio-inductive property that helps in constructive remodeling of injured sites. In fact, it has been extensively and successively used in various clinical applications such as lip augmentation *(Seymour et al., 2008),* abdominal wall reconstruction *(Newman, 2010),* foot and ankle reconstruction *(Bibbo, 2010),* vaginal and perivaginal repair in women (*Geoffrion et al., 2011),* rotator cuff repair *(Phipatanakul and Petersen, 2009)*, Morgagni hernia repair *(Puglisi et al., 2009),* inguinal hernia repair *(Ansaloni et al., 2009),* repair of proximal hypospadias *(Hayn et al., 2009),* urethral stricture repair *(Hauser et al., 2006),* ligament repair *(Liang et al., 2006),* nerve repair *(Smith et al., 2004)*, repair of renal defect *(Schnoeller et al., 2011),* and fistula *(Cintron et al., 2012).* The small intestinal submucosa also heals chronic wounds such as non healing diabetic, venous and pressure ulcers *(Mostow et al., 2005, Hodde and Allam, 2007, Romanelli et al., 2010).* Small intestine submucosa made into sponge and cross linked with 1-ethyl-3-(3-dimethylaminopropyl) carbodiimide hydrochloride showed excellent fluid absorption capacity and enhanced full thickness skin wounds in rats *(Kim et al., 2005).* It can also act as skin flaps carrier to treat arteriovenous fistula in rats *(Zhang et al., 2003).*

However, there are also reports that the most widely used ECM derived from small intestinal submucosa has no significant beneficial effect in treating full thickness skin wounds in dogs *(Schallberger et al., 2008, Winkler et al., 2002).* Small intestine

submucosa is not totally without nuclei and might contain some residual amount of DNA which can elicit some adverse inflammatory response *(Zheng et al., 2005)*. There are also reports of complications arising from the clinical use of small intestine submucosa in regenerative medicine such as irritation and inflammation *(Breyer et al., 2007, John et al., 2008).* Hence, there is a quest for better scaffolds for regenerative medical applications. So, ECM from other sources such as porcine urinary bladder *(Wu et al., 2007, Wang et al., 2006),* dermis of cadaveric human skin *(Yim et al., 2010, Newman, 2010),* bovine pericardium *(Kim et al., 2012)* etc have also been tried with variable success.

2.6.4 Porcine cholecyst derived ECM

Porcine cholecyst derived ECM is a relative new potential biomaterial that can have variable application in the field of regenerative medicine. The scaffold has a mesh like architecture and surface nano topography which is extremely suited for the attachment, proliferation and infiltration of functional cells. The scaffold also has excellent biodegradability and ability to support various types of cells. The acellular scaffold supports the attachment and proliferation of valvular endothelial cells and interstitial cells and thus has the potential to act as scaffold for cardiac tissue engineering. It is shown to act as reinforcing buttressing staples for gastrointestinal resection and anastomotic procedures *(Burugapalli et al., 2008.)* Being a weekly anisotropic scaffold, matrix from cholecyst has the ability to support large strain *(Coburn et al., 2007).* There is also no acute inflammatory response associated with it *(Burugapalli and Pandit,*

2007). Studies have also shown that properties of cholecyst derived ECM can also be functionalized and modified using chemicals *(Chan et al., 2008, Burugapalli et al., 2009).* However, the use of cholecyst derived ECM in skin wound healing application has not been studied yet.

2.7 Factors affecting wound healing potential of the ECM scaffolds

2.7.1 Processing techniques

Apart from the source organ, the various processing technique also contributes to the final outcome of the quality of scaffolds. The production of scaffolds from ECM involves various treatment procedures during transportation, isolation, preparation and packing of scaffolds. Initially the organ selected for scaffold preparation is transported to the laboratory in a suitable transportation solution such as antibiotic containing culture media, normal saline or even in ice cubes. The main aim is to protect the natural architecture, morphology and functional biomolecules in the scaffold and also to prevent bacterial contamination to obtain quality scaffold *(Badylak and Gilbert, 2008).* The separation of scaffolds from the organ may be done at the site of collection also.

2.7.2 Chemicals used for decellularization

The process of decellularization is performed to minimize the antigencity of the scaffold. The ultimate goal of any decellularization protocol is to remove all cellular material without adversely affecting the composition, mechanical integrity and eventual biological activity of the remaining ECM. The decellularization process requires

optimization in different settings and for different organs. There are various methods for decellularization both physical and chemical. The physical methods include freezing, sonication, agitation, direct pressure or by mechanical delaminating *(Badylak et al., 2009).* The chemical methods use various chemicals for the removal of cells. The cocktails of chemicals used for decellularization include alkali/acid (e.g., acetic acid, peracetic acid, hydrochloric acid, sulfuric acid and ammonium hydroxide); nonionic detergents (e.g., Triton X-100); ionic detergents (e.g., sodium dodecyl sulfate, Triton X-200); zwitter ionic detergents (e.g., 3-[(3-cholamidopropyl), dimethylammonio]d-1-propanesulphonate, sulfobetaine-10,sulfobetaine-16); chaotropic agents (e.g., tri(n-butyl)phosphate); chelating agents (e.g., ethylenediaminetetraacetic acid, ethylene glycol-bis(beta-aminoethyl ether)-N,N,N0,N0-tetraacetic acid), hypo-/hypertonic solutions, proteolytic enzymes like pepsin, trypsin or endonucleases, exonucleases etc *(Anilkumar et al., 2014).*

2.7.3 Hydration, dehydration and terminal sterilization

The scaffolds are then washed and hydrated to remove any residual content of reagents or decellularizing agent. This is done by treatment with a neutralizing agent such as trypsin inhibitor or cross linking agent such as glutaraldehyde. Once the scaffold is stabilized after chemical treatment, the scaffold has to be preserved for long term storage. This is achieved by the dehydration of scaffolds. Dehydration prevents loss of growth factors and biomolecules and also facilitates easier handling of scaffolds for packing and storing. Dehydration is done either by lyophilization (freeze drying) or

vacuum pressing. Vacuum pressing is an effective method for constructing a variety of 3-D shapes or multilaminated form of ECM scaffold. Various forms of scaffolds such as gels, sheets, powder or multilaminated sheets can be obtained during this stage. This is followed by terminal sterilization of the scaffold for storage purpose. Various methods adopted for sterilization of scaffolds include ethylene oxide sterilization (750mg/h), gamma irradiation (<15kGy) or electron beam (20kGy) irradiation or their combination *(Badylak et al., 2009).* Hence, a wide range of chemicals are used for the derivation of scaffolds from ECM of mammalian organs. The selection of various procedures for scaffold isolation and the source organ determines the final outcome of the quality of the scaffold. The presence of residual chemicals in the scaffolds not only alters the biophysical properties but may also have some deleterious effect in the end medical use of the scaffold. Thus, it is better to avoid the use of chemicals altogether in the process of scaffold preparation and processing. Hence, a procedure which does not use any chemicals or enzyme was used to produce good quality scaffold from cholecyst organ *(Anilkumar et al., 2014).*

2.7.4 Addition of cells on ECM scaffolds

Addition of cells is known to have modulatory role in wound healing. The added cells interact with the matrix as well as at the niche of the healing site and modulate various activities that are occuring in the granulation tissue of the healing wound. Cell-loaded bioartificial skin grafts open up new approach for repair and regeneration of skin *(Kamel et al., 2013).* This is especially important with complicated wounds such as

cutaneous burns where there is significant destruction of tissue resulting in deficiency of functional cells. Fibroblasts are the most abundant and diverse cell type in the dermis which can be easily isolated and cultured compared to keratinocytes in the epidermis. The dermal fibroblasts are responsible for the synthesis of the native ECM components such as collagen, elastin, laminin, fibronectin GAG etc. The dermal fibroblasts are also known to secrete various growth factors which in turn stimulate the proliferation and migration of other cell types of the skin such as the keratinocytes and endothelial cells *(Osonoi et al., 2011).* So, they are the most easily available cells with plasticity for skin tissue engineering and can be seeded on various scaffolds for fabricating a viable skin construct for wound healing application. However, there are no studies that examine the modulatory role of dermal fibroblast on cholecyst derived scaffold to heal skin wounds.

Chapter 3

Materials and Methods

Section I

3.1 Fabrication and evaluation of tissue engineering scaffolds from ECM of porcine organs for skin tissue engineering

3.1.1 Fabrication of tissue engineering scaffolds

3.1.1.1 List of materials and reagents used

Forceps, scalpel blade, blade holder, stainless steel scale, petri-plate (60 mm), Tyvek* packaging material, aluminium foil, scissors, ultra low -80ºC deep freezer (Sanyo), lyophilization unit (Christ Alpha 2-4LD freeze dryer), electronic analytical balance (Sartorius, CP 224S), ethylene oxide sterilization unit. Fresh porcine gall bladder (cholecyst), small intestine (jejunum) and urinary bladder obtained from Meat products of India, Edayar, Ernakulum, Kerala, 10% neutral buffered formalin.

3.1.1.2 Method

Three types of grafts for cutaneous wound healing application were prepared from three different organs of porcine origin namely gall bladder (cholecyst), small intestine (jejunum) and urinary bladder as described below.

3.1.1.2.1 Fabrication of tissue engineering scaffold from cholecyst

The porcine gall bladder was collected in 10% neutral buffered formalin for transportation to the laboratory. A transverse incision was made at the fundus and the neck of the gall bladder and a horizontal incision was made from one end of the body to the other end to obtain a rectangular piece of tissue. The serosa layer and the inner mucus layer were scrapped off. The remaining layer was peeled off mechanically and washed well in running tap water. The layer so obtained was placed flattened on a petri-plate and lyophilized to get a sheet of scaffold. It was sterilized by ethylene oxide. The

final tissue engineering scaffold prepared from gall bladder was termed as cholecyst derived scaffold (CDS).

3.1.1.2.2 Fabrication of tissue engineering scaffold from small intestine

ECM scaffolds for wound healing application were isolated from submucosal layer of porcine small intestine. The jejunum region was selected for scaffold preparation. About 5 cm of porcine jejunum was collected in 10% neutral buffered formalin for transportation to the laboratory. A horizontal incision was made from one end of the body to the other end and the contents inside the jejunum were emptied. The outer serosa layer was scrapped off and removed completely. The inner mucus layer was also scrapped off. The submucosa layer was peeled off mechanically and was washed well in running tap water. The layer so obtained was placed flattened on a petri-plate and lyophilized. The final product was sterilized by ethylene oxide. The final tissue engineering scaffold prepared from small intestine was termed as jejunum derived scaffold (JDS).

3.1.1.2.3 Fabrication of tissue engineering scaffold from urinary bladder

Fully filled distended porcine urinary bladder was selected for scaffold preparation. It was collected in 10% neutral buffered formalin for transportation to the laboratory. A transverse incision was made at the fundus and the neck of the urinary bladder and a horizontal incision was made from one end of the body to the other end. The serosa layer and the inner muscularis layer were peeled off. The middle layer was separated

mechanically and washed well in running tap water. The layer so obtained was placed flattened on a petri-plate and lyophilized to get a sheet of scaffold. The scaffold so obtained was sterilized by ethylene oxide sterilization. The final tissue engineering scaffold prepared from urinary bladder was termed as urinary bladder derived scaffold (UDS).

3.1.1.2.4 Reference scaffold

Wherever indicated, the commercially available small intestine submucosa (CSIS), marketed by Cook Surgsis^{R} Biodesign^{TM} (one layer tissue graft, Catalogue No – G53614) used for wound healing application, hereafter referred as CSIS was used as the reference biomaterial in the study.

3.1.2 Evaluation of physical properties

3.1.2.1 List of materials and reagents used

Lyophilized ECM scaffolds (CDS, JDS, UDS and CSIS), scissors, measuring scale, 15 ml sterile test tube, aluminium foil, gold coating apparatus, incubator at 37ºC (MRC, DNO series), electronic analytical balance (Sartorius, CP 224S), refrigerator, Universal Testing Machine (Instron, Model 3365, UK), Scanning electron microscope (Hitachi, Model S-2400, Japan), Screw gauge (Mitutoyo digital micrometer), phosphate buffered saline (PBS), 2.5% glutaraldehyde, isopropyl alcohol, distilled water.

Reagent preparation

Phosphate buffered saline

NaCl	8g
KCl	0.2g
Na_2HPO_4	1.44g
KH_2PO_4	0.24g

The contents were dissolved in 800ml distilled water and the pH was adjusted to 7.4 with HCl. The volume was made up to one liter with additional distilled water. The solution was sterilized by autoclaving.

3.1.2.2 Method

3.1.2.2.1 Scanning electron microscopy

The ECM scaffolds were washed in PBS for five minutes and fixed in 2.5% glutaraldehyde overnight at 4ºC. It was then dehydrated using ascending grades of isopropyl alcohol (50%, 60%, 70%, 80%, 90% and 100%) for five minutes in each step, mounted on to aluminium stubs with the luminal surface facing upwards for visualisation, gold spluttered in a coating apparatus and the luminal side was viewed under scanning electron microscope (Hitachi, Model S-2400, Japan).

3.1.2.2.2 Fluid uptake

The specimens were cut into size of one cm^2 and the initial weight was noted. All the samples were soaked in PBS. The samples (N = 4) were taken out of the buffer, blotted

and the wet weight was noted down after 1 hour, 3 hours, 5 hours, 12 hours and 24 hours. Percentage of fluid uptake was calculated as [(wet weight) - (initial weight) x 100]/ (wet weight)].

3.1.2.2.3 Water vapor transmission rate (WVTR)

The mouth of 15 ml tube, filled with 10 ml of water, was sealed with the ECM scaffold. The initial weight was noted (N = 4) using electronic analytical balance (Sartorius, CP 224S). The samples were placed in an incubator at 37ºC (MRC, DNO series) for 24 hours. The weight after evaporation of water from the test tube after 24 hours was noted. The water vapor transmission rate was calculated as follows WVTR = [(initial weight - weight after evaporation) x 10^6]/A x 24 where "A" is the area of bottle mouth (in m^2). The WVTR was expressed in g/m^2h.

3.1.2.2.4 Mechanical strength

3.1.2.2.4.1 Young's modulus

To get the Young's modulus, the scaffolds (N = 8) were first clamped at its cut ends in Universal Testing Machine (Instron Model 3365, UK). The modulus (MPa) as well as the maximum load (Newton) was measured using a 10 Newton maximum load cell with a cross-head speed of 1mm/min and the test was stopped when the load decreased after the onset of failure.

3.1.2.2.4.2 Flexural rigidity

The weight of 5 cm^2 rectangular scaffolds (N = 8) was measured and the moment of inertia of the rectangular piece of the (5cm x 1cm) scaffolds was calculated using the formula Flexural rigidity = m (h^2 + w^2)/12 where m is the moment of inertia, 'h' is the height of the scaffold and 'w' the width of the scaffold. The moment of inertia of each scaffold calculated was multiplied with the Young's modulus of the scaffold to get the flexural rigidity of the scaffolds.

3.1.2.2.4.3 Suture retention strength

The maximum load at the stress strain curve during breakage was read in the Universal Testing Machine (Instron Model 3365, UK) as the suture retention strength (N = 8).

3.1.3 Evaluation of biomolecules and nuclear content

3.1.3.1 List of materials and reagents used

Lyophilized ECM scaffolds (CDS, JDS, UDS and CSIS), scissors, scale, 15 ml test tube, aluminum stubs for gold coating, gold coating apparatus, incubator at 37ºC (MRC, DNO series), refrigerator, Chameleon Multi Technology Plate Reader (Mikrowin 2000), Nanodrop spectrophotometer (Nanodrop, ND-1000), centrifugation unit, vials, 15 test tubes, PBS, 3.14% formaldehyde, propyl alcohol, distilled water, Confocal microscope (Carl Zeiss, Germany), antibodies against collagen IV (C-IV-22, Santa Cruz biotechnologies), laminin (LAM-89, Santa Cruz biotechnologies) and collagen VII (LH7.2, Santa Cruz biotechnologies), Goat anti-mouse IgG F(ab)'2 FITC (fluorescein

iso-thio-cyanate) conjugated (sc-3699, Santa Cruz Biotechnologies USA), Sircol collagen assay kit, Fastin elastin assay kit, Blyscan sulphated GAG assay kit (bicolor life science assays, UK), 10% hydrogen peroxide solution, fetal bovine serum, lysis buffer, phenol, chloroform, isopropanol alcohol, sodium acetate, citiflour antifadent mounting medium (Electron Microscopy Sciences, AF1 17970-100).

3.1.3.2 Method

3.1.3.2.1 Detection of desirable proteins

The scaffolds were fixed in 3.4% formaldehyde for 20 minutes followed by washing with PBS for 5 minutes. The fixed specimens were treated with 10% hydrogen peroxide solution for 5 minutes, followed by washing with PBS for 5 minutes and treatment with 1% fetal bovine serum for 30 minutes. Each of the scaffolds was treated with primary antibodies (Table 2) diluted in PBS against collagen IV, collagen VII and laminin for one hour at room temperature and washed with PBS. It was stained with anti-mouse IgG F(ab)'2 FITC conjugated as secondary antibody for 30 minutes, washed in PBS to remove unbound antibodies and viewed under a confocal microscope (Carl Zeiss, Germany) after mounting in citiflour antifadent mounting medium. The details of source and dilution of the anti-mouse monoclonal IgG antibodies used in the study are given in Table 2.

Table 2 List of antibodies used for immunofluorescence

Sl No	Antibodies	Clone and company	Dilution
1	Collagen IV	COL4a (C-IV-22) (Santa Cruz Biotechnologies, USA)	1:400
2	Laminin α 1	L α 1 (LAM-89) (Santa Cruz Biotechnologies, USA)	1:400
3	Collagen VII	Col7a1(LH7.2) (Santa Cruz Biotechnologies, USA)	1:400

3.1.3.2.2 Quantification of major biomolecules

The amount of biomolecules such as collagen, elastin and sulphated GAG in the scaffolds was estimated biochemically using Sircol collagen assay kit, Fastin elastin assay kit and Blyscan sulphated GAGs assay kit respectively in all the ECM scaffolds using manufacturer's protocol. Chameleon Multi Technology Plate Reader (Mikrowin 2000) was used to measure the spectrophotometry readings.

3.1.3.2.3 Quantification of DNA content

The scaffolds were incubated with lysis buffer 500 µl (proteinase K 20 mg/ml; 50 µl, 1 M Tris-HCl solution; 10 µl, 0.5 M EDTA (Ethylenediaminetetraacetic acid); 2 µl, 10% SDS; 100 µl, distilled water; 838 ml) for 48 hours at 60ºC followed by treatment with 500µl phenol:chloroform:isopropanol alcohol at 25:24:1 ratio. The supernatant obtained after centrifugation was treated with equal volume of chloroform. Isopropanol and 3M sodium acetate (in 10:1 ratio) were added after removing the supernatant and incubated overnight at -20ºC. The precipitated DNA was centrifuged at 12000g at 4ºC and

supernatant was discarded. The pellet was washed in 75% ethanol, dried and was collected in 50µl water. The DNA content was measured using nano drop spectrophotometer (Nanodrop, ND-1000).

3.1.4 Statistical analysis

Student's t-test was performed to determine the level of significant difference between experimental groups, wherever statistical analysis was necessary. A p-value less than 0.05 was considered to be of significance.

Section II

3.2 *In vivo* evaluation of the CDS, JDS, UDS and CSIS for wound healing application.

3.2.1 Animal experiment design

3.2.1.1 List of materials and reagents used

Sterilized scalpel, sterilized blade (22), syringe (5ml), needle, sterilized blade holder, cotton, sterilized rat toothed forceps, ethicon suture, sterilized scaffolds 1cm x 1cm, gloves, mask. PBS, Ketamine, Xylaxin, 70% alcohol

3.2.1.2 Method

The animal experiments were done with the approval and as per requirements of the Institutional Animal Ethics Committee. Two animal experiments (designated as experiment I and experiment II) were conducted to evaluate the wound healing efficiency of the different prototypes of ECM scaffolds as acellular skin grafts. Twenty four healthy rabbits of more than two kg weight were randomly assigned into two groups of twelve animals for the two animal experiments. Each group of twelve animals was again divided into four groups of three each in each animal experiment. Prior to the experiment, fur on either side of the spine was clipped off. Rabbits were anaesthetized using Ketamine (80mg/kg body weight) and Xylaxin (5mg /kg body weight). The skin of the anaesthetized rabbits were lightly swabbed using 70% alcohol and air dried.

3.2.1.2.1 *In vivo* animal Experiment I

On one set of twelve animals, CDS, and CSIS scaffolds were grafted on full thickness excision skin wounds of one cm^2 made dorsally which were created on either side of the vertebra for each of the four time periods of 3, 7, 14 and 30 days (N=3).

3.2.1.2.2 *In vivo* animal Experiment II

On the other set of twelve rabbits, three wounds were created on the rabbit dorsum (N=3) and was grafted with JDS and UDS. The third wound was left open and untreated which was the control in the study.

At the end of each experimental period (3, 7, 14 and 30 days), three rabbits from each group were euthanized by carbon dioxide inhalation and tissue samples were collected from the wound site for routine histology, special staining and histomorphometry evaluations.

3.2.2 Histotechnology

3.2.2.1 List of materials and reagents used

Tissue cassettes, Microtome (Leica RM2255), forceps, Blade (22), blade holder, starFrost adhesive slides, water bath at 60ºC (Leica HI-1210), Paraffin wax dispenser (Slee paraffin wax embeddeding MRS/P1), Tissue processor (Leica TP1020), 10% buffered formalin, xylene, isopropyl alcohol ascending grade (90%, 80%, 70%), paraffin wax.

3.2.2.2 Method

After the animal experiment, the skin graft along with the surrounding normal skin was collected and fixed in 10% neutral buffered formalin. Formalin fixed tissue samples were dehydrated through ascending grades of alcohol, cleared in xylene and

impregnated with paraffin wax using automated tissue processor (Leica TP1020). Paraffin tissue blocks obtained after paraffin embedding (using Slee paraffin wax embeddeding MRS/P1) were mounted on microtome (Leica RM2255). Tissue sections of 4 μm thickness were made after microtomy, floated on water bath (Leica HI-1210) and the sections were obtained on starFrost slides

3.2.3 Histomorphology and histochemistry

The sections were then stained for routine Harris's Hematoxylin and eosin (H and E) and special stains like picro-sirius red. Immunohistochemistry (IHC) staining using primary antibodies against proliferating cell nuclear antigen (PCNA), vimentin and alpha smooth muscle actin (ASMA) was also performed on additional sections.

3.2.3.1 H and E staining

3.2.3.1.1 List of materials and reagents used

Xylene, serial grades of propyl alcohol (70%, 80%, 90% and 100%), water, Harris Hematoxylin stock solution (26041-06090121, Electron Microscopy Science), Eosin Yellowish (60134500251730, Merck) staining solution, 1% acid alcohol solution, ammonia water, DPX (Distrene with butyl phthalate in xylene) mountant.

Reagent preparation

1. Harris Hematoxylin Working Solution

   Harris Hematoxylin stock solution 100 ml

Acetic Acid Glacial	4 ml

The glacial acetic acid was added to Harris Hematoxylin stock solution and mixed well. It was stored at room temperature and filtered before use for removal of metallic sheen.

2. Eosin Yellowish Staining Solution

Eosin Yellowish	1 g
Distilled Water	100 ml
Acetic Acid Glacial	0.1 ml

The eosin yellowish was dissolved in distilled water and the glacial acetic acid was added to it. It was stored at room temperature.

3. 1% Acid - Alcohol

70% Isopropyl Alcohol	99 ml
Concentrated HCl	1 ml

The concentrated HCl solution was added to 70% isopropyl alcohol. It was mixed well and used.

4. Ammonia water

Concentrated ammonium hydroxide	0.2 ml
Distilled Water	100 ml

The concentrated ammonium hydroxide was added to distilled water and mixed well. It was freshly prepared was used immediately.

3.2.3.1.2 Method

The section in slides was dewaxed in three changes of xylene, dehydrated using serial grades of propyl alcohol (70%, 80%, 90% and 100%) and washed in running water. It was treated with Harris Hematoxylin staining solution for 15 minutes, washed in running water for 5 minutes, differentiated in acid alcohol by 1 dipping once, followed by treatment with ammonia water for two minutes. It was rinsed in running tap water and treated with eosin solution for 5 minutes, followed by dehydration, clearing and mounting using DPX.

3.2.3.2 Picro-sirius red staining

3.2.3.2.1 List of materials and regents used

Xylene, serial grades of propyl alcohol (70%, 80%, 90% and 100%), water, Weigert's Iron Hematoxylin (C.I.75290, SD Fine Chemicals Ltd), Picro-sirius red (Direct red 80 C.I. 37580, Fluka) staining solution, 1% acetic acid solution, DPX mountant.

Reagent preparation

1. Picro-sirius red staining Solution.

Sirius red F3BA (C.I. 35780)	0.1 g
Saturated aqueous solution of picric acid	100 ml

The sirius red F3BA (C.I. 35780) was added to saturated aqueous solution of picric acid and a little solid picric acid was finally added to ensure saturation.

2. Acidified water

Glacial acetic acid	1ml
Distilled water	100 ml

The glacial acetic acid was added to distilled water

3. Weigert's Iron Hematoxylin

Stock Solution A:

Weigert's Iron Hematoxylin	1 g
95% Ethyl alcohol	100 ml

It was mixed well and labeled. The resulting solution was stable for 1 year.

Stock Solution B:

29% ferric chloride in water	4 ml
Distilled water	95 ml
Hydrochloric acid	1 ml

It was mixed well, labeled. The resulting solution was stable for 1 year.

Weigert's Hematoxylin Working Solution

Solution A	25.0 ml
Solution B	25.0 ml

Equal amount of solution A and solution B were mixed well. The resulting solution was stable for 3 - 4 days.

3.2.3.2.2 Method

The section in slides was dewaxed in three changes of xylene, dehydrated using serial grades of iso propyl alcohol (70%, 80%, 90% and 100%) and washed in running water.

It was treated with Weigert's Iron Hematoxylin Working Solution for 20 minutes, washed in running water for 5 minutes, followed by staining in Picro-sirius red staining solution for one hour. It was rinsed in acidified water (1% Acetic acid), followed by dehydration, clearing and mounting

3.2.4 Immunohistochemistry

3.2.4.1 List of materials and reagents used

Xylene, serial grades of propyl alcohol (70%, 80%, 90% and 100%), water, Tris-EDTA buffer and citric acid buffer as antigen retrieval buffer, 10% hydrogen peroxide solution for blocking endoperoxidase activity, trisodium citrate (TSC) as working buffer, 10% goat serum, primary antibodies proliferating cell nuclear antigen (PC10, Santa Cruz Biotechnologies), Vimentin (V9, Dako, Denmark) and Alpha Smooth muscle actin (1A 4, Abcam), goat anti mouse Fab'2-biotin conjugate as secondary antibody (Santa Cruz Biotechnologies), streptavidin-horse radish peroxidase (HRP) conjugate (Vector laboratories), HRP substrate (Sigma), Harris's Hematoxylin staining solution (26041-06090121, Electron Microscopy Science), DPX mountant, slides with mounted sections, staining racks, slide trays, coverslips, water bath at 95ºC, timer, stopwatch, gloves, mask etc.

Reagent preparation

1. TSC buffer

Trisodium citrate	2.96 g

Distilled water	1000 ml

The TSC was completely dissolved in 900 ml distilled water and the volume was made up to one liter with distilled water.

2. Tris - EDTA buffer

Tri-base	6.05 g
EDTA	0.74 g
Distilled water	1000 ml

The tris-base and EDTA was completely dissolved in 900 ml distilled water and the volume was made up to one liter with distilled water.

3.2.4.2 Method

Sections of 4µm thickness prepared on glass slides, were incubated at 37°C for 24 hours, de-paraffinised in three changes of xylene and brought to water through descending grades of alcohol. The sections were washed in water and treated in antigen retrieval buffer, either tris-EDTA buffer of pH 9.2 (for PCNA and vimentin) or in citric acid buffer of pH 6 (for ASMA) at 92^{o}C for 20 minutes. The sections were then allowed to cool to room temperature. The endogenous peroxidase activity was blocked by treating the slides with 10% H_2O_2 for 15 minutes. It was washed three times in TSC buffer. The non-specific binding of secondary antibody was blocked by using 10% goat serum. The sections were then washed with TSC buffer and incubated with primary antibody for an hour at room temperature. The section were subsequently washed and treated with goat anti mouse Fab'2-Biotin conjugate for 30 minutes. Sections were again washed followed by treatment with streptavidin-HRP conjugate for 30 minutes.

The sections were again washed thoroughly with TSC buffer and treated with HRP substrate (Sigma) for 5 minutes. The reaction was stopped by immersing the slides in excess distilled water. The section were then counter stained with Harris's Hematoxylin staining solution, dehydrated in ascending grades of alcohol, cleared in xylene, and mounted in DPX. For negative control, sections were stained similarly except that TSC solution was used, instead of primary antibody. The details of antibody and the dilution used are given in Table 3

Table 3 - List of antibodies used for wound healing evaluation

Sl No	Antibodies	Clone and company	Dilution
1	PCNA	PC10 (Santa Cruz Biotechnologies, USA)	1:400
2	Vimentin	V 9 (Dako, Denmark)	1:200
3	ASMA	1A4 (Abcam, UK)	1:200

3.2.5 Histomorphometry and immunohistomorphometry

3.2.5.1 List of materials used

Stained sections, Olympus (BX51) microscope loaded with a DP71 camera and Image-Pro^{TM} software.

3.2.5.2 Method

Histology images were captured using an Olympus (BX51) microscope loaded with a DP71 camera and Image-Pro^{TM} software. The images were further evaluated with the software for the following wound healing parameters.

3.2.5.2.1 Extent re-epithelialization

Re-epithelialization was quantified in images of H and E stained sections. The length of the original wound and non-epithelialized wound were measured and percentage of re-epithelialization was calculated by the formula [Percentage Re-epithelialization = (length of epithelialized wound / length of total wound) x 100. The same was repeated for every histology slides representing the wound site and percentage of re-epithelialization was determined.

3.2.5.2.2 Extent of neo-vascularization

Images from H and E stained sections were used to quantify blood vessels in the vicinity of wound and the 'red' color of erythrocytes was quantified. For each sample, more than six high power fields (40x objective) were captured and the quantified area occupied by erythrocytes was expressed as percentage of RBCs.

3.2.5.2.3 Extent of collagen deposition

Images from picro-sirius red stained sections of wound tissue were used to quantify collagen at the site of wound. The sirius red of picro-sirius red preferentially stained

collagen ‘red’ which was quantified. For each sample, more than six high power fields (40x objective) were captured and the collagen was quantified and expressed as percentage.

3.2.5.2.4 Extent of cell proliferation

This was quantified in IHC slides following staining with antibodies against PCNA. The number of PCNA positive cells in the dermis and the total number of cells in the dermis were counted in the field and the density of proliferating cells in dermis was calculated and represented as percentage proliferation using the formulae [Percentage proliferation in dermis = (number of PCNA positive cells in the field/ total number of cells on the line) x 100]. This was repeated for more than six fields of wound tissue.

3.2.5.2.5 Extent of mesenchymal cell response

This was quantified in IHC slides following staining with antibodies against vimentin. The area positive for vimentin was quantified in six high power fields and was expressed as percentage of vimentin /high power field.

3.2.5.2.6 Extent of myofibroblast response

This was studied in IHC slides following staining with antibodies against ASMA. The area positive for ASMA were quantified for six high power fields and was expressed as percentage of ASMA / high power field.

3.2.6 Statistical analysis

Student's t-test was performed to determine the level of significant difference between experimental groups, wherever statistical analysis was necessary. A p-value less than 0.05 was considered to be of significance.

Section III

3.3 Fabrication of prototypes of cell loaded ECM scaffolds.

3.3.1 Culturing of HaCaT cells on the ECM scaffolds

3.3.1.1 List of materials and reagents used

HaCaT cells, Nunc™ Cell Culture Treated T25 Flasks with filter caps, hemocytometer, pipettes, pipette tips, coverslips, sterilized ECM scaffolds, 50ml tubes sterilized, parafilm tapes, Complete HaCaT culture media [containing DMEM (Dulbecco's Modified Eagle's Medium) high glucose medium (10313 - Gibco), Antibiotic-antimycotic 100X solution (15240-062 Gibco), Fetal bovine serum (10082139, Gibco), Glutamate and (G3126 Sigma) solution], PBS, 0.25% Trypsin EDTA solution (25200-056 Gibco), Trypan blue solution (T8154, Sigma), class II biosafety cabinet (Kleanzone, Class A2), All culture incubations were performed in humidified 37°C, 5% CO_2 in water jacketed carbon dioxide incubator (Thermofisher scientific, forma series II), Inverted microscope (Magnus INVI tissue culture Trinocular microscope).

Reagent preparation

Complete HaCaT culture media

DMEM high glucose medium (10313 - Gibco)	47ml
Antibiotic-antimycotic 100X solution (15240-062 Gibco)	500µl
Fetal bovine serum (10082139, Gibco)	2.5 ml
200 nm Glutamate (G3126 Sigma) solution	500µl

The reagents were aseptically mixed in a 50ml tube inside class II biosafety cabinet and the mouth of the 50ml tube was sealed using parafilm tape. The solution remained suitable for use for 5 days under refrigeration in sterile condition.

3.3.1.2 Method

HaCaT cells were purchased from National Center for Cell Science, Pune. The stock culture was trypisinized, counted and seeded on to three different T25 culture flasks. It was flooded with 2 ml complete culture medium for HaCaT cells containing DMEM medium with 10% fetal calf serum, 1% glutamate and 1% antibiotic-antimycotic solution initially for attachment and placed in incubator. Once the cells got attached the medium was removed and 5 ml fresh complete culture medium was added and further incubated. The complete culture medium was changed every other day.

To determine the cell number and viability 10µl of cell suspension was mixed with 40µl of PBS. This was mixed with 50µl of trypan blue and mixed well. 10µl of this solution was mounted on to hemocytometer. The number of cells (Na) was counted by viewing through a microscope. The cell concentration was calculated as Na x Dilution factor x 10^4 and percentage viability of cells were calculated as (Number of unstained cells/total number of cells) x 100. The scaffold was soaked in PBS solution. HaCaT cells in the density 10^5 were seeded on $1cm^2$ of each of the three scaffolds. Medium was changed every other day and the cells were allowed to grow on the scaffold for 10 days.

3.3.1.2.1 Viability of HaCaT on ECM scaffold

3.3.1.2.1.1 List of materials and reagents used

Six well plates, MTT (3-(4,5-dimethylthiazol-2-yl)-2,5-diphenyltetrazolium bromide) powder (M6494, Gibco), Votex (2T shaker 240VAC, Genie) refrigerated centrifugation apparatus (5430R, Eppendoff), extraction solution (0.01 N HCl in isopropanol) and other materials same as in 3.3.1.1.

3.3.1.2.1.2 Method

The cell viability of HaCaT cells growing on different ECM scaffold were analyzed by monitoring the cellular activity of the cells on scaffold using MTT assay on 3, 7 and 10 days. A stock of 2.5mg/ml MTT was made with PBS solution. The cells were seeded on each scaffold of in triplicates at a density of 10^5/ml on a 6 well plate. The scaffold alone and cells alone was used as control. The culture medium was removed on the 3rd, 7th and 10th day, scaffolds were washed with PBS and 3 ml of MTT solution (1 mg/ml in PBS), and incubated for 3 h at 37 °C. 1 ml of extraction solution (0.01 N HCl in isopropanol) was added on to scaffold after their transfer to small tubes. It was then vortexed for 5 minutes and centrifuged for 5 minutes at 12,000 rpm. The color was read at 570 nm. Triplicate values were analyzed for the scaffolds, scaffolds with cells and cells alone to get average and standard deviation.

3.3.1.2.2 Confocal microscopy analysis

3.3.1.2.2.1 List of materials and reagents used

Four well plates, 3% paraformaldehyde, 0.25% Triton X -100, 1% bovine serum albumin, PBS, FITC conjugated phalloidin (P5282, Sigma), DAPI (4',6-diamidino-2-phenylindole) staining solution (D9542, Sigma), antifadent mounting medium, forceps, coverslips .

3.3.1.2.2.2 Method

The tissue constructs produced by growing HaCaT were transferred to 4 well plates, processed for staining with phalloidin FITC conjugate to visualize the actin filaments of the cells on the scaffold. Briefly, the cells were fixed in 3% paraformaldehyde followed by washing with cold PBS. It was then permeabilized using 0.25% Triton X -100, for improving the presentation of antibody, followed by washing with PBS three times. The tissue construct was blocked using 1% BSA in PBS for 30 minutes followed by treatment with FITC conjugated phalloidin (1:20 dilution) for 4 to 5 hours at 37ºC. It was then washed in PBS and counter stained with (0.1µm/ml) DAPI solution, washed with PBS, mounted on a coverslip using antifadent mountant and viewed under confocal microscope (Carl Zeiss, Germany) .

3.3.1.2.3 Histotechnology processing

3.3.1.2.3.1 List materials and reagents used

Same as in section 3.2.2.1

3.3.1.2.3.2 Method

The scaffolds along with the HaCaT cells were fixed in 10% buffered formalin and processed for histotechnology as in section 3.2.2.2

3.3.1.2.4 Histology evaluation

3.3.1.2.4.1 List materials and reagents used

Same as in section 3.2.3.1.1

3.3.1.2.4.2 Method

The sections obtained after histotechnology were stained for H and E as mentioned in section 3.2.3.1.2

3.3.1.2.5 Immunohistochemistry evaluation

3.3.1.2.5.1 Materials and reagents used

Mouse monoclonal IgG primary antibodies for PCNA (PC10, Santa Cruz Biotechnologies, USA), Involucrin (SY5, Ab17105, Abcam, UK), Vitamin D receptors (CHIP Ab3508, Abcam, UK) and other material as in section 3.2.4.1.

3.3.1.2.5.2 Method

Immunostaining was performed on the slides obtained from blocks of all the three tissue construct using the primary antibodies against PCNA, involucrin and Vitamin D receptors on 7th day using similar protocol as in section 3.2.4.2. The details of antibody and dilutions used is given in Table 4

Table 4 List of antibodies used for immunohistochemistry

Sl No	Antibodies	Clone and company	Dilution
1	PCNA	PC10 (Santa Cruz Biotechnologies, USA)	1:400
2	Involucrin	SY5, Ab17105 (Abcam, UK)	1:200
2	Vitamin D receptor	CHIP Ab3508 (Abcam, UK)	1:200

3.3.2 Culturing of fibroblasts on the ECM scaffolds

3.3.2.1 Primary isolation of dermal fibroblasts from rabbit skin

3.3.2.1.1 Culture plate preparation for explants culture

3.3.2.1.1.1 List of materials and reagents used

Thermofisher Nunc Six well plates, pipettes, pipette tips, 1% gelatin solution

3.3.2.1.1.2 Method

One ml of 1% gelatin solution was poured on plates of 6 well and slightly rotated so that the whole surface of the plate was filled with it. It was kept for about 30 minutes in

the biosafety cabinet. The excess solution was pipette out after 30 minutes and the coated tissue culture plates were incubated at 37ºC for 3-5 hours or until use.

3.3.2.1.2 Collection and transportation of specimen

3.3.2.1.2.1 List of materials and reagents used

Sterilized Scalpel, sterilized blade (22), syringe, needle, sterilized blade holder, cotton, sterilized rat toothed forceps, Ethicon suture, trimmer, scissors, gloves, mask, PBS, Ketamine, Xylaxin, 70% alcohol, Transport medium [containing Hank's balanced modified solution (HBSS) (55021C, Sigma) supplemented with 1% antibiotic-antimycotic solution].

Reagent preparation

Transport medium

HBSS buffer	49.5 ml
100X antibiotic-antimycotic solution	500 µl

The above reagents were aseptically mixed in a 50ml tube inside class II biosafety cabinet and the mouth of the 50ml tube was sealed using parafilm tape. The solution remained suitable for use for 5 days under refrigeration in sterile condition.

3.3.2.1.2.2 Method

The rabbit were anaesthetized using Ketamine (80mg/kg body weight) and Xylaxin (5mg /kg body weight). The hair on the rabbit ventral skin was trimmed using a hair trimmer. The remaining hair was completely shaved using a razor blade. Then, the skin was wiped with 70% alcohol for sterilization. When the skin was completely dry, an

approximate size of 1cm x 3cm skin incision was made using a sterile scalpel blade. With the help of surgical scissors and forceps a side of the cut skin is lifted and cut is made in the dermis parallel to the epidermis to remove the required 1cm x 3 cm skin. The wound site was approximated by suturing and it healed completely by two weeks. The excised tissue was collected in transport medium and immediately transported into the laboratory.

3.3.2.1.3 Processing of skin for explant culture

3.3.2.1.3.1 List of materials and reagents used

Coated 6 well plate, sterilized forceps, pipettes, pipette tips, T25 flasks (Nunc, Thermofisher), T75 flasks (Nunc, Thermofisher), hemocytometer, coverslips, gloves, mask, PBS, Complete culture media for dermal fibroblasts (containing DMEM high glucose with pyruvate (11995-073, Gibco) supplemented with antibiotic-antimycotic 100X solution (15240-062, Gibco) and Fetal bovine serum (10082139, Gibco)), , 0.25% Trypsin EDTA solution (25200-056, Gibco), Trypan blue solution (T8154, Sigma), class II biosafety cabinet (Class A2, Kleanzone), Water jacketed carbon dioxide incubator (Thermofisher scientific).

Reagent preparation

Complete culture medium for dermal fibroblasts

DMEM high glucose with pyruvate (11995-073, Gibco)	39.5 ml
Antibiotic-antimycotic 100X solution (15240-062 Gibco)	500 µl
Fetal bovine serum (10082139, Gibco)	10 ml

The above reagents were aseptically mixed in a 50 ml tube inside class II biosafety cabinet and the mouth of the 50 ml tube was sealed using parafilm tape. The solution remains for 5 days under refrigeration in sterile condition. All culture incubations were performed in humidified 37°C, 5% CO_2 incubator.

3.3.2.1.3.2 Method

After repeated cleaning using antibiotic containing PBS buffer, the skin was cut into further smaller pieces with a sharp sterile scalpel blade and fixed on the centre of each gelatin coated plates of a 6 well plate. One drop of complete culture media was placed over it to prevent it from drying. It was kept undisturbed for 30 minutes for attachment of the explants tissue. Two ml of complete culture media for fibroblasts was poured on each well and placed in incubators. After 7-10 days the cells were trypsinized and all the cells from the 6 well plates were pooled and seeded on to a T 25 flask. One third day the T25 was trypsinized and seeded on to a T75 flask. The cells on 3^{rd} or 4^{th} passage were further characterized and taken for the study. To determine the cell number and viability 10 µl of cell suspension was mixed with 40 µl of PBS. This was mixed with 50 µl of trypan blue and mixed well and 10 µl of this solution was mounted on to hemocytometer. The number of cells (Na) was counted by viewing through a microscope. The cell concentration was calculated as Na x Dilution factor x 10^4 and percentage viability of cells were calculated as (No of unstained cells/total number of cells) x 100.

3.3.2.2 Characterization of isolated fibroblasts

3.3.2.2.1 Immunocytochemistry

3.3.2.2.1.1 List of materials and reagents used

Thermofisher Nunc four well plates, coverslips, Methanol: acetone, Serial grades of propyl alcohol (70%, 80%, 90% and 100%), water, Triton X 100, 10% peroxide solution for blocking endoperoxidase activity, TSC as working buffer, 10% goat serum, primary antibodies of prolyl hydroxylase (EPR2745, Abcam) collagen III (COL3a1, Santa Cruz Biotechnologies, USA), vimentin (V9 Dako, Denmark), fibronectin (IST9, Abcam, UK), laminin (LAM-89, Santa Cruz Biotechnologies, USA), ASMA (1A4, Abcam, UK), goat anti mouse Fab'2-Biotin conjugate as secondary antibody (1:400), Streptavidin-HRP conjugate, HRP substrate (Sigma), Harris's Hematoxylin. The details of antibodies and the dilution used are given in Table 5.

Table 5 List of antibodies used for immunophenotyping

Sl No	Antibodies	Clone and company	Dilution
1	Prolyl hydroxylase	EPR2745 (Abcam)	1:400
2	Collagen III	COL3a1 (Santa Cruz Biotechnologies)	1:400
3	Fibronectin	IST9 (Abcam)	1:400
2	Vimentin	V 9 (Dako)	1:200
3	ASMA	1A4 (Abcam)	1:200
2	Laminin α 1	LAM-89, (Santa Cruz Biotechnologies)	1:400

3.3.2.2.1.2 Method

The fibroblasts were seeded and cultured on to four well plates. Immunocytochemistry was performed using primary antibodies for collagen III, vimentin, fibronectin, laminin, ASMA, after 24 hours of incubation. The cells on 4 well plates were fixed using cold acetone methanol and immunostaining was performed as mentioned in section 3.2.4.2.

3.3.2.2.2 Flow cytometry

3.3.2.2.2.1 List of materials and reagents used

T25 flask confluent with cells, 15 ml culture tubes, centrifuge, flow cytometer (FACS ARIA, BD Biosciences, San Jose, CA, USA), BD FACS Diva software (BD Biosciences, San Jose, CA, USA), PBS, 0.25% Trypsin-EDTA, 3.7% formaldehyde, Triton X-100, 1% bovine serum albumin, antibodies against vimentin, FITC-conjugated secondary antibody.

3.3.2.2.2.2 Method

Fibroblasts from a confluent T 25 flask were harvested after trypsinization (0.25% Trypsin-EDTA for 3 minutes). It was then washed with PBS and fixed with 3.7% formaldehyde in PBS for 20 minutes, again washed with PBS, and permeated with Triton X-100 (0.1%) in PBS for 5 minutes. The cells were blocked with 1% bovine serum albumin (Sigma-Aldrich, St. Louis, MO, USA) in PBS for 30 minutes and incubated with antibodies against vimentin (1:100) antibody for 2 hours. The cells were washed and treated with FITC-conjugated secondary antibody (1:200) for 1 hour. After

the staining procedure, the cells were washed in PBS and analyzed by using a flow cytometer (FACS ARIA, BD Biosciences, San Jose, CA, USA). The percentage of vimentin-expressed cells was calculated by using BD FACS Diva software (BD Biosciences, San Jose, CA, USA).

3.3.2.3 Viability of dermal fibroblast on ECM scaffold

3.3.2.3.1 List of materials and reagents used

Same as in section 3.3.1.2.1.1

3.3.2.3.2 Method

The scaffold was immersed in PBS solution. The fibroblasts of second passage were seeded on $1cm^2$ of the three scaffold at a concentration of 10^5/ml. Medium was changed every other day and the cells were allowed to grow on the scaffold. The cell proliferation of dermal fibroblasts growing on different ECM scaffold was analyzed by monitoring the cellular activity of the cells on scaffold using MTT assay on 3, 7 and 10 days as mentioned in section 3.3.1.2.1.2

3.3.2.4 Cell attachment on ECM scaffolds

3.3.2.4.1 List of materials and reagents used

Coated 6 well plate, sterilized forceps, pipettes, pipette tips, T25 flasks (Nunc Thermofisher), T75 flasks (Nunc Thermofisher), hemocytometer, coverslips, gloves, mask, PBS, Complete culture media for dermal fibroblasts (containing DMEM high

glucose with pyruvate (11995-073, Gibco) supplemented with antibiotic-antimycotic 100X solution (15240-062 Gibco) and Fetal bovine serum (10082139, Gibco)), 0.25% Trypsin EDTA solution (25200-056 Gibco), Trypan blue solution (T8154, Sigma), class II biosafety cabinet (Class A2, Kleanzone), Water jacketed carbon dioxide incubator (Thermofisher scientific). All culture incubations were performed in humidified 37°C, 5% carbon dioxide incubator, gold coating apparatus, scanning electron microscope (Hitachi, Model S-2400, Japan).

3.3.2.4.2 Method

The scaffold was immersed in PBS solution. The fibroblasts of second passage were seeded on $1cm^2$ of the three scaffold at a concentration of 10^5/ml. Medium was changed every other day and the cells were allowed to grow on the scaffold for 3 days. This was used for scanning electron microscopy as mentioned in section 3.1.2.2.2

3.3.2.5 Fibroblast loaded CDS construct

3.3.2.5.1 List of materials and reagents used

Same as in section 3.3.1.2.2.1

3.3.2.5.2 Method

The fibroblasts from third passage were seeded on $1cm^2$ of the CDS scaffold at a concentration of 10^5/ml. Medium was changed every other day and the cells were allowed to grow on the scaffold for two days. The tissue construct was fixed in

glutaraldehyde and proceeded for confocal scanning microscopy on 3rd day as mentioned in 3.3.1.2.2.2.

3.3.3 Statistical analysis

Student's t-test was performed to determine the level of significant difference between experimental groups, wherever statistical analysis was necessary. A p-value less than 0.05 was considered to be of significance.

Section IV

4.4 *In vivo* evaluation of wound healing by homologous fibroblast loaded CDS scaffold in full thickness burn model

3.4.1 Fabrication of burn making device

3.4.1.1 List of materials used

Soldiering station of 230 V and 50W (Model Signetic-DSD), 1cm x 1cm brass template fabricated.

3.4.1.2 Method

A device for inducing burn wound was fabricated by slightly modifying a (Model Signetic-DSD) soldiering station. A 1cm x 1 cm brass template was connected to the nozzle of the soldiering station. The temperature was controlled using the temperature control knob and the actual temperature was displayed on the screen. The temperature knob as well as the display was set at 180ºC. Accordingly, the brass template also got heated up at the temperature displayed on the screen. Burns were induced on the rabbit dorsum by keeping the heated template on the dorsum. The burn wound obtained in rabbit model by this device was excised, fixed in 10% neutral buffered formalin, processed for histology and histomorphometry to confirm whether the burns were of uniform size.

3.4.2 Tagging of dermal fibroblast and seeding on CDS scaffold

3.4.2.1 List of materials and reagents used

Culture tubes (15 ml), propylene vials, T75 confluent dermal fibroblasts, sterilized CDS scaffolds, refrigerated centrifugation apparatus (5430R, Eppendoff), Diluent C solution (G-8278, Sigma), PKH26 dye (PKH Mini26-1, Sigma), Fetal bovine serum, Complete

culture medium for dermal fibroblasts without serum, complete culture medium for dermal fibroblasts.

3.4.2.2 Method

The cells from two T75 flasks (4^{th} passage) was trypsinized and used for animal experiment. The concentrations of fibroblasts were adjusted to $2X10^7$ cells and were washed in medium (without serum) in a conical bottom propylene tube for removing residual serum. The pellet was re-suspended in 1ml Diluent C solution and mixed well, followed by mixing with the staining solution (4µl PKH26 dye in 1ml Diluents C). The vial was incubated at 37ºC for 2 minutes, followed by addition of 2ml serum to stop the staining reaction. It was allowed to stand for 1 minute and the cells were re-suspended in 2 ml of complete serum containing medium after washing the cells to remove excess unbound dye. The final concentration of cells was 10^7/ml for seeding on to CDS scaffold. Scaffolds of 1cm x 1cm were seeded with 1ml of cell suspension in a 4 well plate and incubated for 30 minutes for cells attachment. The presence of PKH26 stained cells in the CDS scaffold were confirmed using confocal microscopy and viability confirmed by live dead assay. Tagging of dermal fibroblast with PKH26 was thus performed and it was seeded on the CDS scaffolds at a density of more than 10^6 cells. This tissue construct was termed as homologous fibroblast loaded CDS (HFCDS).

3.4.3 Full thickness burn wound experiment in rabbit model

3.4.3.1 List of materials and reagents used

Burn making device, other materials same as mentioned in 3.2.1.1

3.4.3.2 Method

Nine healthy rabbits of more than two kg body weight were randomly assigned into three groups of three each. The animal experiments were done with the approval and as per requirements of the Institutional Animal Ethics Committee. Prior to the experiment, fur on either side of the spine was clipped off. Rabbits were anaesthetised using Ketamine (80mg/kg body weight) and Xylaxin (5mg/kg body weight). The skin of the anaesthetised rabbits were lightly swabbed using 70% alcohol and air dried. Third degree burn wounds were induced on the dorsum of each rabbit using the burn making device by pressing the 1x1 cm^2 brass template of soldering station for 45 seconds at 180ºC. The HFCDS graft and non cell loaded CDS grafts were grafted on full thickness cutaneous burn wounds of one cm^2 made dorsally (N=3). The third wound was left open and served as the control. At the end of each experimental period (7, 14 and 28 days), 3 rabbits were euthanized by carbon dioxide inhalation and samples were collected from the wound site for histomorphology and histomorphometry evaluations. At the end of the animal experiment, the skin graft along with the surrounding normal skin was collected and fixed in 10% neutral buffered formalin. The fixed tissue samples were dehydrated through ascending grades of alcohol, cleared in xylene and impregnated

with paraffin wax. Tissue sections of 4 μm thickness were made from paraffin tissue blocks using Leica RM2255^{TM} Microtome.

3.4.4 Histology and histomorphology

3.4.4.1 H and E staining

Same as in Section 3.2.3.1

3.4.4.2 Masson's Trichrome staining

3.4.4.2.1 List of materials and regents used

Xylene, serial grades of propyl alcohol (70%, 80%, 90% and 100%), water, Bouin's fixative, Weigert's iron Hematoxylin (C.I.75290, SD Fine Chemicals Ltd) staining solution, Acid fuchsin (C.I.42685, SD Fine Chemicals) staining solution, 5% phosphomolybdic acid solution, 1% acetic acid solution, aniline blue solution (C.I.42775, Loba Chemi), DPX mountant.

Reagent preparation

1. Bouin's Fixative

Saturated picric acid	150 ml
Formaldehyde	50 ml
Glacial acetic acid	10 ml

The above reagents were mixed well. It was stable for 2 years.

2. Acid fuchsin staining solution

Acid fuchsin	0.5 g

Distilled water	100.0 ml
Glacial acetic acid	1.0 ml

The acid fuchsin was added to distilled water, followed by addition of glacial acetic acid. The solution was mixed well and it remained stable for 6 months.

3. Phosphomolybdic acid Solution:

Phosphomolybdic acid	5 ml
Distilled water	95 ml

The above reagents were mixed well. The solution was stable for 6 months.

4. Aniline blue staining solution:

Aniline blue	2.5 g
Distilled water	100 ml
Glacial acetic acid	1 ml

The aniline blue was added to distilled water followed by addition of glacial acetic acid. The solution was mixed well and it remained stable for 6 months.

3.4.4.2.2 Method

The sections on slides were dewaxed in three changes of xylene, dehydrated using serial grades of propyl alcohol (70%, 80%, 90% and 100%) and fixed in Bouin's solution overnight at 37ºC. It was washed in running tap water to remove the yellow color of secondary fixative. It was treated with Weigert's iron Hematoxylin staining solution for 20 minutes, washed in running water for 5 minutes, followed by staining in acid fucshin staining solution for 5 minutes. It was rinsed with water and treated with 5% phosphomolybdic acid solution. It was directly transferred to aniline blue solution for

20 seconds and rinsed acidized water (1% acetic acid), followed by dehydration, clearing and mounting.

3.4.4.3 Herovici staining

3.4.4. 3.1 List of materials and regents used

Xylene, serial grades of propyl alcohol (70%, 80%, 90% and 100%) water, Herovici staining solution, Weigert's iron Hematoxylin (C.I.75290, SD Fine Chemicals Ltd) staining solution, 1% acetic acid solution, DPX mountant.

Reagent preparation

1. Herovici staining solution

Van Gieson’s stain	50ml
Methyl blue (0.05%) aqueous	50ml
Glycerol	10ml
Lithium carbonate, saturated aqueous	0.5ml

The above reagents were mixed well and used freshly for staining.

2. van Gieson's stain

Picric acid sat. aqueous	100ml
Acid fuchsin 1% aqueous	100ml

The above reagents were mixed well and kept refrigerated until use. The staining solution is stable for 6 months.

3.4.4.3.2 Method

The sections on slides were dewaxed in three changes of xylene, dehydrated using serial grades of propyl alcohol (70%, 80%, 90% and 100%) and washed in running water. It was treated with Weigert's iron Hematoxylin staining solution for 20 minutes, washed in running water for 5 minutes, followed by staining in Herovici staining solution for 2 minutes. It was rinsed acidized water (1% Acetic acid), followed by dehydration, clearing and mounting.

3.4.4.4 Immunohistochemistry

Same as in section 3.2.4

3.4.4.5 Histomorphometry and immunohistomorphometry

The following wound healing parameters were studied using histomorphometry as described in section 3.2.5

3.4.4.5.1 Thickness of epidermis

This was quantified in H and E stained section. The images of neo-epidermis were taken and thickness of newly formed epidermis was measured. This was repeated for more than 7 high power field of the wound tissue.

3.4.4.5.2 Extent of re-epithelialization

Re-epithelialization was quantified in H and E stained sections in low power field (4 x objectives). The length of the original wound and non-epithelialized wound length were

measured and percentage of re-epithelialization was calculated by the formula [Percentage re-epithelialization = (length of epithelialized wound / length of total wound) x 100]. The same was repeated for each wound site and percentage of re-epithelialization was determined.

3.4.4.5.3 Extent of neo-vascularization

Neo-vascularization in the vicinity of the wound was quantified in Masson's trichrome stained sections by identifying blood vessels containing red blood cells (RBC). For each wound site, 7 high power field were taken (high power objective, 40x) with all other microscope settings kept constant. The area with color intensity similar to RBCs within the newly formed blood vessels was quantified, and the percentage was calculated.

3.4.4.5.4 Extent of collagen deposition

Collagen at the wound site was quantified morphometrically in Masson's trichrome stained sections of wound tissue. The collagen appears blue in color and this blue colored area was quantified for each wound site. More than 7 high power field were taken (high power objective, 40x) for each sample and percentage of collagenous area was calculated.

3.4.4.5.5 Collagen remodeling

This was quantified morphometrically in Herovici-stained tissue sections. With this staining procedure, the type I collagen stained red while the type III collagen stained

blue in colour. Each of these was determined by area morphometry and the ratio of type I to type III collagen was calculated.

3.4.4.5.6 Extent of cell proliferation

This was quantified in IHC slides following staining with PCNA antibodies. The number of PCNA positive cells in the dermis and the total number of cells in the dermis were counted in the field and the density of proliferating cells in dermis was calculated and represented as percentage proliferation using the formulae [Percentage proliferation in dermis = (number of PCNA positive cells in the field/ total number of cells on the line) x 100].

3.4.4.5.7 Extent of myofibroblast response

This was quantified in IHC slides following staining with vimentin antibodies. The area positive for vimentin was quantified and expressed as percentage of vimentin-stained area/high power field.

3.4.4.6 *In vivo* imaging and cryosectioning

3.4.4.6.1 List of materials and reagents used

Forceps, PBS buffer, mountant, cryostat (Leica, CM 3050S), confocal microscope (Carl Zeiss, Germany), optical imaging system (Xenogen IVIS *in vivo* imaging system), tissue freezing medium (Leica, 3808609E)

3.4.4.6.2 Method

This was done to track the cells tagged with PKH 26 dye loaded on the CDS healing skin. The whole skin was excised and viewed for *in vivo* imaging. *In vivo* optical imaging was performed by the Xenogen ivis *in vivo* optical imaging system having excitation filters in the range 430-780 nm and emission filters in the range 500-800 nm. The dermis region showing PKH26 signal was sectioned using cryostat and scanned under confocal scanning microscope.

3.4.5 Statistical analysis

Student's t-test was performed to determine the level of significant difference between experimental groups, wherever statistical analysis was necessary. A p-value less than 0.05 was considered to be of significance.

Chapter 4

Results

Section I

4.1 Fabrication and evaluation of tissue engineering scaffolds from ECM of porcine organs for skin tissue engineering

4.1.1 Fabrication of tissue engineering scaffolds.

The gross appearance of the acellular scaffolds prepared from gall bladder or cholecyst, small intestine or jejunum and urinary bladder is shown in Figure 1 and the various features of the scaffolds are summarized in Table 6.

Table 6 Features of the fabricated acellular grafts

Scaffolds	CDS	JDS	UDS
Color	Greenish yellow	Ivory white	Creamy
Thickness (mm)	0.095±.04	0.134±0.028	0.118±0.0451

4.1.2 Evaluation of physical properties

4.1.2.1 Scanning electron microscopy

The scanning electron microscopy revealed a fibrous porous surface morphology for all the three grafts as seen in Figure 2.

4.1.2.2 Fluid uptake

After one hour itself all the scaffolds showed more than 100% fluid uptake. There was no significant difference in the pattern of fluid uptake between the scaffolds (Figure 3).

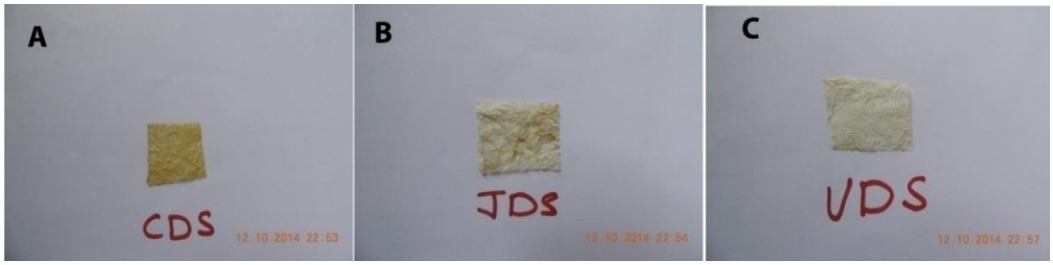

Figure 1: Tissue engineering scaffolds: CDS derived from porcine cholecyst (A), JDS derived from jejunum (B) and UDS derived from urinary bladder (C).

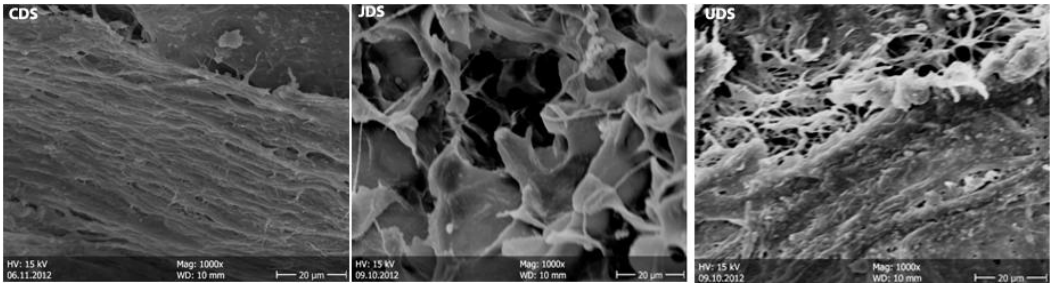

Figure 2 Scanning electron micrograms of the scaffolds

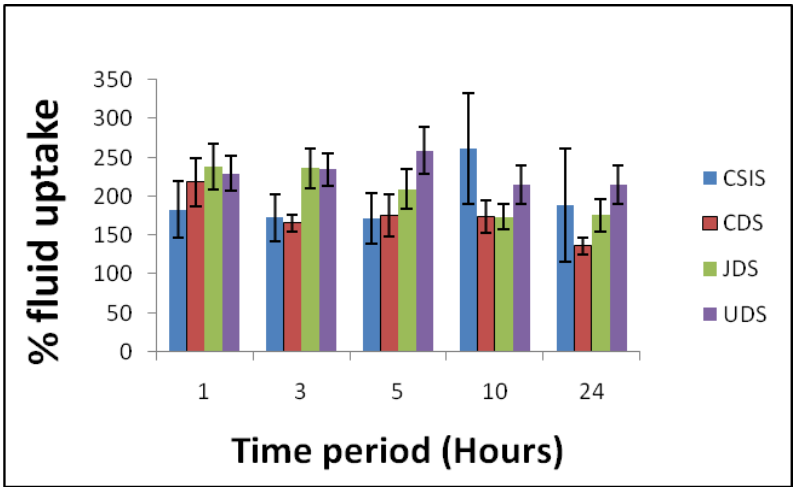

Figure 3 Fluid uptake by the scaffolds

4.1.2.3 Water vapor transmission rate (WVTR)

The WVTR of CDS was significantly lower compared to CSIS (p value = 0.03), JDS (p value = 0.001) and UDS (p value = 0.01) (Figure 4).

4.1.2.4 Mechanical strength

4.1.2.4.1 Young's modulus

The Young's modulus of CDS was similar to the reference material while that of the other scaffolds were significantly lower than the reference material (Figure 5). However, the Young's modulus of CSIS was significantly higher than JDS (p value = 0.0006) and UDS (p value = 0.0004).

4.1.2.4.2 Flexural rigidity

The flexural rigidity of CDS was similar to the reference material (Figure 6). The flexural rigidity of UDS was significantly lower compared to JDS (p value =0.0008), CDS (p value =0.02) and CSIS (p value =0.02). The flexural rigidity of JDS was significantly higher compared to the reference material (p value = 0.04).

4.1.2.4.3 Suture retention strength

The suture retention of the CSIS, CDS, JDS and UDS were 6±2 N, 2±1 N, 6±2 N and 3±2 N respectively. The CDS had the least suture retention strength compared to CSIS and JDS (Figure 7). It was significantly lower compared to CSIS (p value = 0.003) and JDS (p value = 0.001).

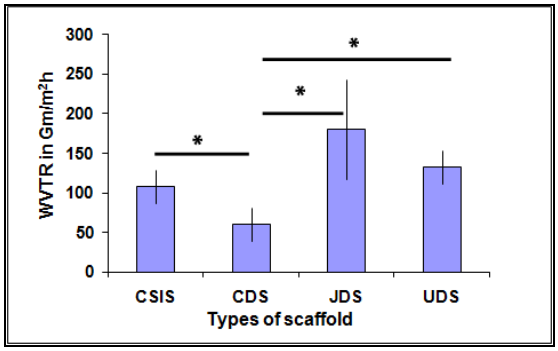

Figure 4 WVTR of the scaffolds (* p value < 0.05)

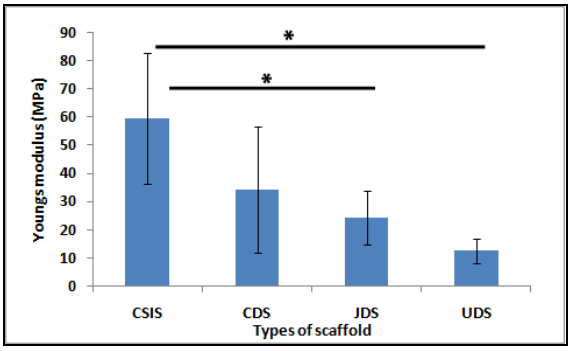

Figure 5 Mechanical strength of the scaffolds (* p value < 0.05)

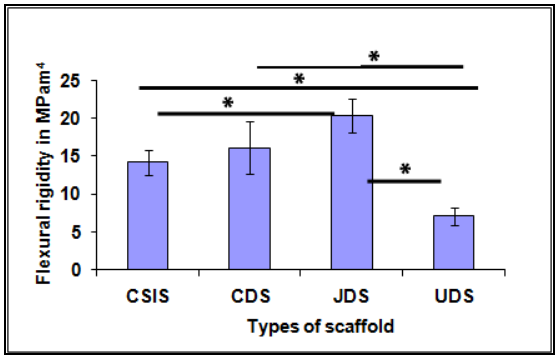

Figure 6 Flexural rigidity of the scaffolds (* p value < 0.05)

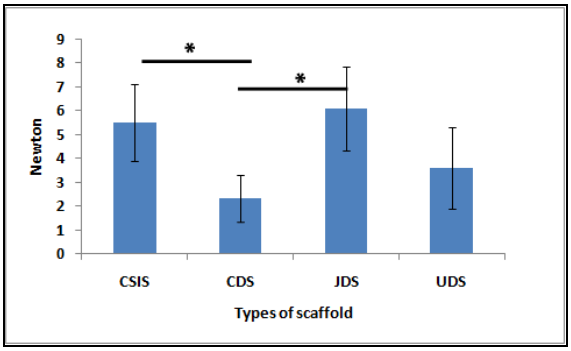

Figure 7 Suture retention strength of the scaffolds (* p value < 0.05)

4.1.3 Evaluation of biomolecules and nuclear content

4.1.3.1 Detection of desirable proteins

The immunofluorescence staining with antibodies to laminin, collagen IV and collagen VII antibodies followed by treatment with secondary antibodies conjugated with FITC showed the presence of these linker proteins in the scaffolds. The relative intensity of

fluorescence for all the linker proteins – laminin, collagen IV and collagen VII was much higher in the CDS compared to both JDS and UDS (Figure 8).

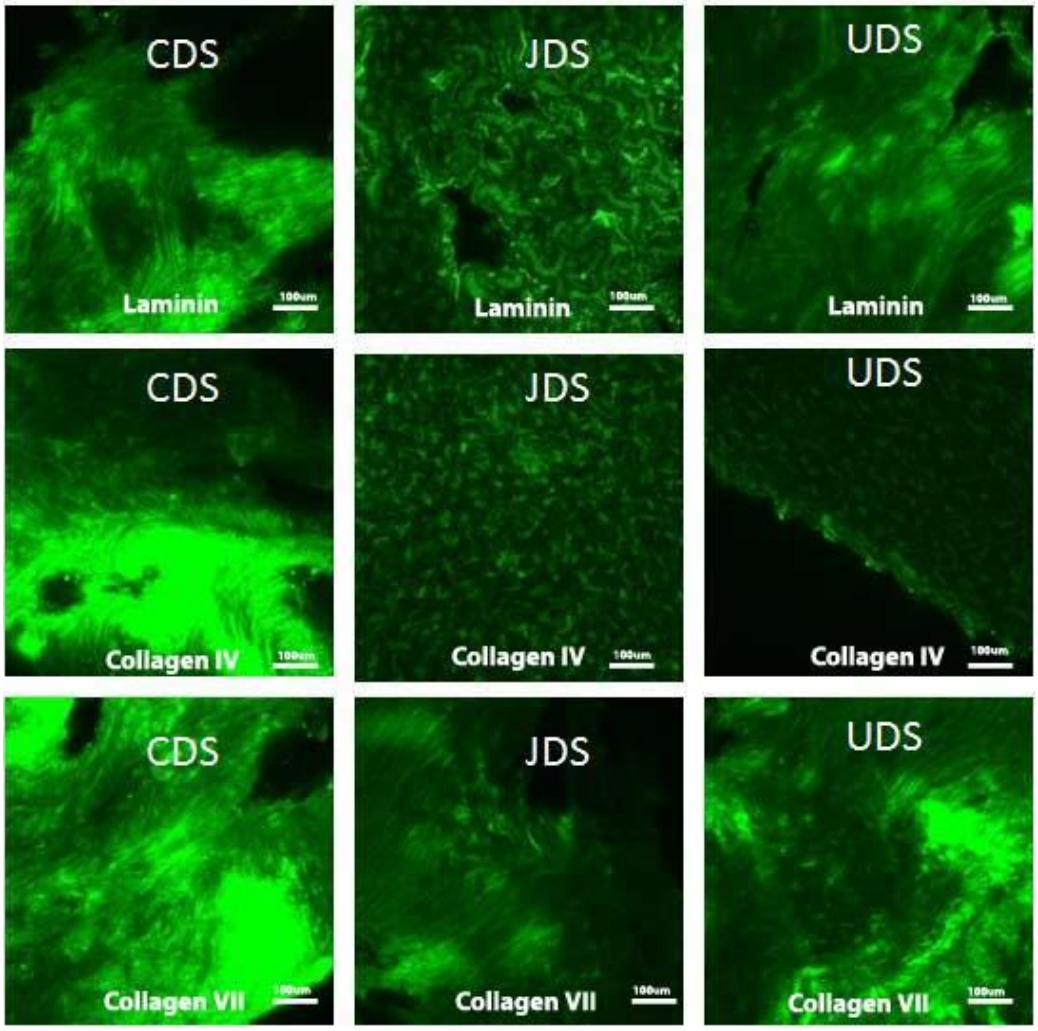

Figure 8 Presence of desirable linker proteins in the scaffolds

4.1.3.2 Quantification of major biomolecules

There was no significant difference between JDS and UDS in their collagen, elastin and GAG content. The amount of collagen content was also similar in CDS and CSIS but the elastin (p value = 0.001) and GAG (p value = 0.03) contents in the CDS were

significantly higher than in CSIS (Figure 9). The elastin content was higher in CDS compared to JDS (p value =0.01). The elastin content in CSIS was lower compared to JDS (p value = 0.001) and UDS (p value = 0.002) also.

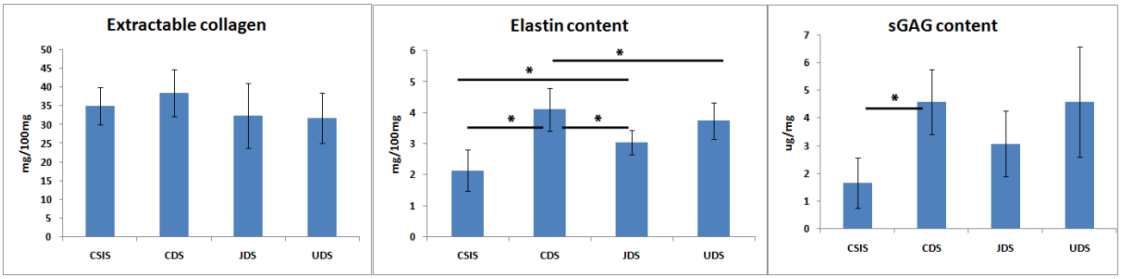

Figure 9 Biomolecules in the scaffolds: (* p value < 0.05)

4.1.3.3 Quantification of DNA content

The DNA content in CDS was much lower (p value = 0.03) than in the reference material. There was no significant difference between JDE and UDE grafts in their DNA content (Figure 10).

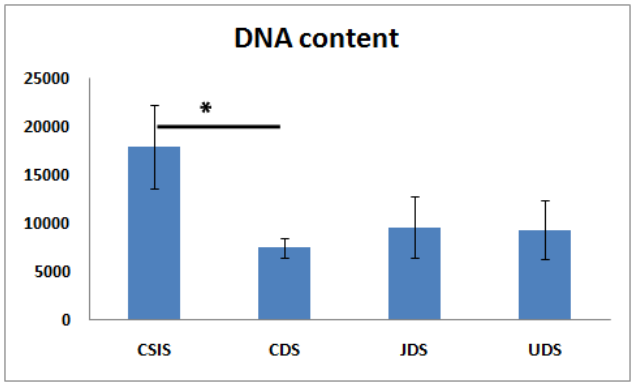

Figure 10 DNA content in the scaffolds (* p value < 0.05)

Section II

4.2 *In vivo* evaluation of the CDS, JDS, UDS and CSIS for wound healing application.

4.2.1 Animal experiment

The overall condition of all experimental animals remained satisfactory throughout the period of experiment and all the animals showed good progressive healing response as shown in Figure 11 and 12. There was no gross evidence of infection or necrosis in the grafted wound tissue retrieved.

4.2.1.1 *In vivo* animal Experiment 1

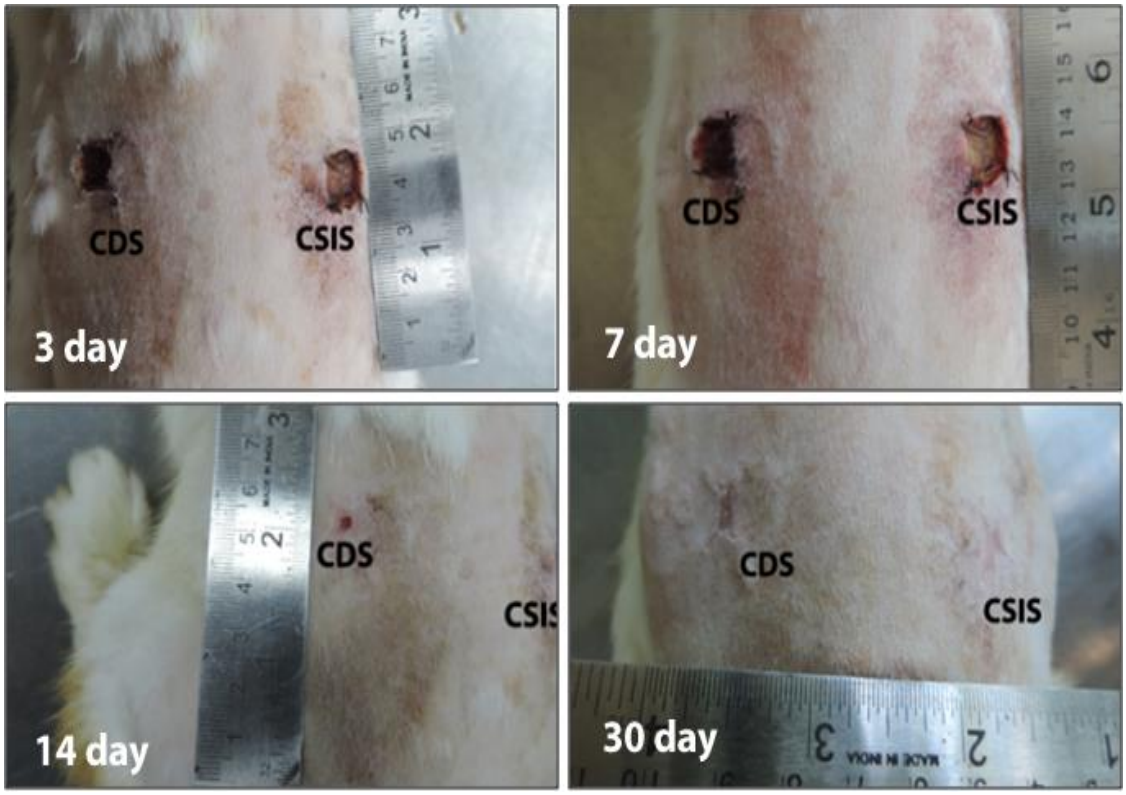

Figure 11 Healing progresses of CDS and CSIS grafted wounds

4.2.1.2 *In vivo* animal Experiment II

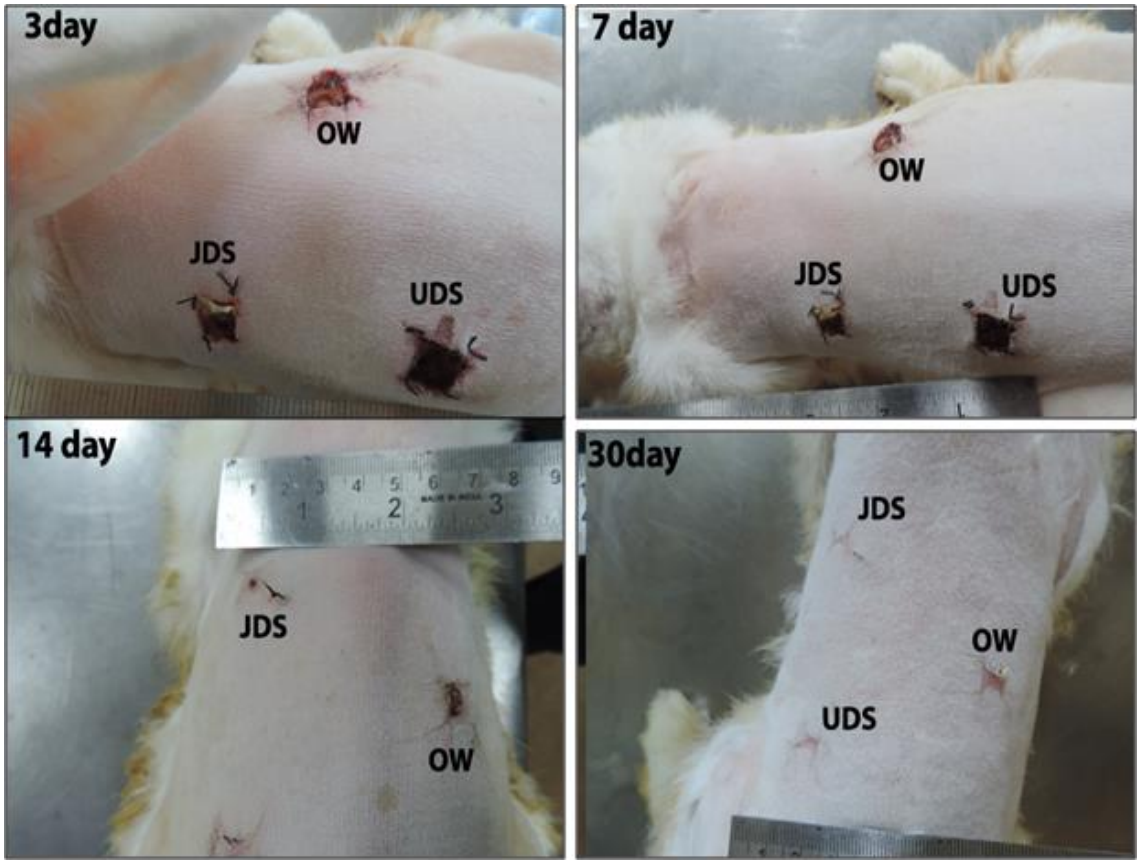

Figure 12 Healing progresses of JDS and UDS grafted wounds

4.2.2 Histomorphology and histochemistry

When evaluated by light microscopy on H and E and picro-sirius red stained histology sections, all the wounds appeared to have progressive healing reaction over time evidenced by the extent of re-epithelialisation, granulation tissue formation, angiogenesis and collagen deposition/remodelling as expected for skin-wound healing by second intention.

4.2.2.1 H and E staining

4.2.2.1.1 H and E staining in Experiment 1

The CDS and CSIS grafted wounds (Figure 13) healed by complete re-epithelialization and granulation tissue formation. On 3rd day, the CDS and CSIS grafts were present over the healing wound tissue. The neo-epithelium though present was not yet complete. The granulation tissue included scattered collagen fibers and newly forming blood vessels (A and B). On 14th day (C and D), the rete pegs and ridges (arrow) was seen in both groups. The epidermis was thicker and the granulation tissue occupied a large part of the dermis (E and F). On the 30th day (G and H), there was formation of complete epidermis with a few rete pegs and ridges. The dermis was also well developed with newly formed blood vessels and well organized collagen fibers.

4.2.2.1.2 H and E staining in Experiment II

In the JDS and UDS grafted wounds and open control (Figure 14), on the 3rd day (A, B and C), there was some evidence of re-epithelialisation. On the 7th day (D, E and F), there was significant re-epithelialisation in all the wounds. On the 14th day (G, H and I), there was complete formation of neo-epithelium in the epidermis at least in one sample in all the three groups. By 30 days (J, K and L), all the wounds healed completely with the deposition of well organized collagen fibres in the neo dermis beneath the neo epidermis. Rete pegs and ridges were evident in the epidermis in both 14th and 30th days providing evidence for complete healing.

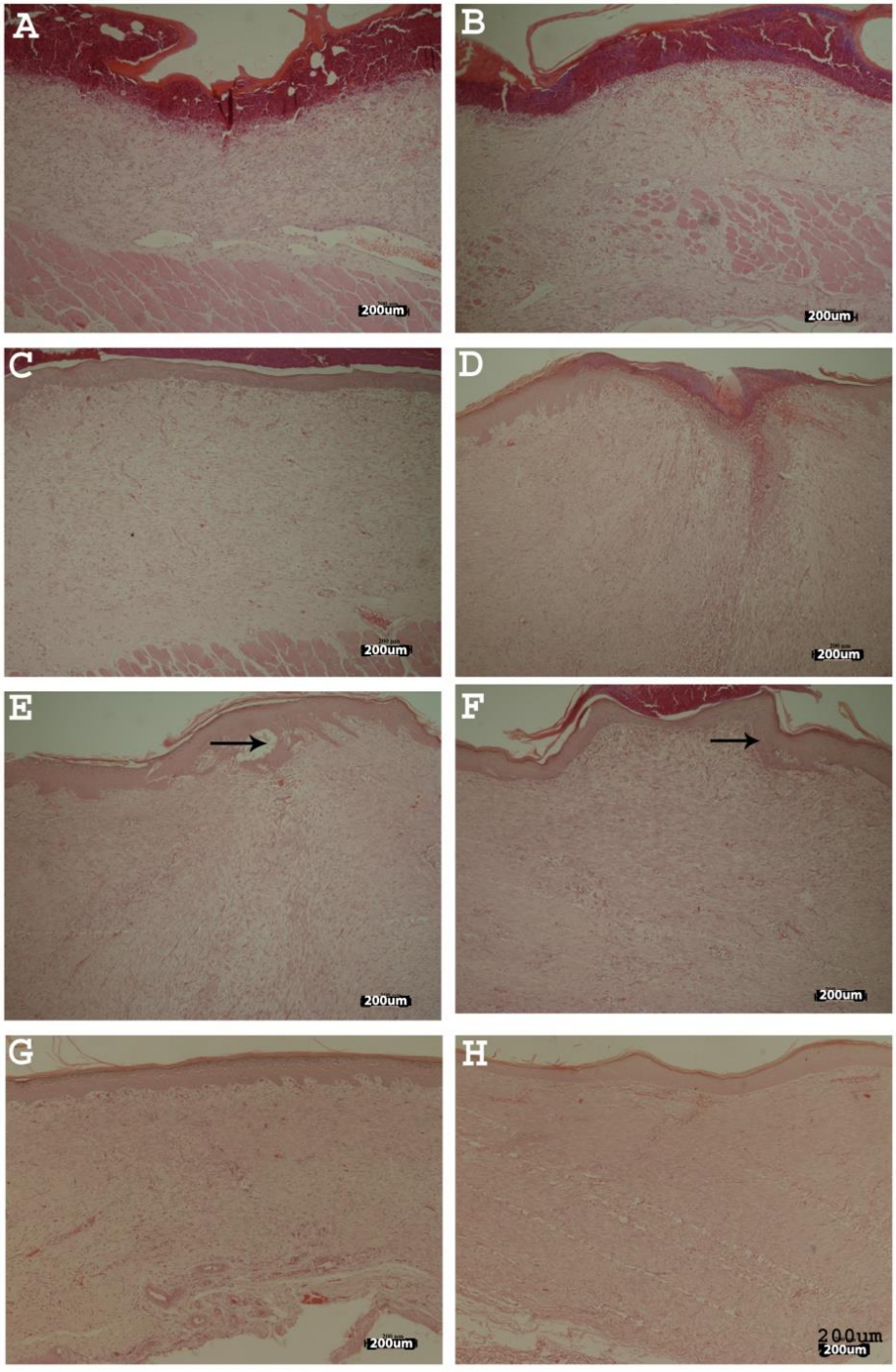

Figure 13 H and E staining of CDS (A, C, E and G) and CSIS (B, D, F and H) grafted wounds (10x); 3rd (A and B), 7th (C and D), 14th (E and F) and 30th (G and H) day.

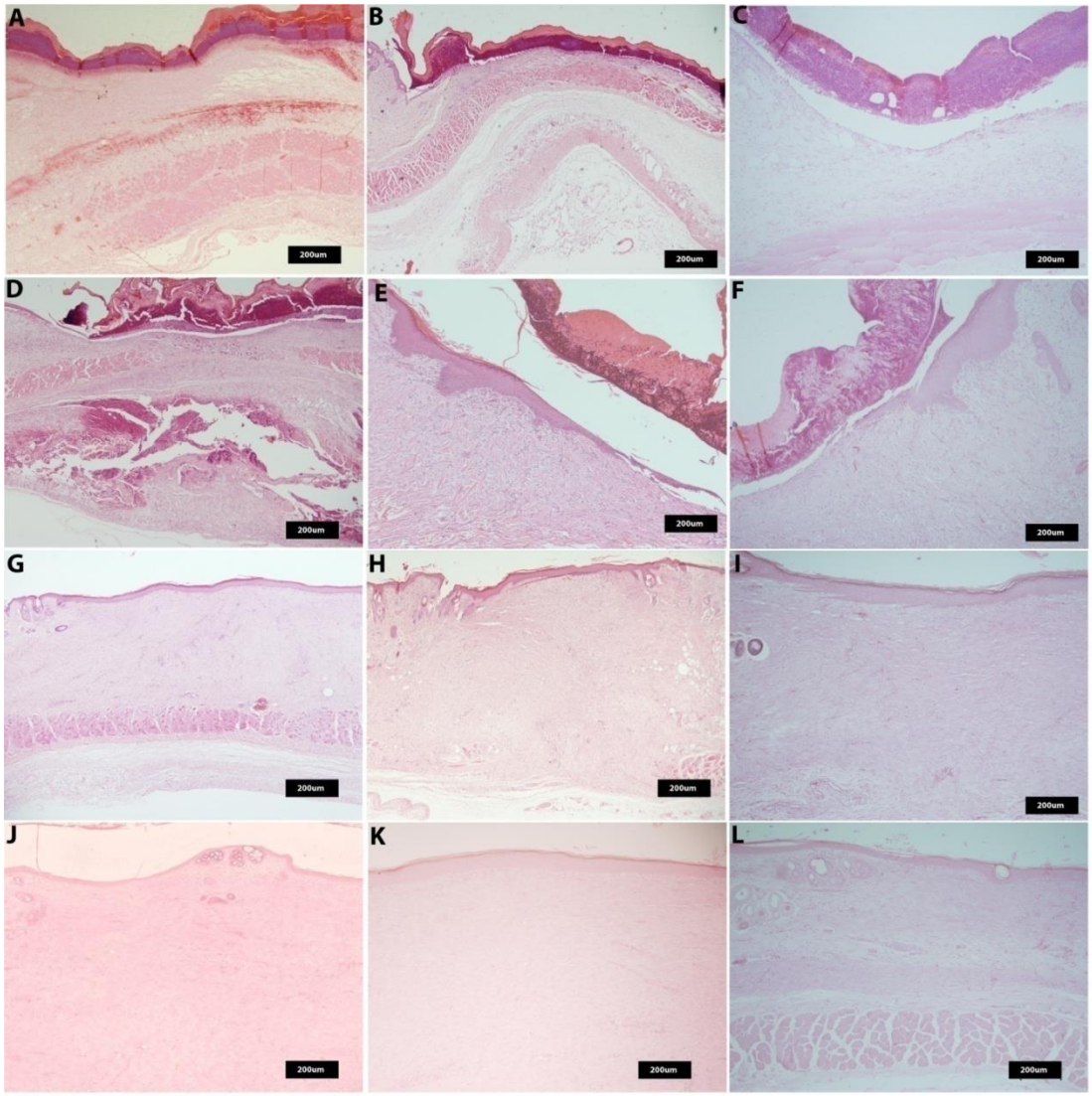

Figure 14 H and E staining in JDS (A, D, G and J) and UDS (B, E, H and K) grafted and open (C, F, I and L) wounds (10x); 3rd (A, B and C), 7th (D, E and F), 14th (G, H and I) and 30th (J, K and L) day

In the dermis (Figure 15) of the JDS and UDS grafted wound and the open wound (OW), significant granulation tissue formation with neovascularisation was apparent as early as 3 days (A, B and C) and subsequently by 7th day (D, E and F) and 14th day (H, I and J) significant fibroblast proliferation with collagen deposition was evident. The

angiogenesis was more in JDS treated wound compared to UDS treated and OW during 3rd day but, there was no significant difference between the OW and graft assisted wound on day 7. During the later time periods of the study by 14 and 30 (J, K &L) days, the blood vessels were more defined and organized compared to early time periods.

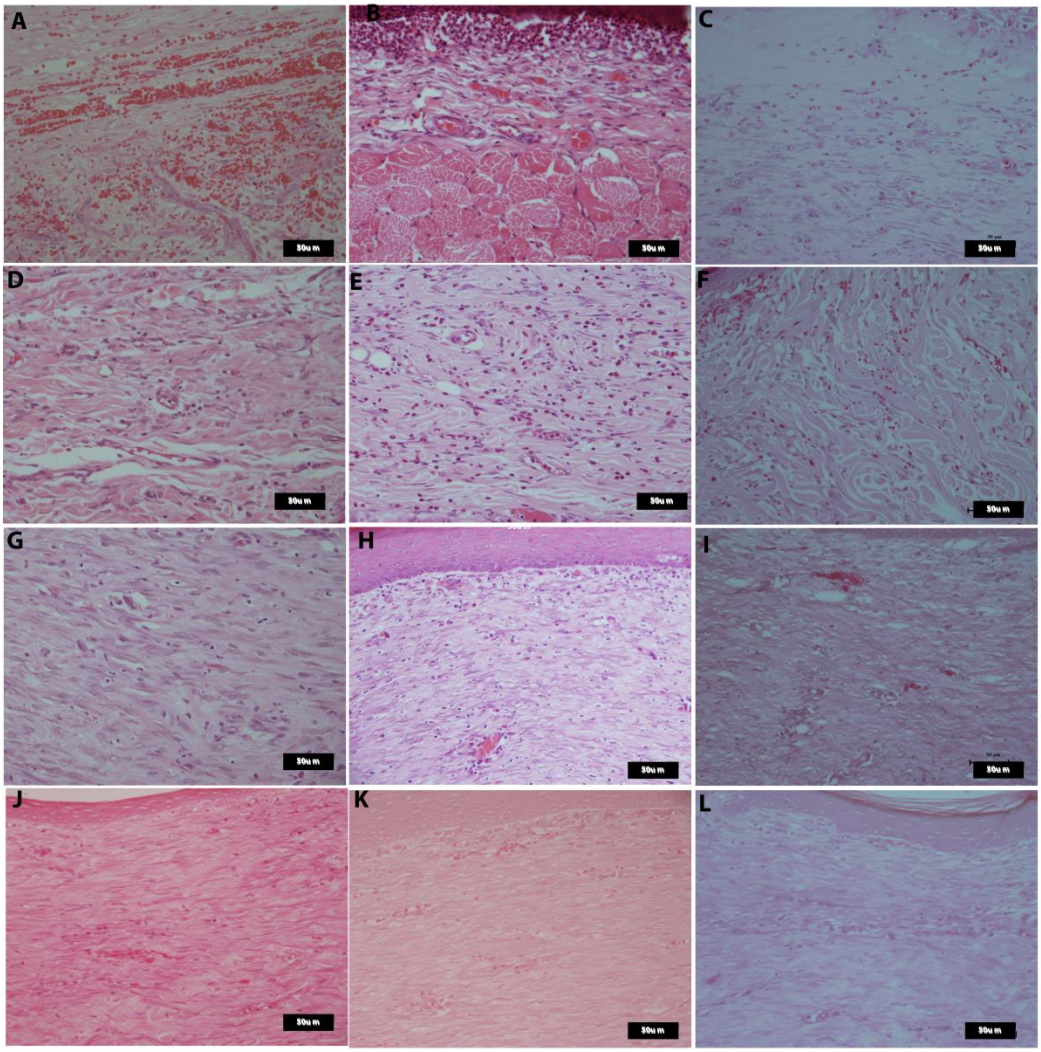

Figure 15 H and E staining in JDS (A, D, G and J) and UDS (B, E, H and K) grafted and open (C, F, I and L) wounds (40x); 3rd (A, B and C), 7th (D, E and F), 14th (G, H and I) and 30th (J, K and L) day

4.2.2.2. Picro-sirius red staining

The collagen fibers stain red color following picro-sirius red staining. This staining facilitated the quantitative assessment of collagen fiber orientation in the healing wound. The orientation of collagen fibers varied with the stages of healing. Generally, the fibers were denser, patchy and appeared in clusters during initial stages of healing but the fibers underwent elongation during the later wound healing phases.

4.2.2.2.1 Picro-sirius red staining in Experiment I

In the CDS and CSIS grafted wounds (Figure 16), collagen deposition increased from 3 to 7 days. On 14 days (E and F) and 30 days (G and H), the collagen fibers were elongated and closely arranged (star) compared to 3 (A and B) and 7 days (C and D) where collagen fibers are seen as bundles and patchy (arrow).

4.2.2.2.2. Picro-sirius red staining in Experiment II

The remodelling occurring during wound healing process was evident from the pattern of collagen deposition in JDS and UDS grafted wounds and in the OW (Figure 17). A progressive change occurred in the organization of collagen fibres from patchy thick collagen bundles in the early time periods of 3^{rd} (A, B and C) and 7^{th} day (D, E and F) to long, slender and thin strands of collagen fibres signifying the remodelled form during the later time periods of 14^{th} (G, H and I) and 30^{th} (J, K and L) days.

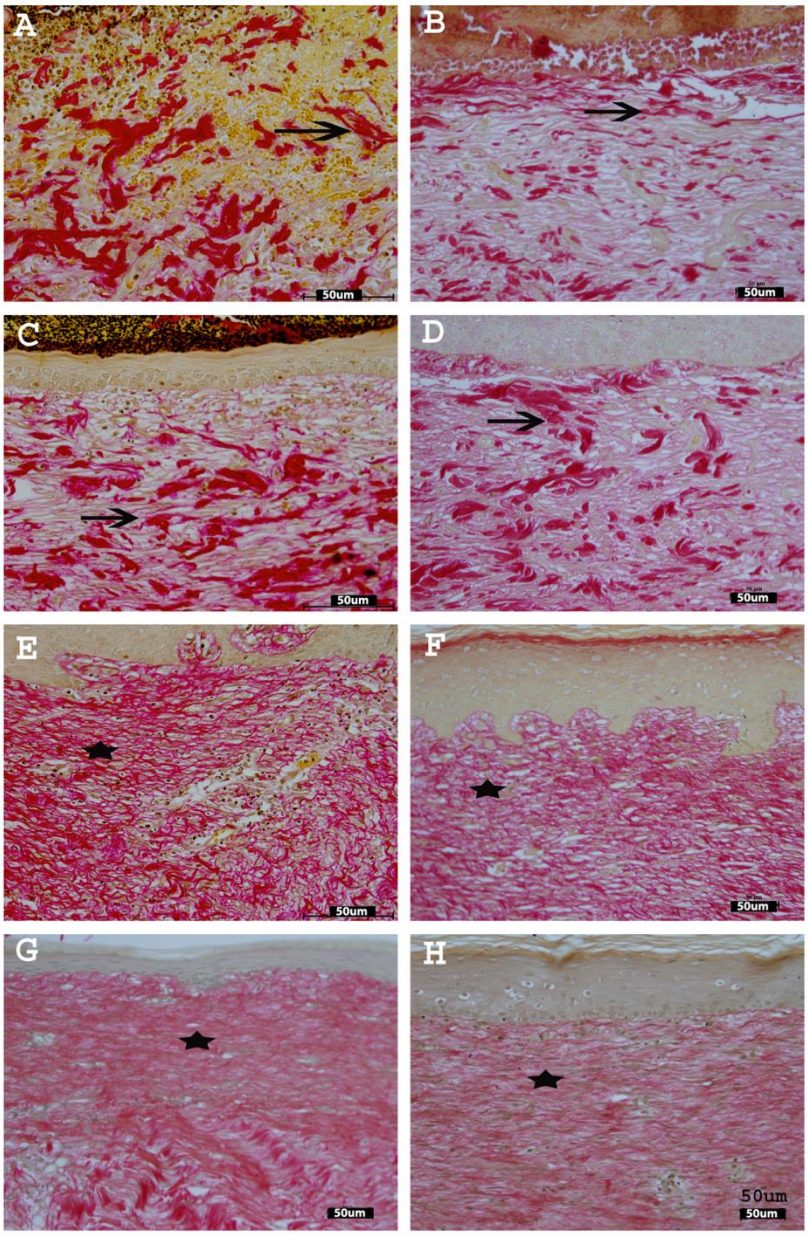

Figure 16 Picro-sirius red staining on CDS (A, C, E and G) and CSIS (B, D, F and H) grafted wounds (40x); 3rd (A and B), 7th (C and D), 14th (E and F) and 30th (G and H) day

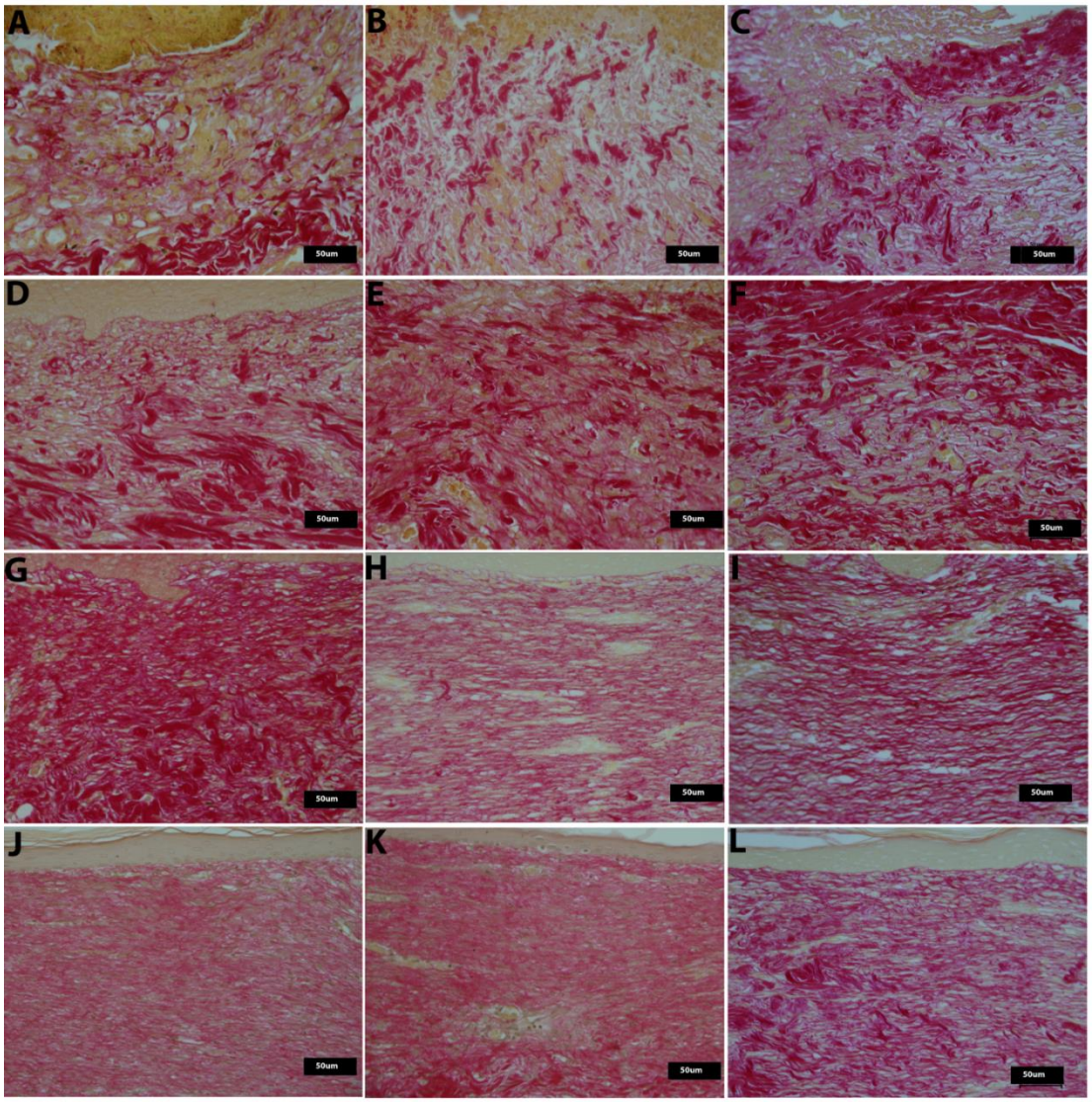

Figure 17 Picro-sirius red staining on JDS (A, D, G and J) and UDS (B, E, H and K) grafted and open (C, F, I and L) wounds (40x); 3rd (A, B and C), 7th (D, E and F), 14th (G, H and I) and 30th (J, K and L) day.

4.2.3 Immunohistochemistry

4.2.3.1 Immunohistochemistry with PCNA antibodies

The immunohistochemistry with antibody raised against PCNA revealed the extent of cell proliferation in the healing wounds. The PCNA antibodies bound to dividing nuclei

usually before or in the S phase of cell cycle and appeared brown in colour. The nuclei of the non dividing cells in the granulation tissue took up the counter stain, Harris Hematoxylin and appeared purple in colour.

4.2.3.1.1 Immunohistochemistry with PCNA antibodies in Experiment I

In CDS and CSIS grafted wounds (Figure 18) on 3rd day (A and B), most of the basal cells in the newly forming epidermis and the dermis immediately beneath were positive for PCNA (black arrow). During 7th day (C and D), both the basal and supra basal cells in the epidermis were positive for PCNA however the outer layers of epidermis remained negative in all cases. By 14th (E and F) and 30th day (G and H), only basal cells in epidermis (white arrow) were positive for PCNA and suprabasal cells ceased to show PCNA positivity.

4.2.3.1.2 Immunohistochemistry with PCNA antibodies Experiment II

In JDS and UDS grafted and OWs (Figure 19), the early time periods of 3rd (A, B and C) and 7th day (D, E and F), there were higher numbers of randomly distributed proliferating cells both in the dermis and epidermis. However, the proliferating cells were confined to the basal layers of epidermis during the later phase of healing, *i.e.* 14th (G, H and I) and 30th day (J, K and L). The cell proliferation also contributed for granulation tissue formation especially, angiogenesis and fibroblast proliferation.

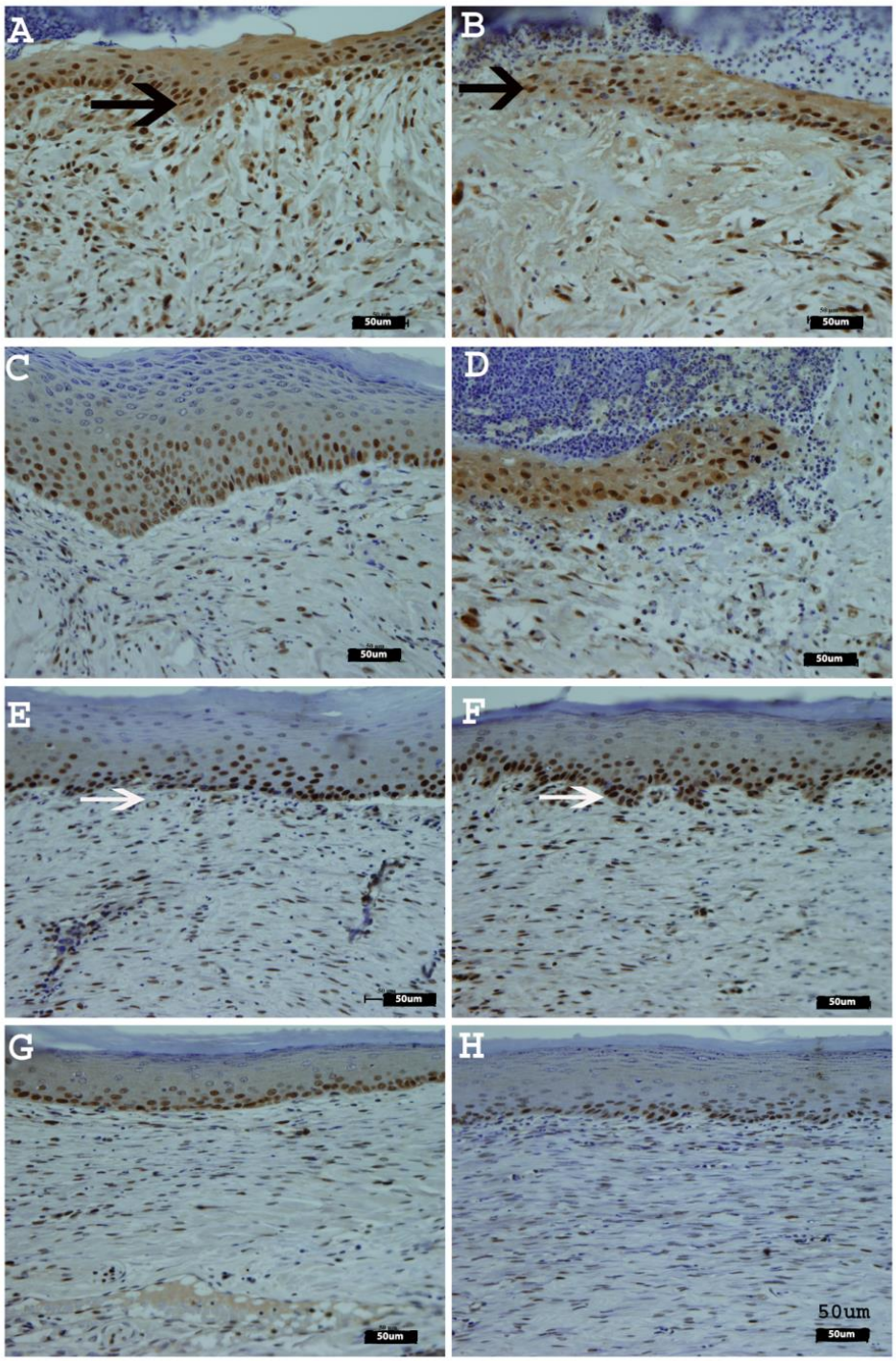

Figure 18 Immunohistochemistry using PCNA antibodies in CDS (A, C, E and G) and CSIS (B, D, F and H) grafted wounds (40x); 3rd (A and B), 7th (C and D), 14th (E and F) and 30th (G and H) day

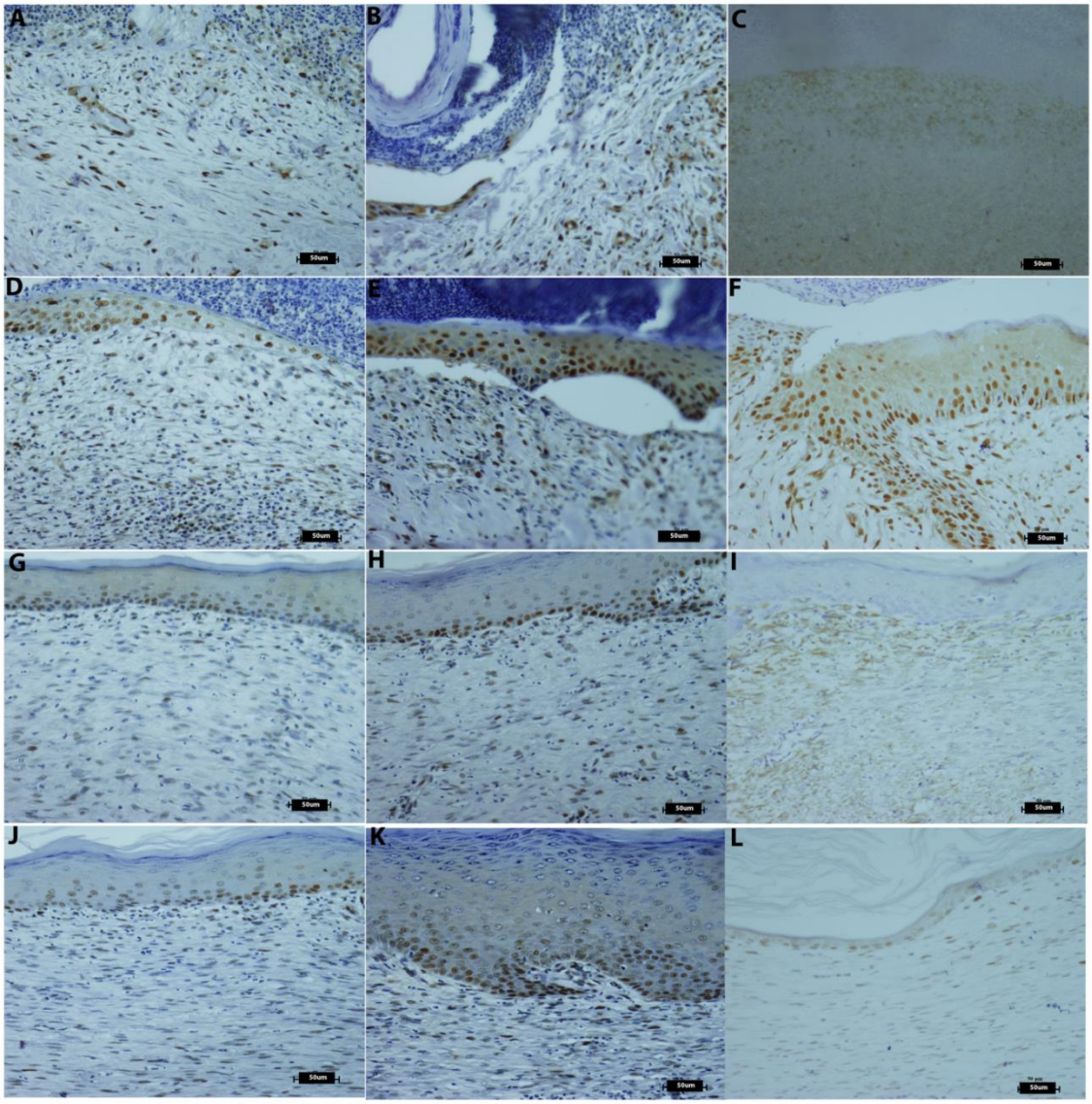

Figure 19 Immunohistochemistry using PCNA antibodies in JDS (A, D, G and J) and UDS (B, E, H and K) grafted and open (C, F, I and L) wounds (40x); 3rd (A, B and C), 7th (D, E and F), 14th (G, H and I) and 30th (J, K and L) day

4.2.3.2 Immunohistochemistry with Vimentin antibodies

The vimentin antibodies bound to intermediate filament expressed by mesenchymal cells as expected. IHC to vimentin showed the extent of mesenchymal infiltration in the healing wounds.

4.2.3.2.1 Immunohistochemistry with Vimentin antibodies Experiment I

The CDS and CSIS induced healing reactions (Figure 20), showed heterogeneous distribution of vimentin throughout the wound area on 3rd day (A and B) and they appeared like elongated spindles (white arrow). On 7th (C and D) and 14th day (E and F), the vimentin content increased with scattering and elongation (white arrow). In some slides, they were concentrated immediately below the neo-epidermis. On 30th day (G and H), the vimentin proteins were sparse, faint, thin (star) and assumed the shape of an 'elongated wavy thread'.

4.2.3.2.2 Immunohistochemistry with Vimentin antibodies Experiment II

The vimentin positivity was more intense and abundant during 3rd (A, B and C) and 7th day (D, E and F), compared to later stages of healing in the JDS and UDS grafted wounds and the OWs (Figure 21). During 14th (H, I and J) and 30th day (K, J and L), the vimentin filaments appeared dispersed, faint and elongated signifying the later phases of wound healing. There was significant delay in mesenchymal re-population in OW compared to the graft assisted healing wounds.

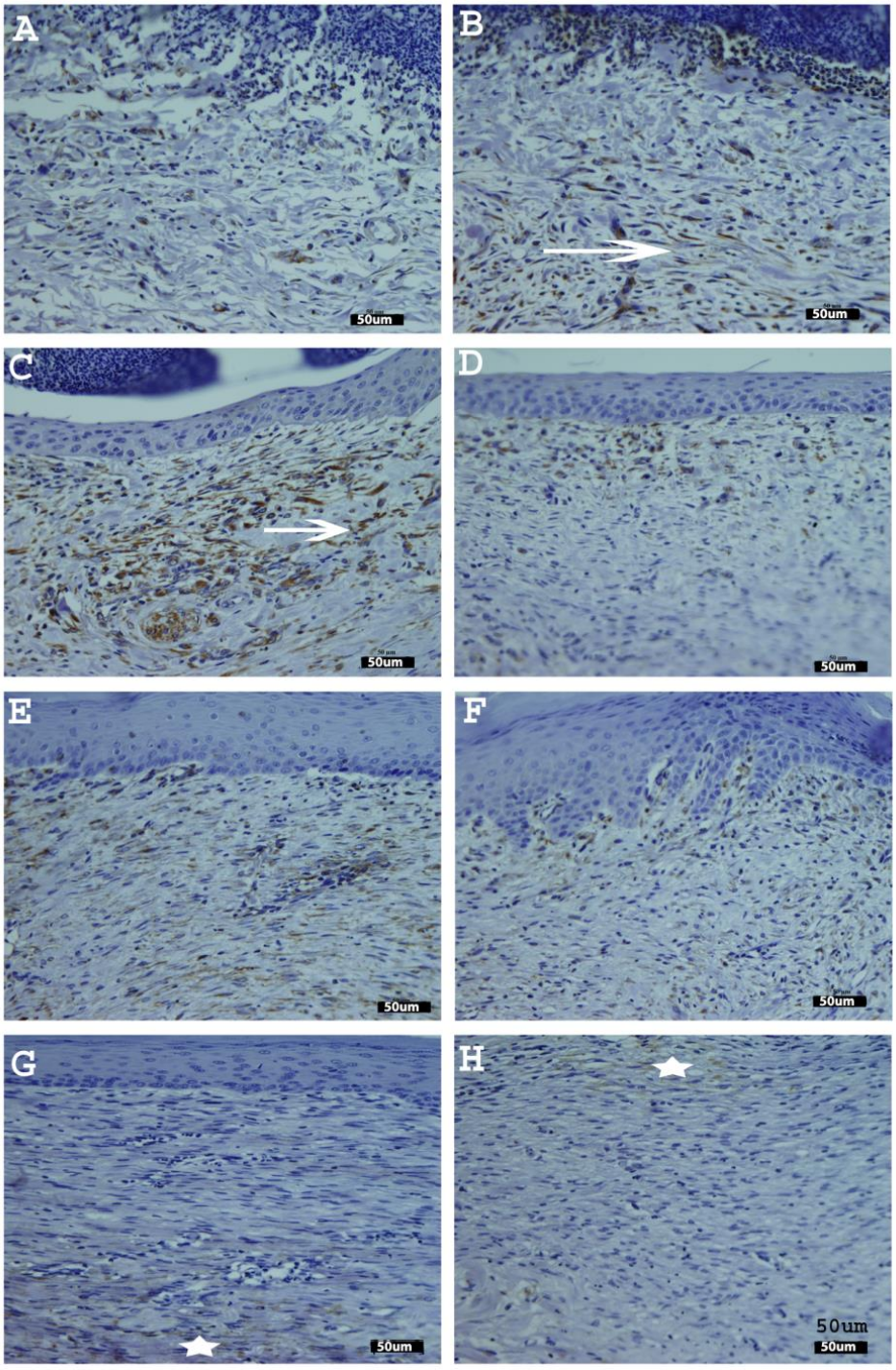

Figure 20 Immunohistochemistry using Vimentin antibodies in CDS (A, C, E and G) and CSIS (B, D, F and H) grafted wounds (40x); 3rd (A and B), 7th (C and D), 14th (E and F) and 30th (G and H) day

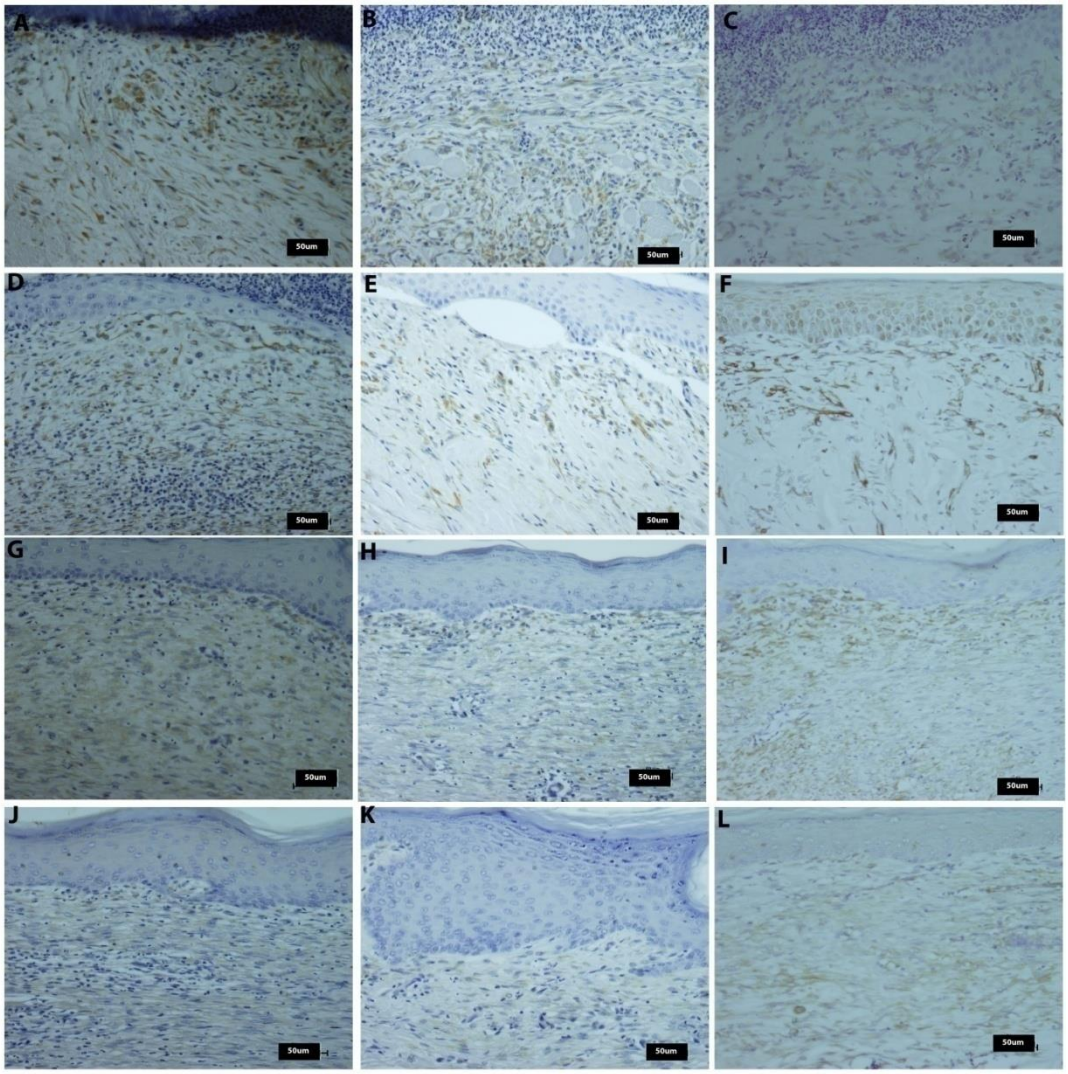

Figure 21 Immunohistochemistry using Vimentin antibodies in JDS (A, D, G and J) and UDS (B, E, H and K) grafted and open (C, F, I and L) wounds (40x); 3rd (A, B and C), 7th (D, E and F), 14th (G, H and I) and 30th (J, K and L) day

4.2.3.3 Immunohistochemistry with ASMA antibodies

The ASMA antibodies were bound to myofibroblasts as expected. Immunohistochemistry to ASMA showed the extent of myofibroblast response in the healing wounds.

4.2.3.3.1 Immunohistochemistry with ASMA antibodies in Experiment I

In CSIS and CDS grafted wounds (Figure 22), on 3rd day (A and B), ASMA was distributed throughout wound area and showed spindle shape pattern (arrow). On 7th day (C and D), ASMA further increased and on 14th day (E and F), it was abundant immediately below the newly formed epidermis and at the wound tissue interface (star) in the dermis. During 30th day (E and F), ASMA concentration was found to decrease.

4.2.3.3.2 Immunohistochemistry with ASMA antibodies in Experiment II

In JDS and UDS grafted wounds (Figure 23), compared to the 3rd (A, B and C) day, the ASMA immunopositivity was relatively higher on the 7th day (D, E and F). By the 7th day, spindle shaped and elongated ASMA deposition was prominent. The ASMA-immunoreactivity decreased thereafter by 14 (G, H and I) and 30 days (J, K and L) with a clear peak reaction by the 7th day. On the other hand, OW showed highest number of ASMA response during the 14th day. On 30th day, the ASMA declined in all the samples.

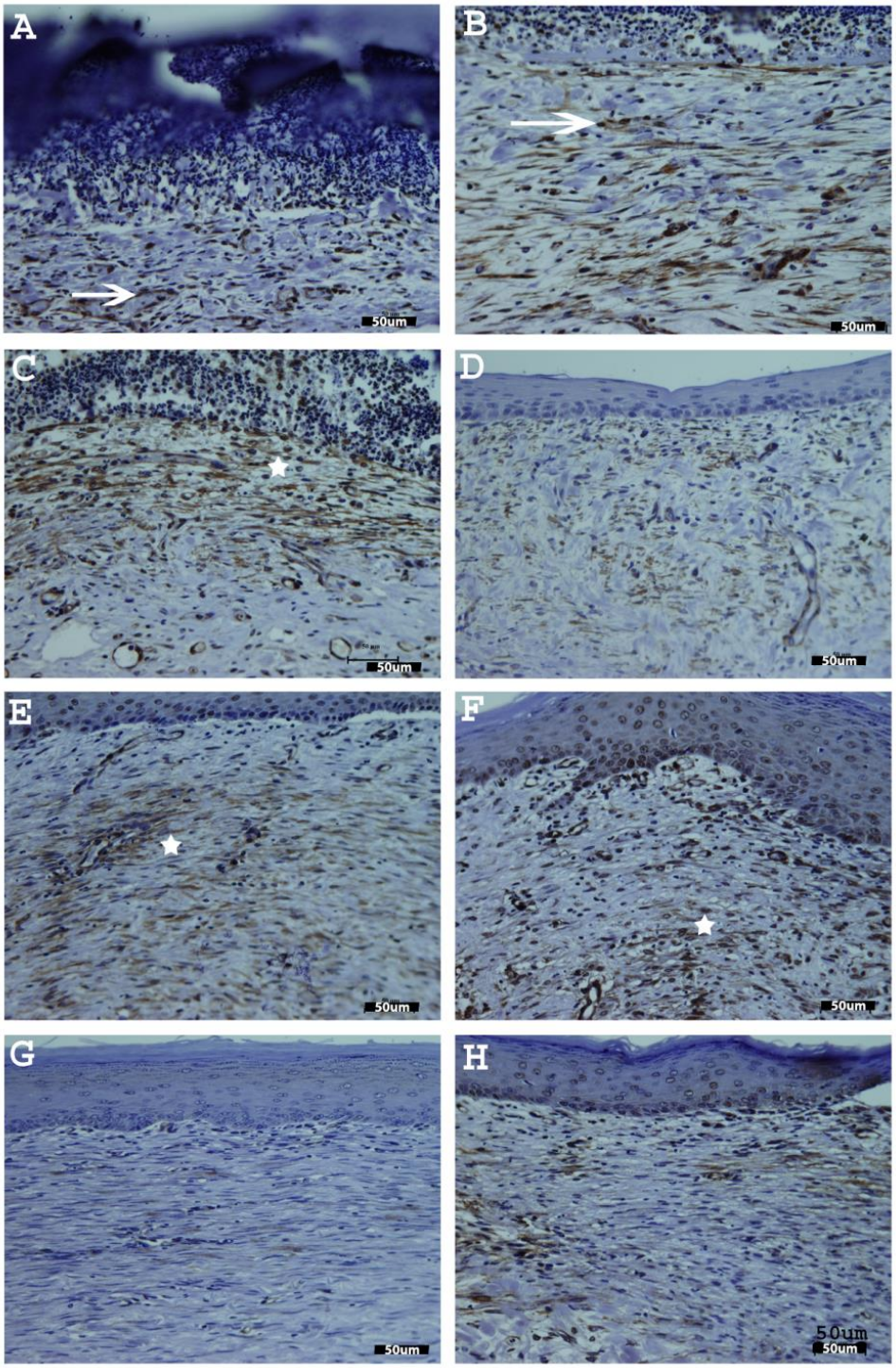

Figure 22 IHC using ASMA antibodies in CDS (A, C, E and G) and CSIS (B, D, F and H) grafted wounds (40x); 3rd (A and B), 7th (C and D), 14th (E and F) and 30th (G and H) day

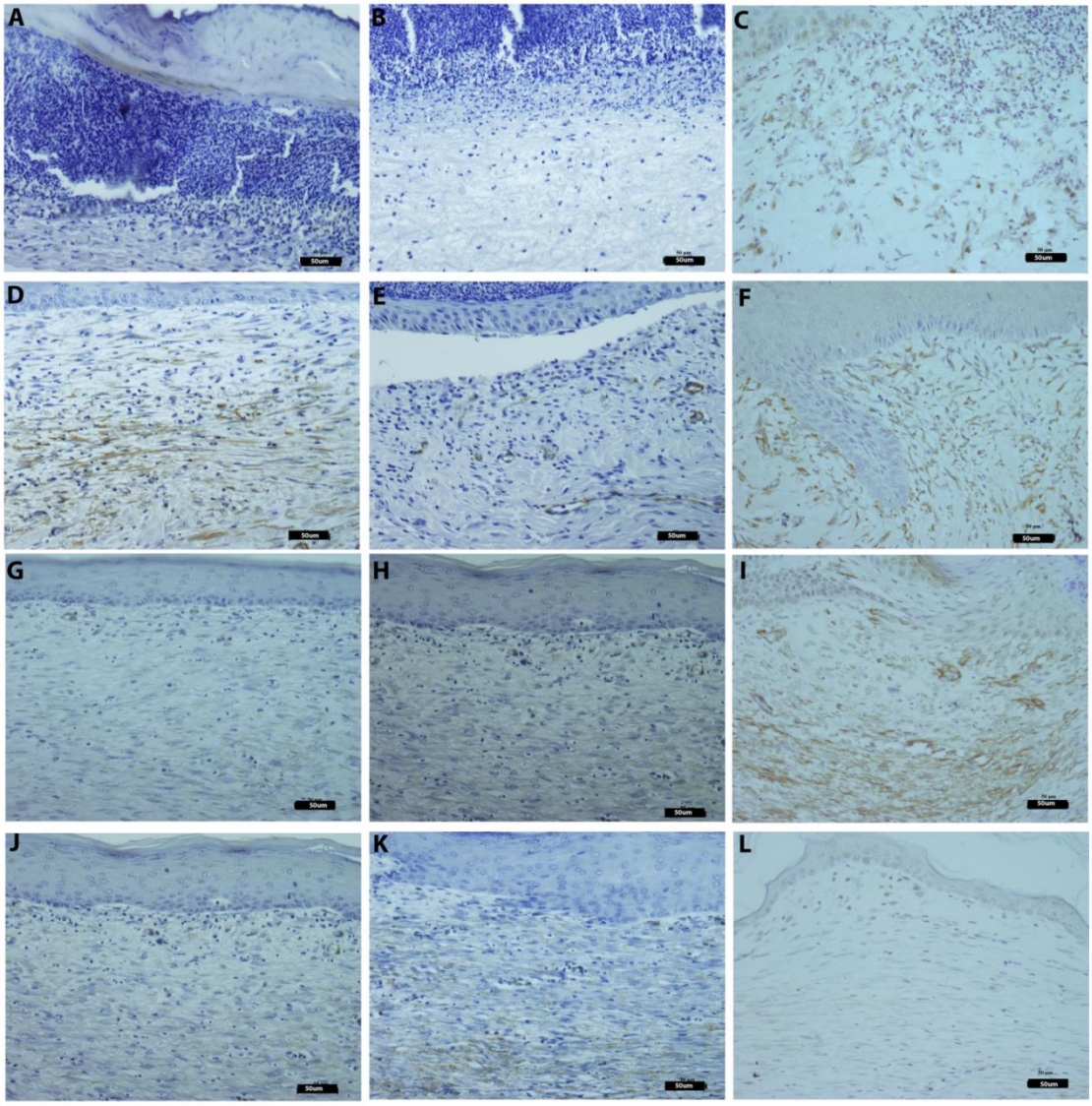

Figure 23 IHC using ASMA antibodies in JDS (A, D, G and J) and UDS (B, E, H and K) grafted and open (C, F, I and L) wounds (40x); 3rd (A, B and C), 7th (D, E and F), 14th (G, H and I) and 30th (J, K and L) day

4.2.4 Histomorphometry and immunohistomorphometry

4.2.4.1 Extent of re-epithelialization

4.2.4.1.1 Extent of re-epithelialization in Experiment I

Re-epithelialization was similar in both CSIS and CDS. At least in one sample of CDS and CSIS grafted wounds, 100% re-epithelialization was seen on 14th day (Figure 24 A). Re-epithelialization was complete by 30 days in all the samples.

4.2.4.1.2 Extent of re-epithelialization in Experiment II

The extent of re-epithelialisation was faster in the graft assisted healing wound compared to the OWs. Complete re-epithelisation was observed in JDS and UDS treated wound as early as 14 days. All the three wounds acquired 100% re-epithelialisation by 30 days (Figure 24 B).

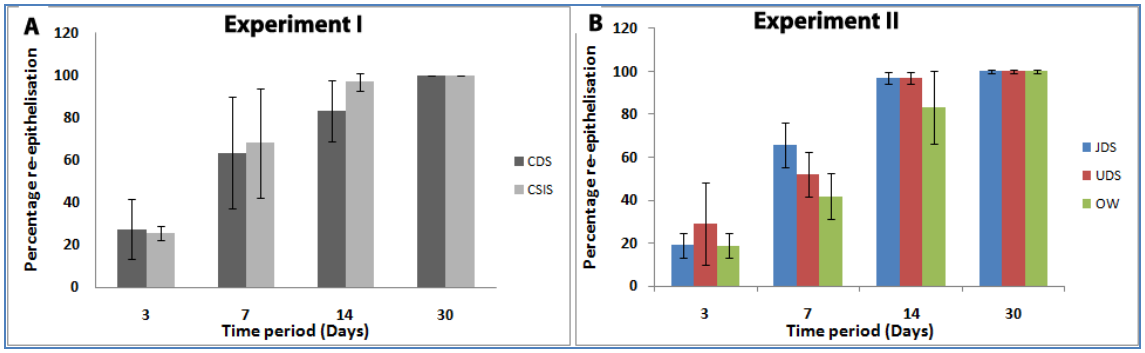

Figure 24 Extent of Re-epithelialization: A) CDS v/s CSIS grafted wounds, B) JDS and UDS grafted wounds v/s OW

4.2.4.2 Extent of neo-vascularization

4.2.4.2.1 Extent of neo-vascularization in Experiment I

There was no significant difference in the extent of formation of blood vessels between CSIS and CDS as both the grafts showed similar pattern in formation of blood vessels (Figure 25 A).

4.2.4.2.2 Extent of neo-vascularization in Experiment II

The extent of formation of blood vessels in JDS-treated wound was higher than to UDS treated wound on the 3rd day (p value = 0.04). On 14th day, the UDS treated wound showed higher neo-vascularization compared to OW (p value = 0.005) but no difference was seen thereafter (Figure 25 B).

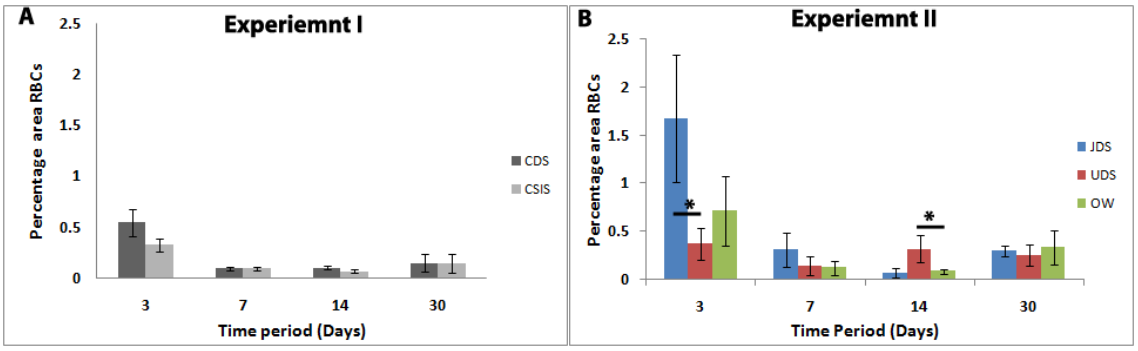

Figure 25 Extent of neo-vascularization: A) CDS v/s CSIS grafted wounds, B) JDS and UDS grafted wounds v/s OW (* represents p value ≤ 0.05)

4.2.4.3 Extent of collagen deposition

4.2.4.3.1 Extent of collagen deposition in Experiment I

The extent of collagen deposition also was similar in both CDS and CSIS treated wounds. About 20% of the scanned areas were stained with picro-sirius red on 3rd day which increased to about 40% by 7th day in both CDS and CSIS treated wounds (Figure 26 A).

4.2.4.3.2 Extent of collagen deposition in Experiment II

There was no significant difference between OW, JDS and UDS with respect to the extent of collagen deposition. The JDS and UDS treated wounds as well as open control wound had steady increase in the collagen deposition from day 3 to 14 and subsequently decreased by 30 days. Thus, by 30 days all the wounds had similar collagen deposition (Figure 26 B).

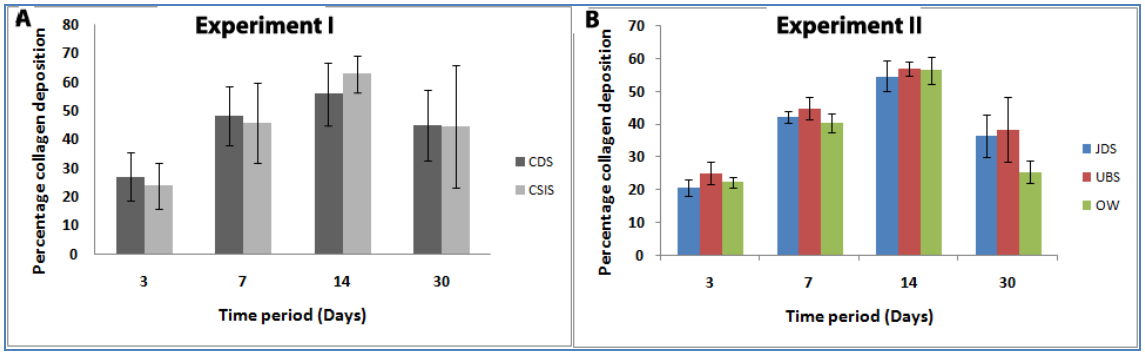

Figure 26 Extent of collagen deposition: A) CDS v/s CSIS grafted wounds, B) JDS and UDS grafted wounds v/s OW

4.2.4.4 Extent of cell proliferation

4.2.4.4.1 Extent of cell proliferation in Experiment I

During 7th day, the percentages of PCNA positive cells were similar in CDS and CSIS treated wounds. However, the cell proliferation was higher in CDS during the early time period of 3rd day (p value = 0.02) and late time period of 14th day (p value = 0.008) after grafting (Figure 27 A).

4.2.4.4.2 Extent of cell proliferation in Experiment II

The OW had a fewer proliferating cells during the early phases of healing (3rd day) compared to JDS and UDS treated wounds. Both the JDS (p value =0.002) and UDS (p value =0.0005) treated wounds had high cell-proliferation potentials compared to the OW on 3rd day. However, the cell-proliferation induction potential for UDS was poor on the 7th day (p value =0.008) which later increased to significant level by 14th day (p value= 0.02) compared to JDS**.** However, the proliferation of cells in all the wounds was similar during 30 day (Figure 27 B).

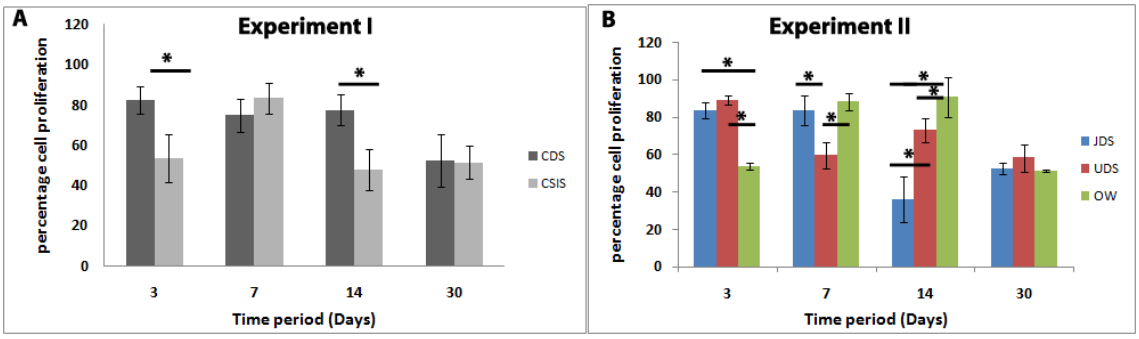

Figure 27 Extent of cell proliferation: A) CDS v/s CSIS grafted wounds, B) JDS and UDS grafted wounds v/s OW (* represents p value ≤ 0.05)

4.2.4.5 Extent of mesenchymal cell response

4.2.4.5.1 Extent of mesenchymal cell response in Experiment I

There was no significant difference in the extent of mesenchymal cell infiltration in CDS and CSIS grafted wound during any time period as both CDS and CSIS showed similar pattern in vimentin positive cells (Figure 28 A).

4.2.4.5.2 Extent of mesenchymal cell response in Experiment II

The extent of mesenchymal cell infiltration was higher in JDS (p value=0.02) compared to UDS on the 3rd day. There was no significant difference between JDS and UDS on the 7th day. However the mesenchymal cell infiltration for UDS peaked higher than JDS (p value=0.001) on the 14th day. On the 30th day, both JDS and UDS showed similarity in the extent of mesenchymal cell infiltration. In the case of OW, mesenchymal cell infiltration peaked only by the 14th and the reaction persisted during the later time periods (30 days) compared to JDS or UDS (Figure 28 B).

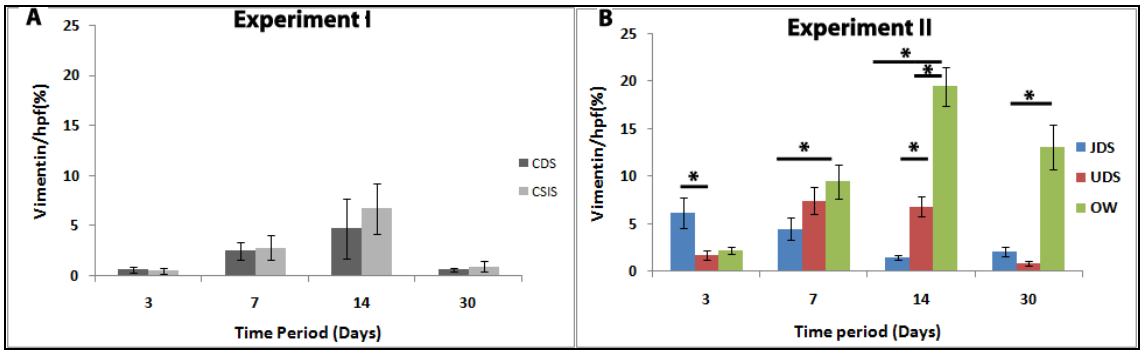

Figure 28 Extent of mesenchymal cell response: A) CDS v/s CSIS grafted wounds, B) JDS and UDS grafted wounds v/s OW (* represents p value ≤ 0.05)

4.2.4.6 Extent of myofibroblast response

4.2.4.6.1 Extent of myofibroblast response in Experiment I

There was significantly higher number of myofibroblasts in the CDS grafted (p value = 0.009) wound during early phases (3rd day) of wound healing. However, the number of ASMA positive cells was similar in both CDS and CSIS after 3rd day (Figure 29 A).

4.2.4.6.2 Extent of myofibroblast response in Experiment II

The myofibroblast response peaked and declined much earlier for both the JDS and UDS treated wounds compared to OWs. Also, the myofibroblast response was higher in JDS during the 7th day (p value=0.02) than UDS. There was presence of higher number of myofibroblast in the OW on the 14th day compared to both JDS (p value ≤ 0.0001) and UDS (p value ≤ 0.0001). However, the myofibroblast response was much less by 30 days in all the wounds. (Figure 29 B).

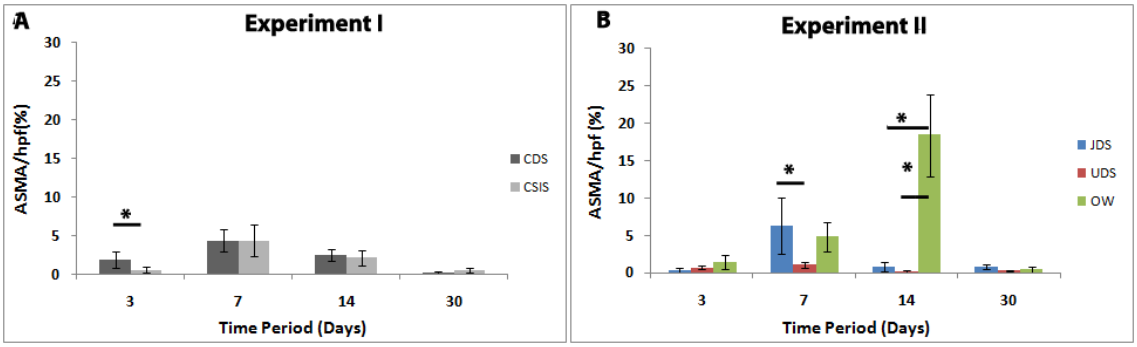

Figure 29 Extent of myofibroblast response: A) CDS v/s CSIS grafted wounds, B) JDS and UDS grafted wounds v/s OW (* represents p value ≤ 0.05)

Section III

4.3 Fabrication of prototypes of cell loaded ECM scaffolds.

4.3.1 Culturing of HaCaT cells on the ECM scaffolds

HaCaT cells became confluent within 2 days in T 25 flask. They maintained a typical cobble stone morphology as shown in Figure 30. The stock culture was trypsinized. It had a cell concentration of $2.5X10^6$. The stock was split into 1:3 ratios into 3 T25 flasks and allowed to expand. All the flasks had more than 90% cell viability. The flasks were further trypsinized and expanded for yielding more number of cells. These cells were seeded on to the ECM scaffolds.

4.3.1.1 HaCaT viability on ECM scaffold

For further confirming the viability of cells on the ECM scaffold, MTT assay was performed on 3, 7 and 10 days. All the three scaffolds facilitated growth of HaCaT cells. The results showed more than 100% viability in scaffolds because the scaffolds had more surface area for cellular attachment compared to the bare 6 well plates. The results are shown in Figure 31.

4.3.1.2 Confocal microscopy analysis

The polygonal cobblestone morphology of the HaCaT cells were confirmed after staining with phalloidin FITC conjugate as seen in Figure 32. The actin filaments bound to phalloidin and appeared green in color while the nuclei took the stain of DAPI and appeared blue. The HaCaT cells covered the entire surface of the ECM scaffolds.

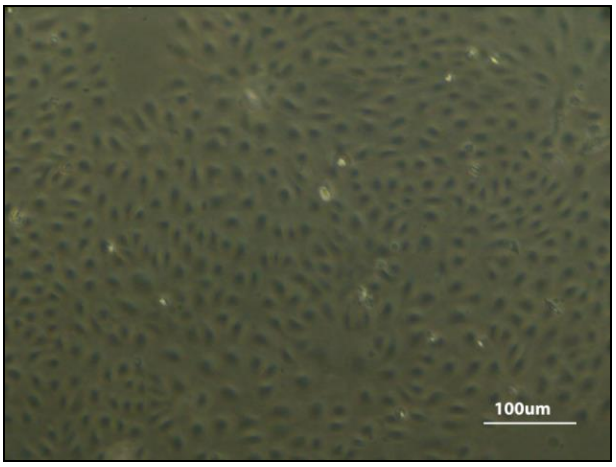

Figure 30 HaCaT cells

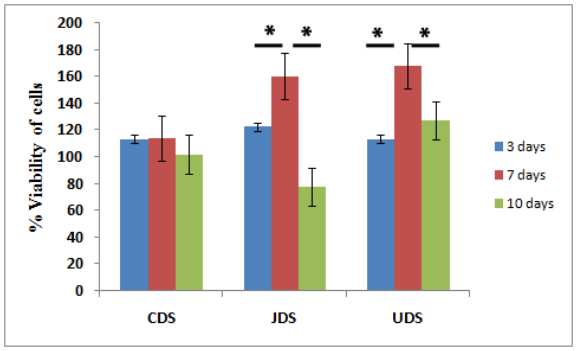

Figure 31 Viability of HaCaT cells on ECM scaffolds (* indicates p value ≤ 0.05)

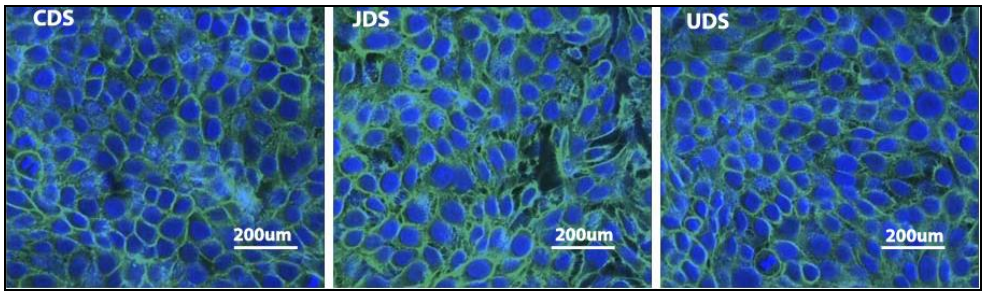

Figure 32 HaCaT cells on ECM scaffolds

4.3.1.3 Histology evaluation of the tissue construct

The histology slides of HaCaT seeded scaffolds were observed under light microscopy after H and E staining. The HaCaT cells grew as layers over the ECM scaffolds as shown in Figure 33.

4.3.1.4 Immunohistochemistry evaluation

4.3.1.4.1 Immunohistochemistry with PCNA

The Figure 34 shows IHC of slides stained with PCNA antibodies. Most of the HaCaT cells on the ECM scaffold were positive for PCNA which showed that the cells were actively proliferating on the ECM scaffolds.

4.3.1.4.2 Immunohistochemistry with involucrin

Most of the HaCaT cells on the ECM scaffold were positive for involucrin antibodies and this showed that the cells were stable (Figure 35).

4.3.1.4.3 Immunohistochemistry with Vitamin D receptor

A few of the HaCaT cells on the ECM scaffold were positive for Vitamin D receptor and this indicated that the some of HaCaT cells were functionally active on the scaffold (Figure 36).

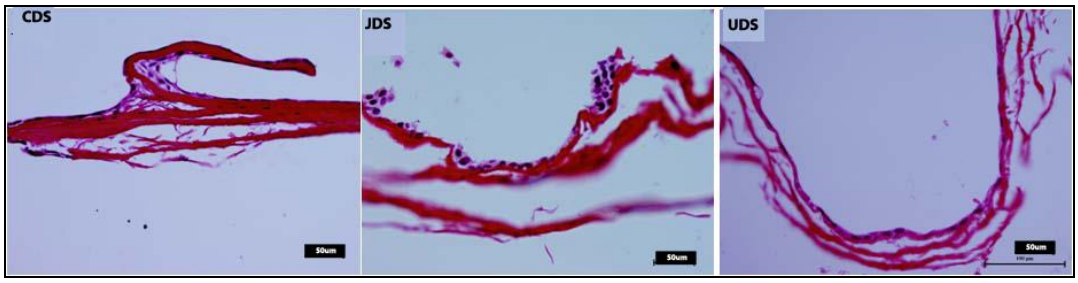

Figure 33 Histology of HaCaT cells on ECM scaffolds

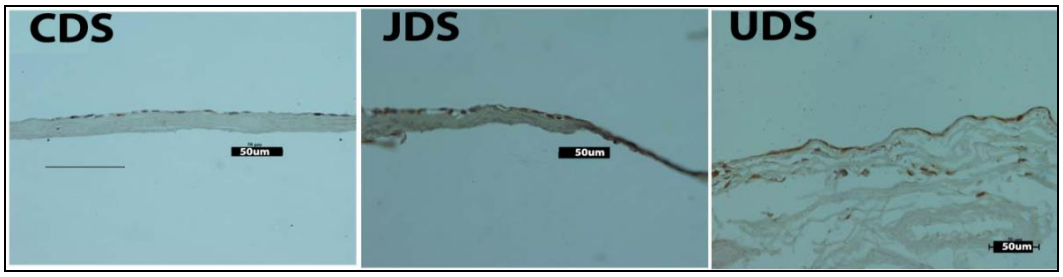

Figure 34 Immunohistochemistry using PCNA antibodies

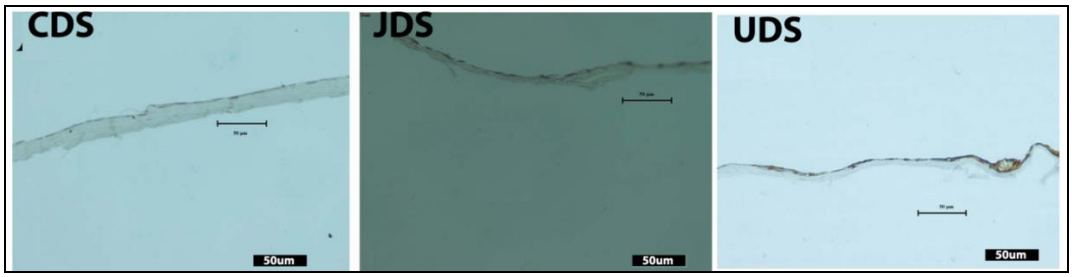

Figure 35 Immunohistochemistry using Involucrin

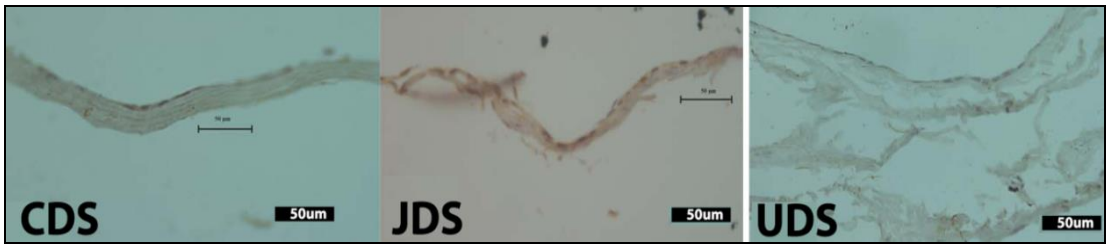

Figure 36 Immunohistochemistry using Vitamin D receptors

4.3.2 Culturing of fibroblasts on the ECM scaffolds

4.3.2.1 Primary isolation of dermal fibroblasts from rabbit skin

After five to six days fibroblasts were seen to migrate from the fixed explants tissue. Fibroblast grew confluent outside the explants by 7 days. On day 10, the fibroblasts were collected by trypsinization and pooled. The different stages of explants culture during 3, 5, 7 and 10 days are shown in the representative Figure 37. The pooled cells on day 10 was seeded and allowed to grow in T25 flask. The 3^{rd} or/and 4^{th} passages were taken for fabrication of graft and animal experiment.

4.3.2.2 Characterization of dermal fibroblasts

4.3.2.2.1 Immunocytochemistry

Most of the isolated fibroblasts were positive for vimentin, laminin and fibronectin. Some of the cells also contained of collagen III, collagen IV and ASMA in the cytoplasm as depicted in Figure 38.

4.3.2.2.2 Flow cytometry

The flow cytometry further confirmed the fibroblast nature of isolated cells. Almost 90% of the cells in the preparation were positive for vimentin as seen in Figure 39. The fibroblasts confirmed were seeded on the ECM scaffolds at a concentration of 10^6 cells/cm^2 scaffold.

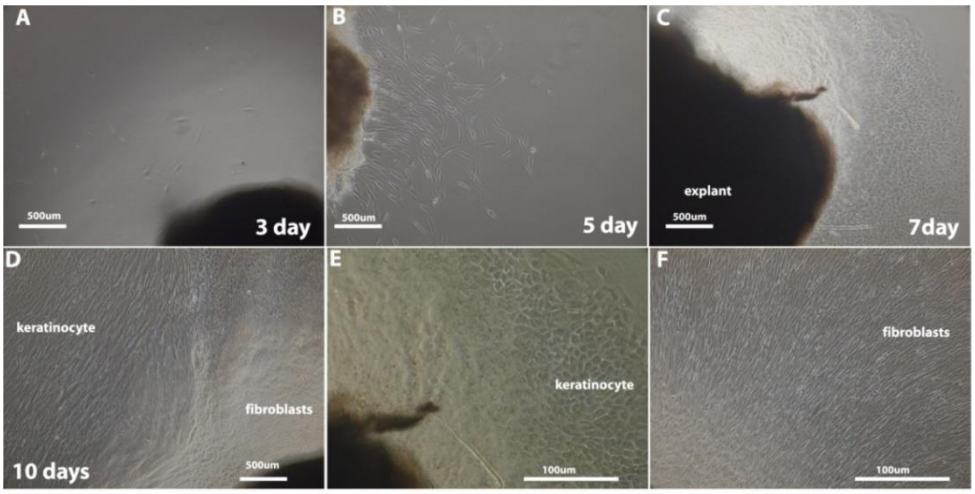

Figure 37 Primary isolation of dermal fibroblast by explants culture

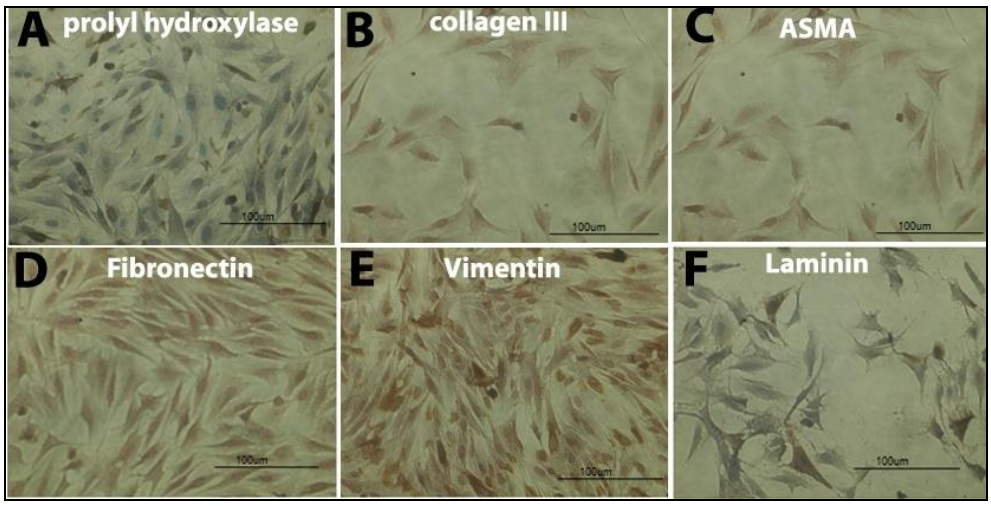

Figure 38 Immunophenotyping of isolated fibroblasts

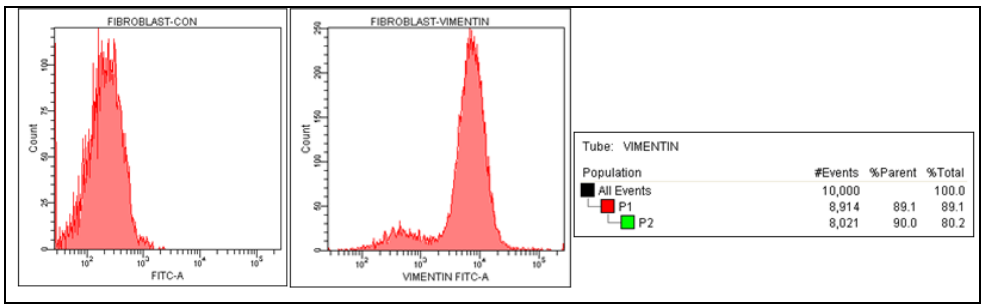

Figure 39 Flow cytometry analysis: ≥ 90% vimentin positivity

4.3.2.3 Viability of fibroblast on ECM scaffolds

For further confirming the viability of cells on the ECM scaffold, MTT assay was performed on 3, 7 and 10 days. All three scaffolds facilitated more than 100% viability for fibroblasts in different time points. The scaffolds had more surface area for cellular attachment compared to the bare plates and the calculated viability exceeded 100% (Figure 40).

4.3.2.4 Attachment of fibroblast on ECM scaffolds

To further study the attachment and morphology of fibroblasts on ECM scaffold, scanning electron microscopy was performed. The fibroblasts on the ECM scaffolds showed good attachment and covered the entire surface of ECM (Figure 41).

4.3.2.5 Confocal analysis of fibroblast loaded CDS

The dermal fibroblasts were seen growing on the CDS scaffolds and confocal analysis attachment of dermal fibroblasts on CDS scaffolds with typical spindle shape morphology (Figure 42).

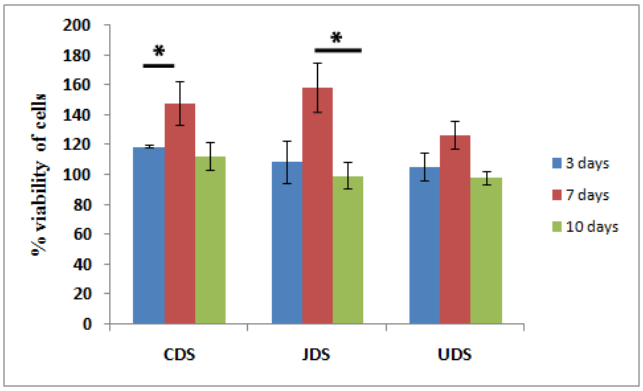

Figure 40 Viability of fibroblasts on ECM scaffolds (* indicates p value ≤ 0.05)

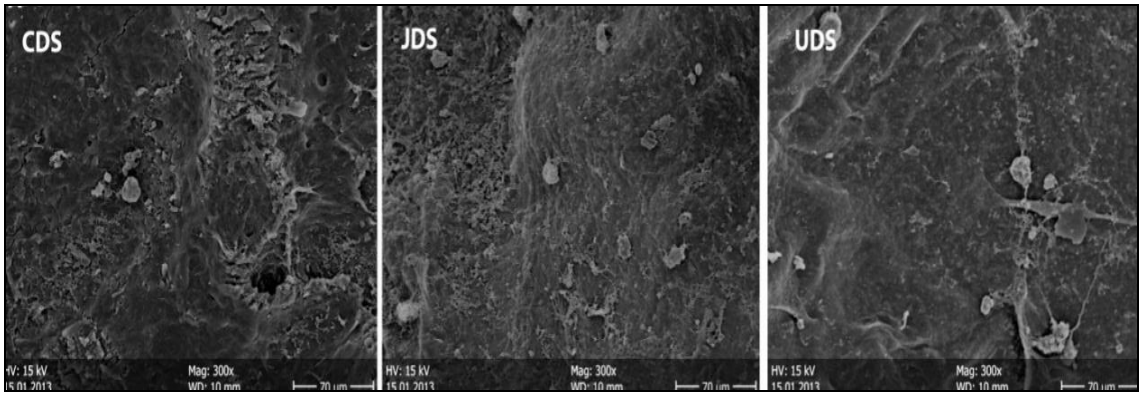

Figure 41 Scanning electron microscopy of fibroblasts loaded ECM scaffolds

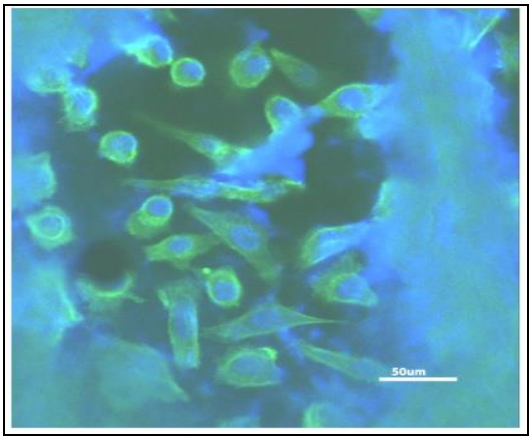

Figure 42 Confocal microscopy of HFCDS

Section IV

4.4 *In vivo* evaluation of wound healing by homologous fibroblast loaded CDS scaffold in full thickness burn model

4.4.1 Fabrication of burn wound device

With the help of the fabricated wound inflicting device, third degree burn wounds of uniform area and thickness were obtained by applying the brass template of the heated device for 45 seconds at 180ºC. The Figure 43 shows the device containing soldiering station (A) whose nozzle is replaced with a brass template (B). The heated template was capable of making burn wounds of uniform area (C) and thickness (D) in rabbit model as confirmed by histomorphometry.

4.4.2 Tagging of dermal fibroblast and seeding on CDS scaffold

The tagged dermal fibroblasts on CDS were visualized using confocal microscopy and the uptakes of PKH26 dye by the dermal fibroblasts were confirmed (Figure 44). The cytoplasm of labeled cells appeared red in color and all the cells took the PKH26 stain label.

4.4.3 *In -vivo* wound healing experiment in rabbit burn model

All the animals survived the experiments and the progression of the healing of burn wounds was uneventful. There was no necrosis or infection in any of the animals. Complete wound closure was observed in both CDS and HFCDS grafted full burns by 28 days in gross observation (Figure 45).

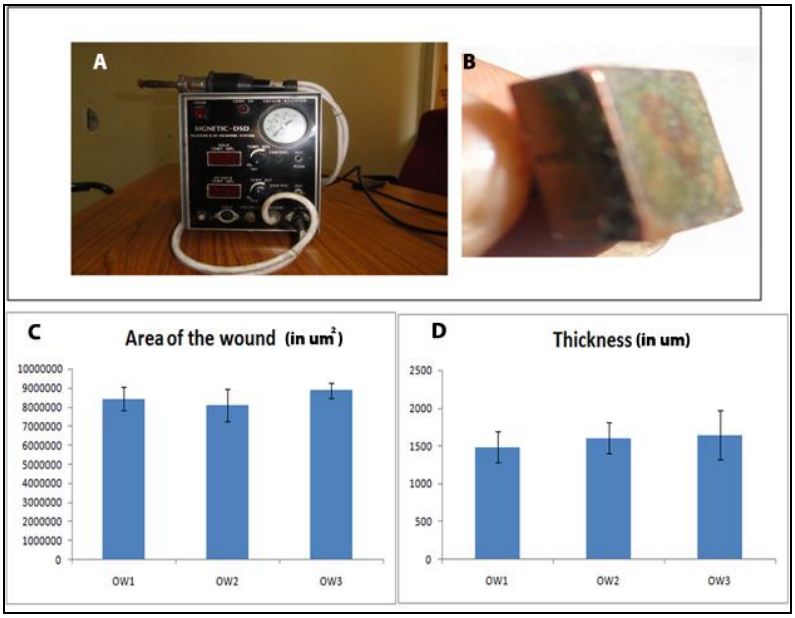

Figure 43 Fabricated burn making device

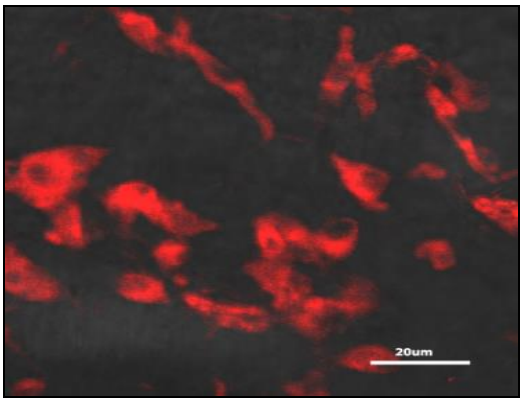

Figure 44 PKH26 tagged fibroblast on CDS

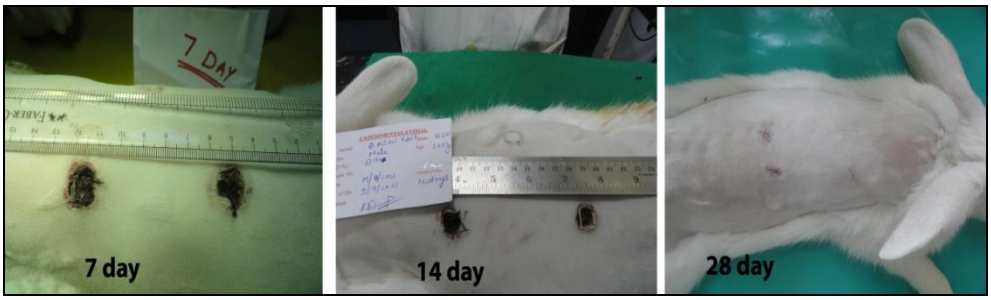

Figure 45 Healing progress in full thickness burn wounds in rabbit model

4.4.4. Histology and histomorphology

4.4.4.1 H and E staining

The epidermis (Figure 46) of CDS (A, B and C) and HFCDS (D, E and F) treated wounds showed progressive healing response. On 7th day (A and D), partial re-epithelialization was seen in both the wounds. On 14th day (B and E), HFCDS grafted burn wounds showed thicker epidermis compared to CDS treated wounds. On 28th day (C and F), complete re-epithelialization and generation of a new dermis were evident in both the graft treated wounds.

In the dermis (Figure 47) of non cell loaded CDS (A, B and C) and HFCDS (D, E and F) treated wounds healed by progressive collagen deposition and cell proliferation in the granulation tissue in the dermis of both the groups. On 7th day (A and D), the HFCDS treated wounds had muscle regeneration as evidenced by centrally placed nucleus. On 14th (B and E) and 28th (C and F) day, complete generation of dermis with parallel arrangement of collagen fibers and blood vessels were seen in both the grafts.

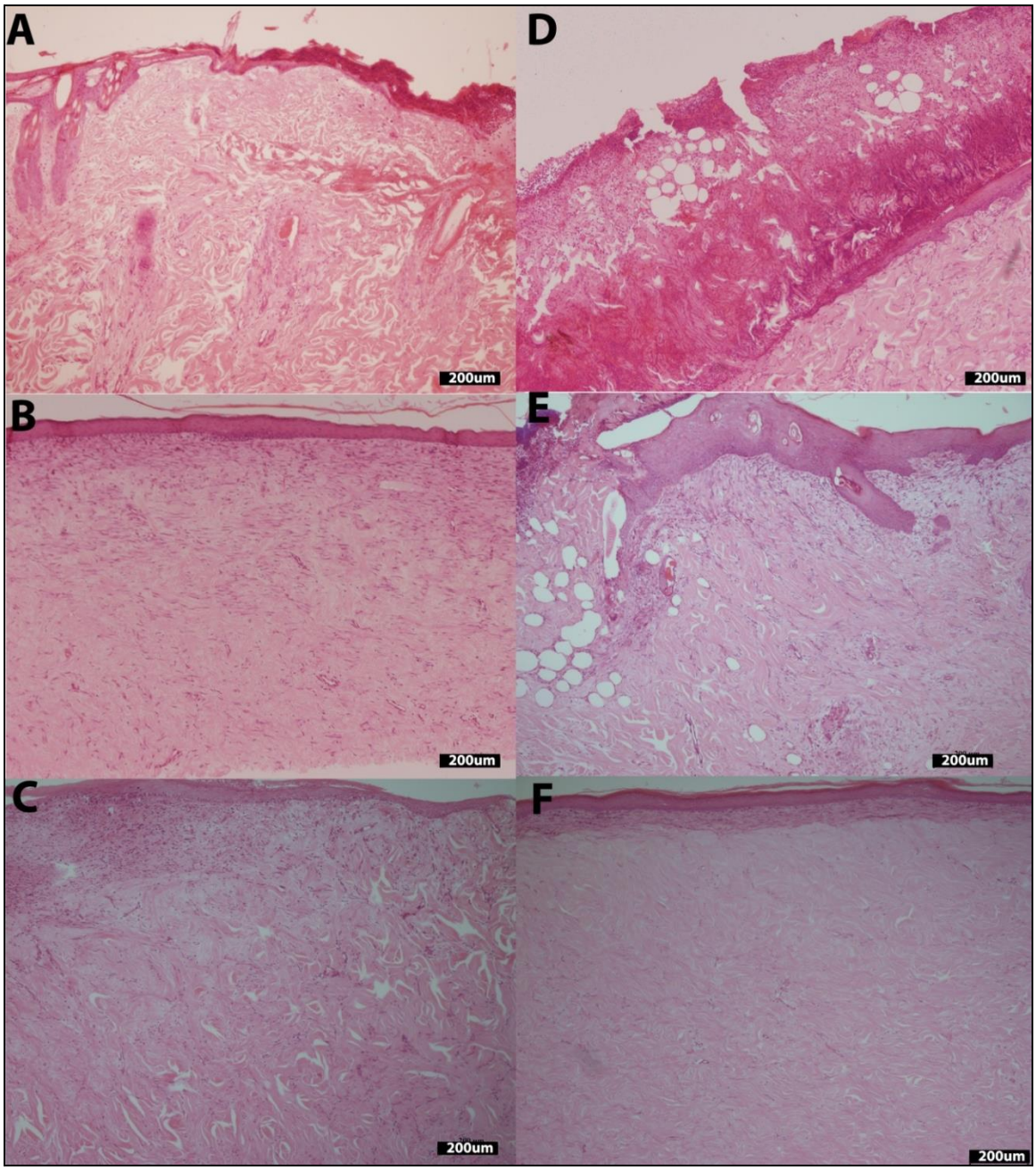

Figure 46 H and E staining in CDS (A, B and C) and HFCDS (D, E and F) treated burn wounds (10x); 7th (A and D), 14th (B and E) and 28th (C and F) day

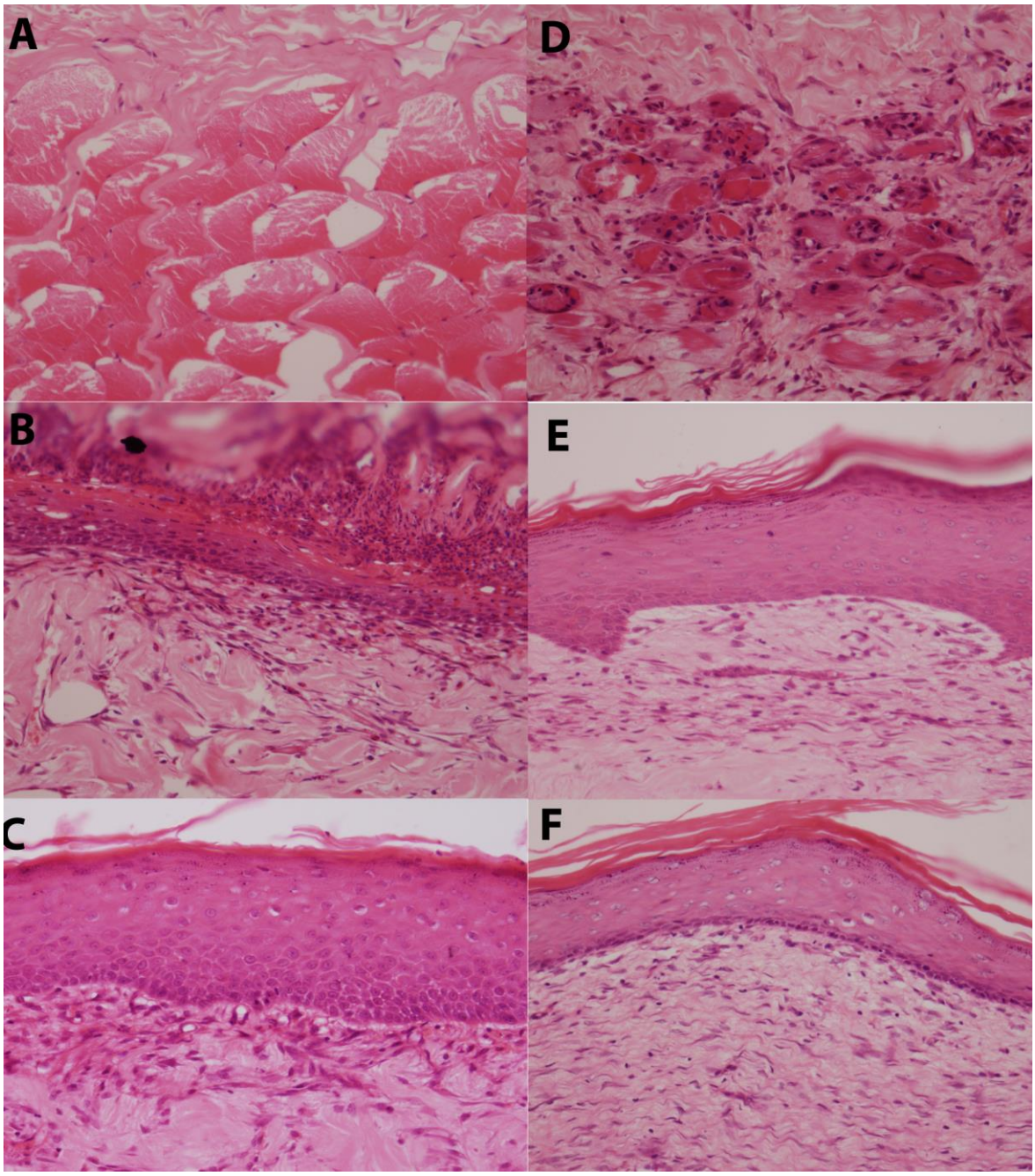

Figure 47 H and E staining in CDS (A, B and C) and HFCDS (D, E and F) treated burn wounds (40x); 7th (A and D), 14th (B and E) and 28th (C and F) day

4.4.4.2 Masson's Trichrome

The Masson's Trichrome stained sections (Figure 48) of CDS (A, B and C) and HFCDS (D, E and F) treated wounds showed progressive collagen deposition and angiogenesis in the granulation tissue in the dermis of both the groups. On 7^{th} day (A and D), the HFCDS treated wounds showed presence of blood vessels and regenerating muscles. On 14^{th} (B and E) and 28^{th} (C and F) day, well organized and compact arrangement of collagen fibers, blood vessels in between the fibers and regenerating muscle bundles were seen in both the grafts.

4.4.4.3 Herovici staining

The Figure 49 shows Herovici staining of CDS (A, B and C) and HFCDS (D, E and F) treated wounds. The collagen type I appeared pink in color while collagen type III appeared blue in color after the Herovici staining. The type I collagen appeared as thicker and denser bundles compared to type III which appeared as finer and longer fibers. Both HFCDS and CDS showed larger proportion of type I collagen over type III in 7 (A and D), 14 (B and E) and 28 days (C and F). On 7^{th} day, both type I and type III collagen fibers were patchy and denser compared to 14^{th} and 28 days where both type I and type III collagen fibers appeared elongated and compact.

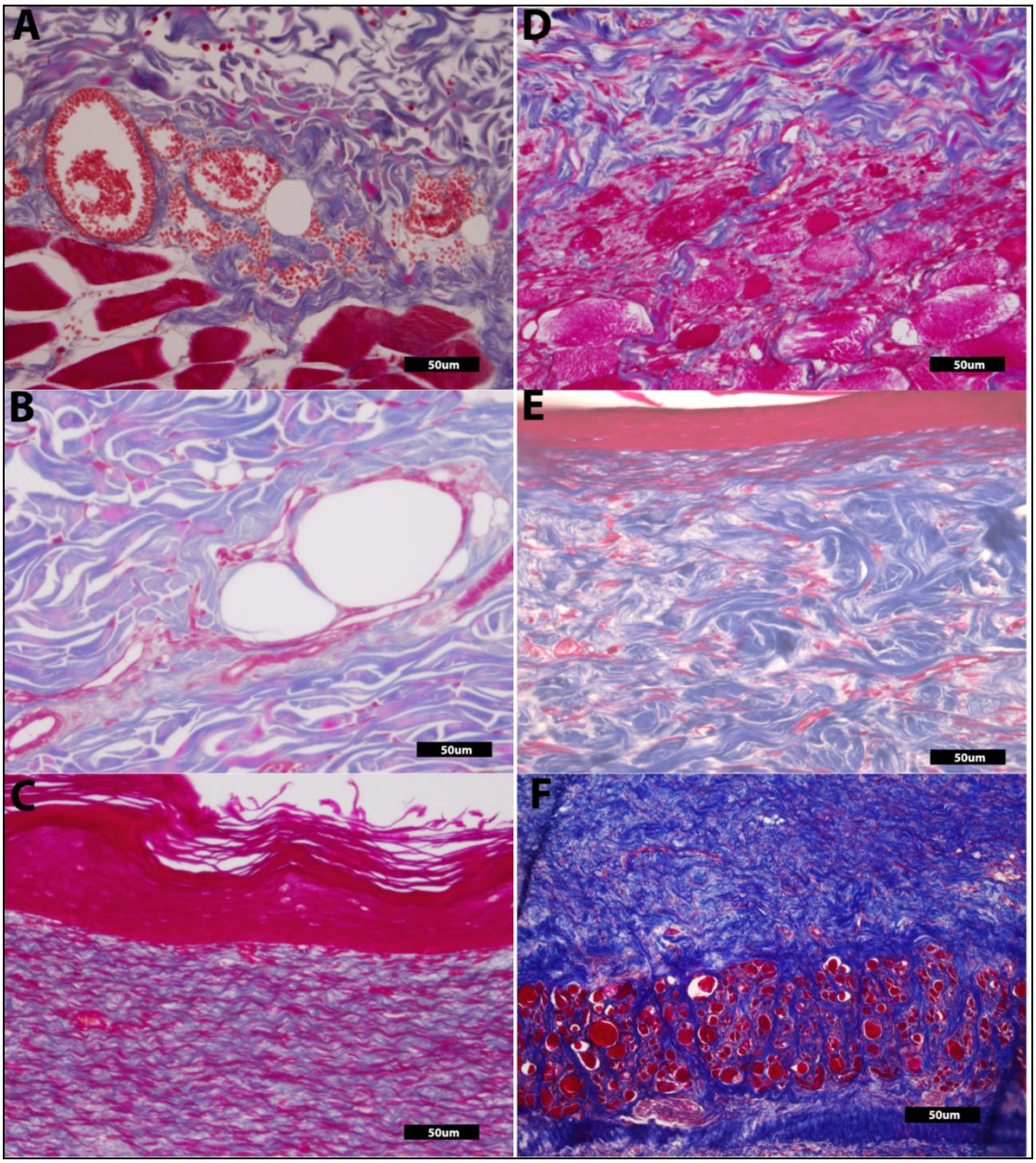

Figure 48 Massons Trichrome staining in CDS (A, B and C) and HFCDS (D, E and F) treated burn wounds (40x); 7th (A and D), 14th (B and E) and 28th (C and F) day

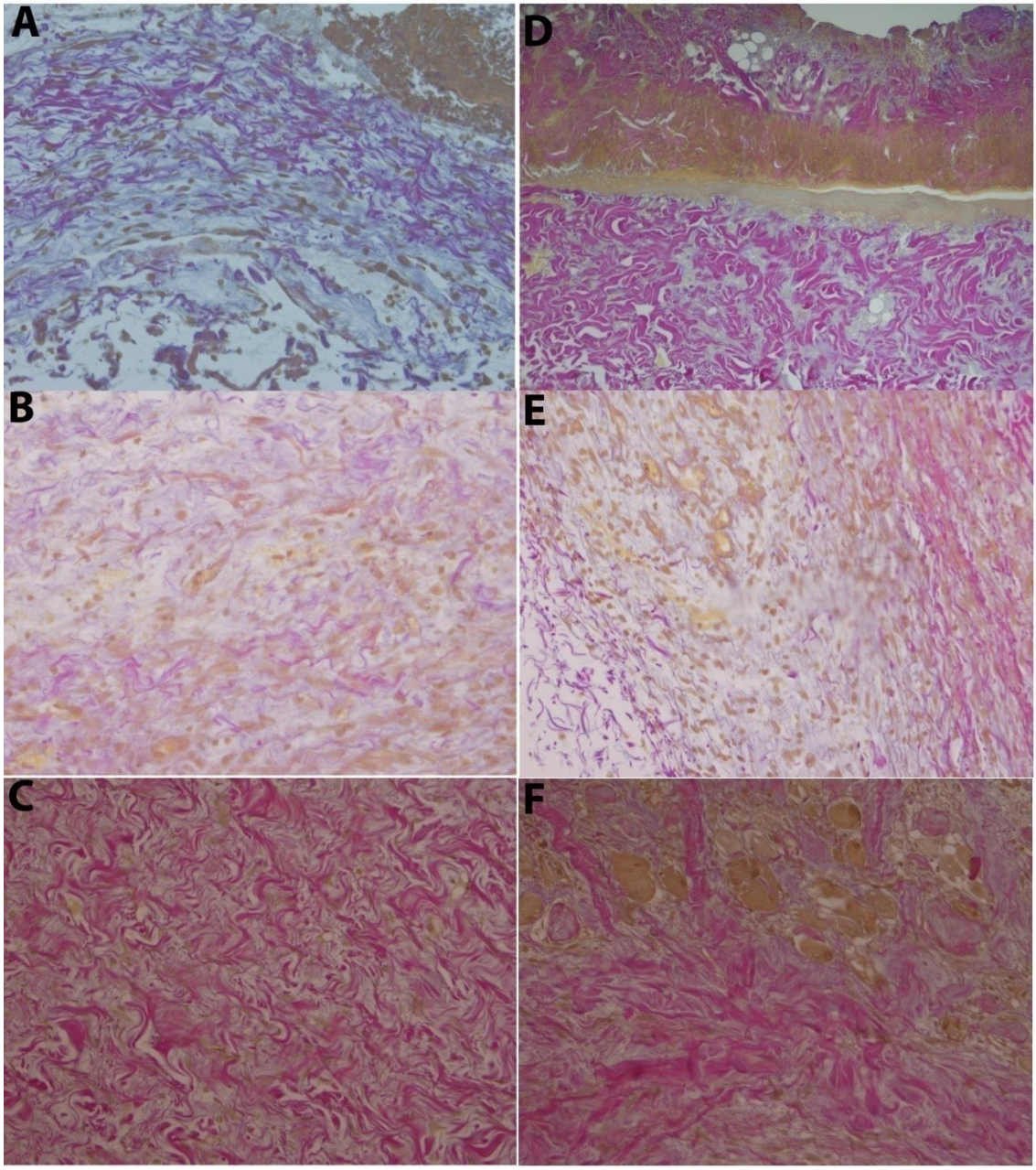

Figure 49 Herovici staining in CDS (A, B and C) and HFCDS (D, E and F) treated burn wounds (40x); 7th (A and D), 14th (B and E) and 28th (C and F) day

4.4.5 Immunohistochemistry

4.4.5.1 Immunohistochemistry with PCNA

Immunohistochemistry with PCNA (Figure 50) antibodies of non cell loaded CDS (A, B and C) and HFCDS (D, E and F) treated wounds is shown in Figure 51. On 7th day, partial (A and D) the proliferating cells were higher in HFCDS treated wounds compared to non cell loaded CDS treated wounds. On 14th day (B and E) and 28th day (C and F), the cell nuclei were smaller and some of the nuclei were elongated in both types of graft treated wounds.

4.4.5.2 Immunohistochemistry with ASMA

IHC with ASMA (Figure 51) antibodies of non cell loaded CDS (A, B and C) and HFCDS (D, E and F) treated wounds is shown in Figure 52. On 7th day, partial (A and D), the myofibroblasts were seen in both the CDS and HFCDS treated wounds. On 14th day (B and E), the ASMA were more abundant in HFCDS treated wounds compared to CDS treated wounds. On 28th day (C and F), the myofibroblast response declined in both the CDS and HFCDS graft treated wounds.

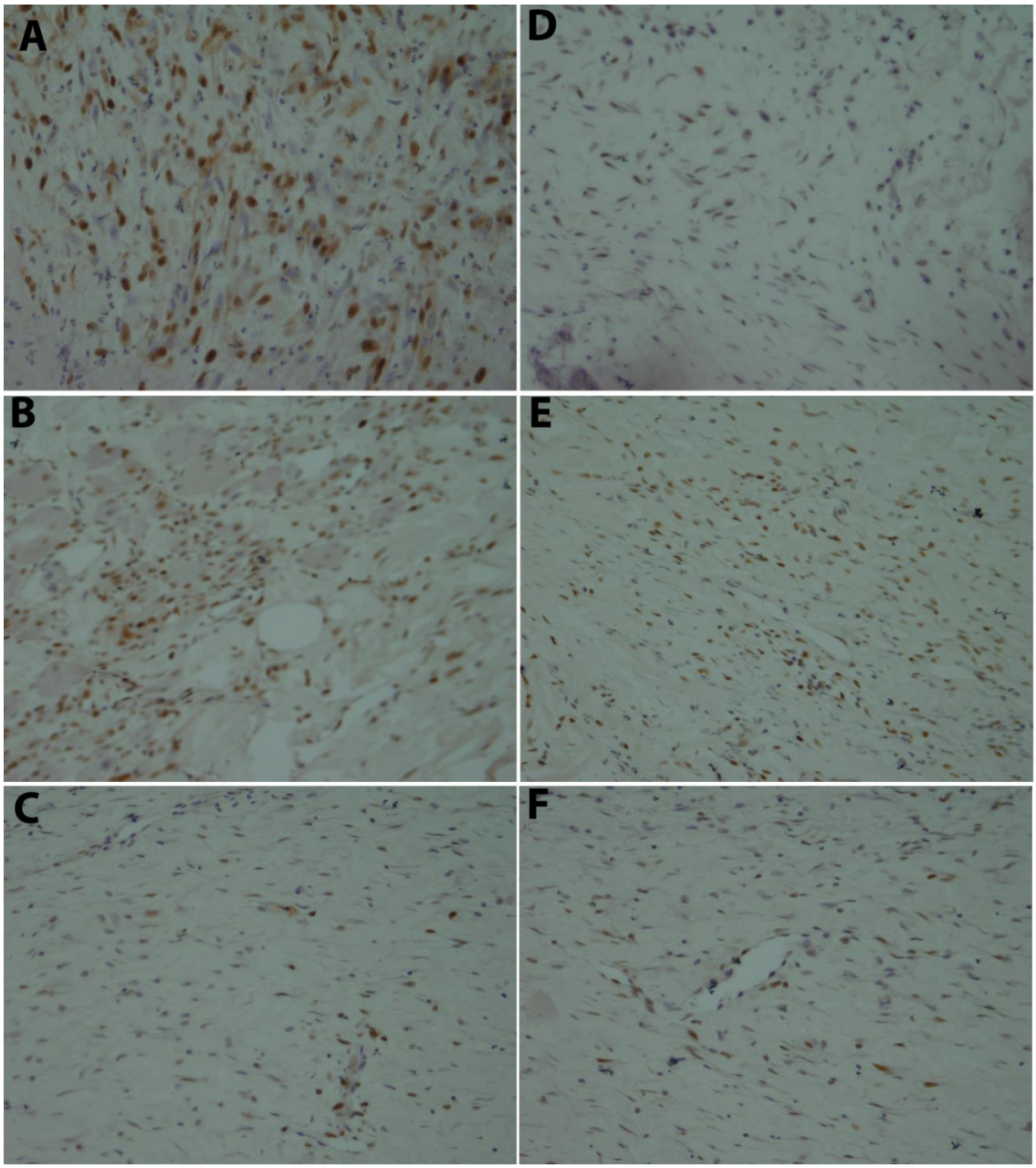

Figure 50 Immunohistochemistry with PCNA in CDS (A, B and C) and HFCDS (D, E and F) treated burn wounds (40x); 7th (A and D), 14th (B and E) and 28th (C and F) day

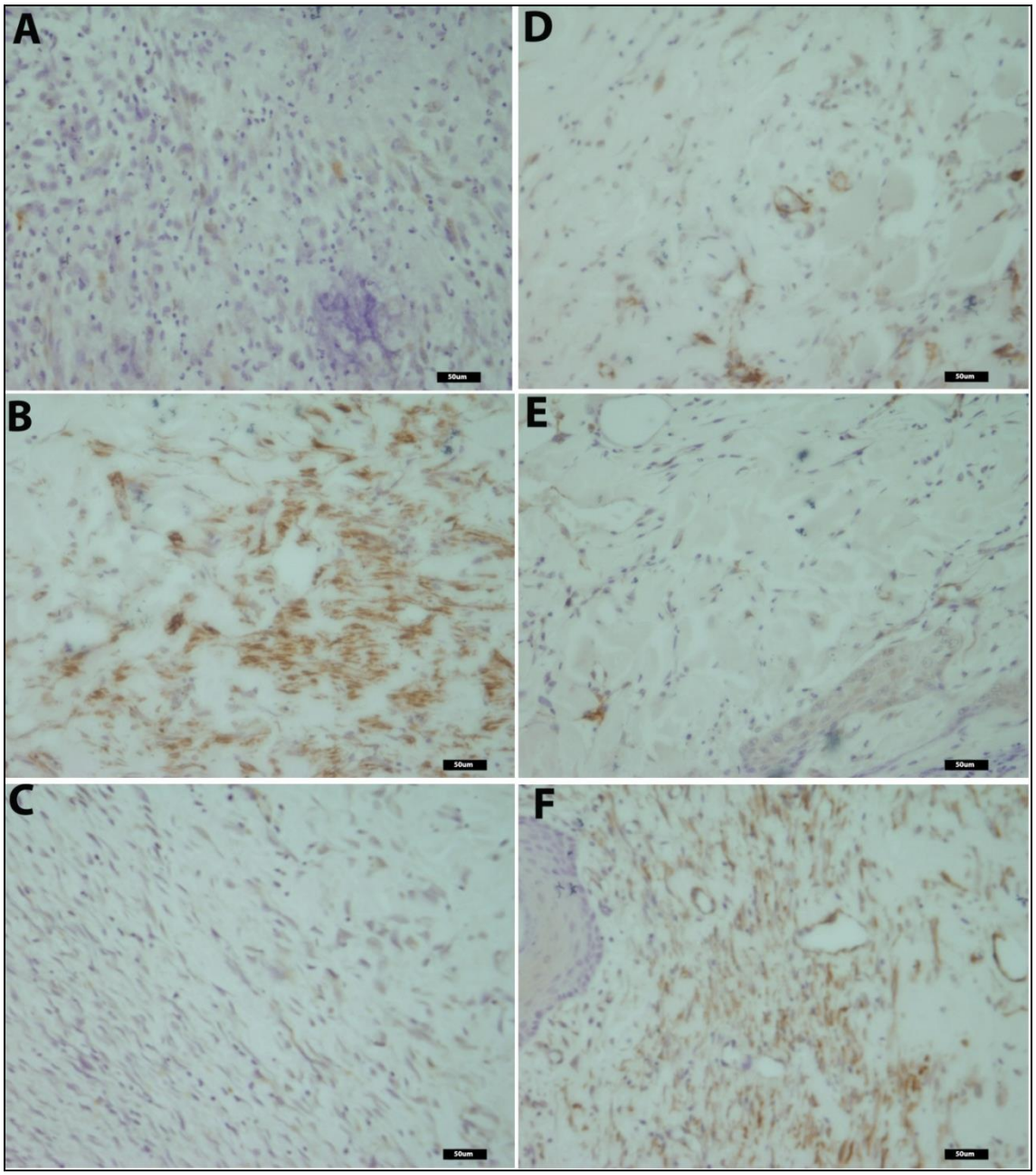

Figure 51 Immunohistochemistry with ASMA in CDS (A, B and C) and HFCDS (D, E and F) treated burn wounds (40x); 7th (A and D), 14th (B and E) and 28th (C and F) day

4.4.6 Histomorphometry

4.4.6.1 Thickness of epidermis

The epidermal thickness of skin was much higher in HFCDS treated compared to CDS treated wounds (p value = 0.0001) on day 14. There was no significant difference in epidermal thickness between CDS and HFCDS grafted wounds in 7 and 28 days of healing (Figure 52).

4.4.6.2 Extent of re-epithelialization

The extent of re-epithelialization was faster in HFCDS scaffold treated burns compared to CDS treated burns (p value = 0.01) on day 7. Complete re-epithelialization was seen in both CDS and HFCDS treated wounds during 28 days (Figure 53).

4.4.6.3 Extent of collagen deposition

The deposition of collagen was much higher in the wounds treated with HFCDS grafts on 14^{th} day when compared with CDS (p value = 0.01) treated grafts (Figure 54).

4.4.6.4 Extent of collagen remodeling

The type I collagen was always higher in skin wounds treated with HFCDS grafts in all the time points. However, there was no significant difference in the ratio of type I/type III collagen between CDS and HFCDS treated wounds at any time point (Figure 55).

4.4.6.5 Extent of neo-vascularization

There was no significant difference between the extent of neo-vascularization between HFCDS and non cell loaded CDS treated wounds (Figure 56).

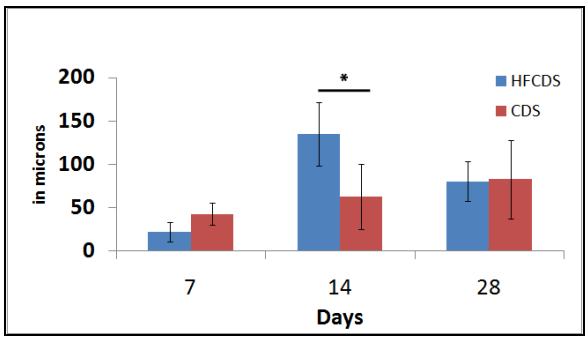

Figure 52 Thickness of epidermis (* p value ≤ 0.05)

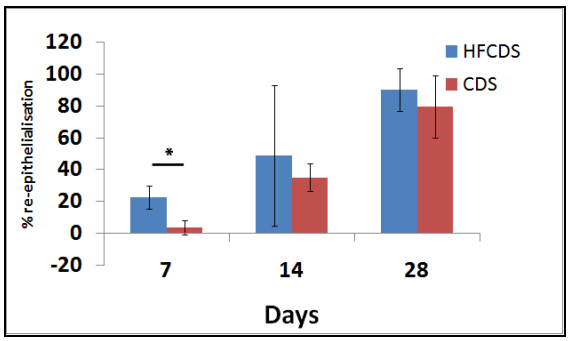

Figure 53 Extent of re-epithelialization (* p value ≤ 0.05)

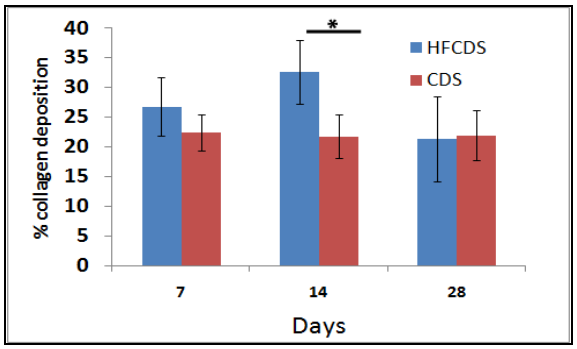

Figure 54 Extent of collagen deposition (* p value ≤ 0.05)

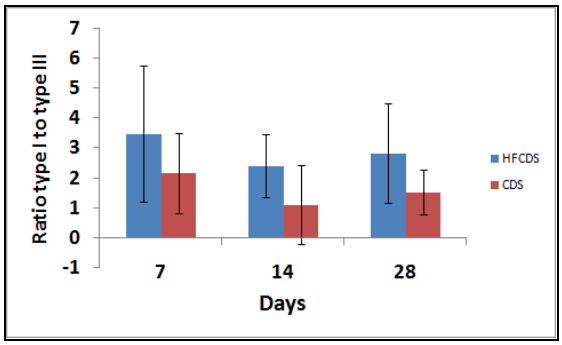

Figure 55 Ratio of type I/type III collagen (* p value ≤ 0.05)

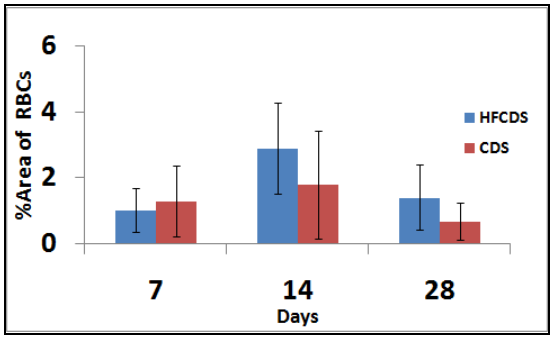

Figure 56 Extent of neo-vascularization (* p value ≤ 0.05)

4.4.6.6 Extent of cell proliferation

There was high cell proliferation in the HFCDS treated wounds compared to CDS treated wounds during 7^{th} day (p value ≤ 0.0001) and 14^{th} day (p value = 0.02). (Figure 57)

4.4.6.7 Extent of myofibroblast response

There was increased ASMA positive cells in HFCDS treated wounds with compared to non cell loaded CDS treated during 7^{th} day (p value = 0.01) as seen in Figure 58. This pattern reversed during 28 days (p value = 0.03) with CDS treated burns having higher myofibroblast compared to HFCDS treated burns.

4.4.7 *In vivo* imaging and cryosectioning

PKH26- labeled cells were tracked in the dermis of healing wound on 7 and 14 day as red fluorescence in HFCDS grafted wounds (Figure 59). The PKH26 labeling was not detected in CDS grafted wound at any time point as expected. The PKH26- labeled cells were also not detected in HFCDS treated wounds on 28 days.

This was further confirmed by scanning the sections from the HFCDS treated wounds under confocal microscope. The confocal microscopy images (Figure 60) showing cells as red dots on 7 and 14 days in the healing sections of skin detected the presence of PKH26 tagged loaded cells in HFCDS treated wounds.

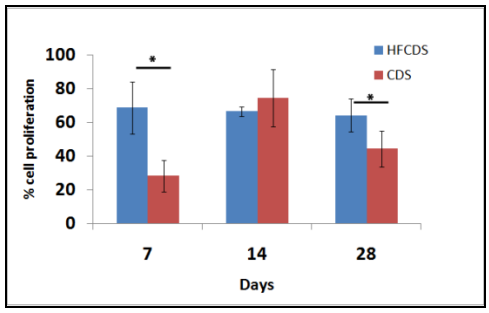

Figure 57 Extent of cell proliferation (*p value ≤ 0.05)

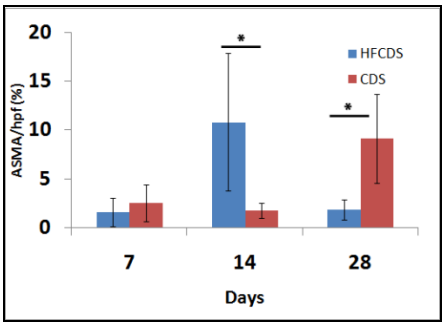

Figure 58 Extent of myofibroblast response (*p value ≤ 0.05)

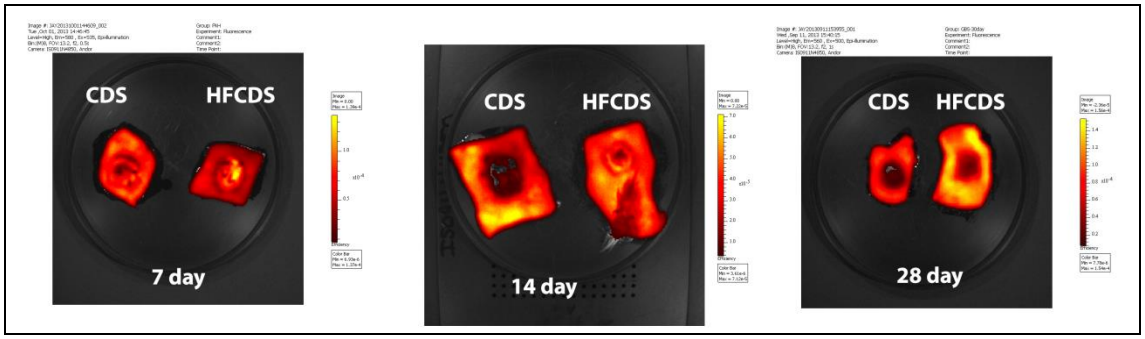

Figure 59 *In vivo* imaging of healing skin samples: The HFCDS (on left) has brighter fluorescence compared to CDS samples on 7, 14 and 28 days

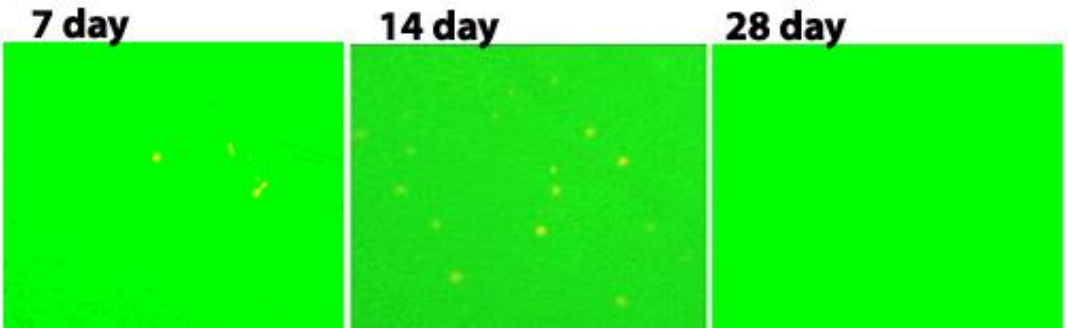

Figure 60 Confocal images of corresponding HFCDS treated wounds

Chapter 5

Discussion

SECTION 1

4.1 Fabrication and evaluation of tissue engineering scaffolds from ECM of porcine organs for skin tissue engineering

This section of the thesis examines the quality of CDS, JDS and UDS (Figure 1) prepared by a non-detergent/non-enzymatic treatment method *(Anilkumar et al., 2014)* for their suitability as potential skin-graft substitute based on their *in vitro* properties. In order to study the probable nature of cell adhesion and attachment, the surface topography and micro architecture of the scaffolds were analysed by scanning electron microscopy (Figure 2). The physiochemical properties of the different scaffolds, physical parameters like fluid uptake (Figure 3), WVTR (Figure 4), mechanical strength (Figure 5), flexural rigidity (Figure 6) and suture retention strength (Figure 7) of the scaffolds were also determined. The presence of linker proteins present in the basement membrane of skin was also examined in the scaffolds (Figure 8). The collagen, elastin, GAG (Figure 9) and DNA content (Figure 10) in the scaffolds were also quantified.

All the three scaffolds showed a highly fibrous porous surface topography (Figure 2) probably indicating their likely nature as a substrate for cellular attachment. The CDS is known to have a weakly anisotropic nature with strength and compliance in the range of physiological stress and strain *(Burugapalli et al., 2007).* It is also reported to have collagen fibre orientation that enables it for a wider range of use including multi axial loading applications *(Coburn et al., 2007).* The scaffold derived from small intestinal submucosa is also reported to have a collagen fibre orientation that ranges from cross-

hatch to random-weave pattern giving the scaffold enough porosity that can aid in cellular infiltration and rapid vasculogenesis or in growth of blood vessels. The scaffolds derived from urinary bladder submucosa have a dense microporous collagenous network in the luminous surface giving it a smooth sheet like appearance *(Callanan et al., 2012).*

The fluid uptake (Figure 3) of a scaffold gives the ability to bind fluids which is important during wound healing *in vivo* and absorption of culture medium and physiologically relevant buffers in tissue culture application *in vitro.* Cross linking is known to significantly reduce hydrophilic nature of scaffolds *(Roh et al., 1999)* and hydrophilic scaffolds are known to have higher fluid uptake ability and wider applications in tissue engineering *(Silva et al., 2013).* The CDS, JDS and UDS had 100% fluid uptake similar to the reference material and hence deemed to have the potential to provide a moist environment for healing *in vivo* and also have excellent ability to bind to fluids *in vitro* for skin tissue engineering (Figure 3).

Another important physical parameter often studied for evaluating healing potential of scaffolds is the WVTR, which indicates the ability to retain absorbed water *(Mittal and Kumar, 2012, Mi et al., 2001).* High WVTR rate might cause the wound bed to become desiccated and consequently lead to loss of integrity. It may also modulate various tissue responses in the healing wound, for example, too much water loss increases the possibility of tissue necrosis and slowing of epithelial cell migration leading to impediment of re-epithelisation and decreased oxygen availability for

bacterial killing leading to increased risk of infection and impaired nutrient flow *(Chang et al., 1996).* These are all poor prognosis for wound healing. The CDS had lower WVTR compared to JDS, UDS and the reference scaffold (Figure 4) and hence, has the potential to provide a moist environment for wound healing. Adequate moisture is also required for satisfactory activity of growth factors and proteolytic enzymes *(Bryan, 2004).* Furthermore, moisture enhances fibroblast/endothelial cell proliferation and is known to increase the immune defence of wound surface *(Jones, 2005).* Epithelial cells need a moist ground to migrate and re-epitheliate faster *(Junker et al., 2013).* Hydrated surrounding provides a better environment for healing. Indeed, hydration is required for transport of oxygen, nutrients in the form of glucose, amino acids, vitamins and mineral ions into the proliferating wound bed and also for removing wastes from active cells in healing wounds. Moisture is also required for the optimal activity of growth factors and proteolytic enzymes which can bring about speedy wound healing *(Junker et al., 2013).* The other hydration parameter, percentage fluid uptake of the CDS graft was similar with that of the commercially available reference graft. Hence, CDS was considered as a preferred skin graft for wound healing application compared to the other three scaffolds with respect to WVTR.

The Young's modulus, flexural rigidity and suture retention efficiency are three parameters that indicate suitability of a scaffold as skin graft. Flexural rigidity corresponds to the ability of a wound dressing or skin graft to drape over the wound and it should be sufficiently low. But, high flexural rigidity means a rigid scaffold that will not be flexible to be in touch with the wound surface *(Yannas and Burke, 1980).* In the

present instance, the Youngs modulus (Figure 5) and flexural rigidity of CDS (Figure 6) was similar to that of the reference product. On the other hand, CDS (2.3± 9 N) had lower suture retention ability than that of CSIS (Figure 7). But, the actual measure of the suture retention strength was higher than 1.2 N as expected for scaffold sheets used in soft tissue engineering applications *(Tran et al., 2010).* Hence, CDS has acceptable mechanical properties and can be considered for skin graft applications (Figure 4). The flexural rigidity was very low in UDS compared to JDS. The probable reason for this might be the difference in orientation of collagen between UDS *(Callanan et al., 2012)* and JDS *(Burugapalli et al., 2007).* The UDS has thinner and finer collagen fibres compared to the denser fibres of JDS which makes JDS more rigid and easier to handle than UDS. However, high flexural rigidity of a graft prevents intimate contact between the graft and wound, creating dead space and impeding wound healing *(Yannas and Burke, 1980).* The suture retention strength of JDS was also higher compared to UDS (Figure 7). But, both these scaffolds and CDS had suture retention strength of more than 1.2N which is the minimum requirement of a biomaterial for tissue engineering application *(Tran et al., 2010).* Hence, all the scaffolds CDS, JDS and UDS isolated by this method were deemed suitable for skin-tissue engineering application.

The CDS, JDS and UDS retained proteins like laminin, collagen IV and collagen VII (Figure 8) even after the treatment procedures adopted for the recovery of scaffolds from respective source organs. Considering these are important proteins in the basement membrane of the skin, the observation has significance. The endothelial cells require

laminin rich basement membrane for their assembly. Laminin has a central role in the formation of the architecture and maintenance of the stability of basement membranes. It connects different tissues, *i.e.* the parenchymal and the interstitial connective tissues. Laminin also acts as a mechanical scaffold which provide adjacent cells with biological information either directly (by interacting with cell surface components) or indirectly (by trapping growth factors). Thus, laminin can trigger as well as control various cellular functions *(Aumailley and Smyth, 1998).* The network of collagen IV is thought to define the nature of scaffold, as collagen IV is involved in integrating other components such as, laminins, nidogens or perlecan, into highly organized supramolecular architectures. This property is fundamental for the maintenance of integrity and function of basement membrane under conditions of increasing mechanical demands and also for the deposition and initial assembly of components of basement membrane. Laminin is essential for maintaining the basement membrane-like matrices during early development, but at later stages the specific composition of components including collagen IV defines integrity, stability and functionality *(Poschl et al., 2004).* Type VII collagen was identified as the protein component of anchoring fibrils that extend into the papillary dermis and entrap fibrous dermal components thus mediating the attachment and interaction of basement membrane with the dermis *(Burgeson, 1993).* Thus, all the three scaffolds obtained by the non enzymatic/non detergent method contains the essential component in the basement membrane of skin and can act as a scaffold for the migration of epithelial cells and modulate its interaction with the cells in the dermis, hence stimulating wound healing.

The CDS had higher content of macromolecules like elastin and sulphated GAGs than CSIS while the collagen content was similar (Figure 9). It was not sure if the higher elastin and sulphated GAG content reflected the native content of these molecules in normal cholecyst wall. Nevertheless, higher content of these biomolecules in CDS made it a better scaffold than SIS for skin graft application. It is known that, elastin enhances angiogenesis *(Robinet et al., 2005),* promotes proliferation of endothelial cells *(Long et al., 1989)* and also supports proliferation of dermal fibroblasts *(Rnjak et al., 2009).* The GAG facilitate specific interactions to cytokines *(Coombe, 2008)* and chemotactic growth factors which are important for wound healing as they can regulate the release of growth factors in the healing environment *(Shipp and Hsieh-Wilson, 2007).* In addition, GAG can also trap water in the form of gel and prevent loss of water *(Kirker et al., 2002)* and corroborated the observations made about CDS with respect to physical property like WVTR (Figure 4). The chemicals used in the decellularization process also can cause leeching of bio active molecules resulting in the decrease in its content. For example, use of sodium dodecyl sulphate for decellularization process is known to decrease the GAG content of scaffolds revived from animal tissues *(Faulk et al., 2014).* The CDS in the present instance was prepared using a method that does not involve the use of any chemicals, detergents or enzymes for decellularization. This might be another reason for getting better quality CDS with retention of biomolecules and also growth factors like fibroblast growth factor and vascular endothelial growth factor *(Anilkumar et al., 2014)* compared to the reference material CSIS.

Upon grafting to appropriate host, presences of excess cellular content especially DNA in a scaffold are known to cause inflammatory reactions that are not congenial for a good scaffold *(Badylak and Gilbert, 2008).* However, the CDS contained lower DNA-content compared to CSIS (Figure 10). This is probably because gall bladder is not a very cellular organ and its main functions are storage and release of bile *(Jacyna, 1990)* unlike the small intestine which is involved in digestion, peristalsis and secretion with wide absorptive surface organized into primary and secondary folding *(Laster and Ingelfinger, 1961).* Thus, compared to the reference material, the higher content of sulphated GAG and elastin and the lower content of DNA in CDS make it a preferred biomaterial for graft assisted healing and for tissue engineering application.

All the scaffolds CDS, JDS and UDS, for skin graft application, also passed preclinical safety evaluation procedures, performed according to ISO standards *(Anilkumar et al., 2014). In vitro* cytotoxicity tests as per ISO 10993 part 5 using L929 fibroblast cell lines ($2.5X10^4$ cells/well) by direct contact method, showed that the scaffolds were non cytotoxic to L929 cells (score 0). *In vivo* biocompatibility test as per ISO 10993 (Part 6 - local effects after implantation) by subcutaneous implantation in rabbit model, showed that the scaffolds were biocompatible. Test for endotoxins with Limulus amoebocyte lysate (LAL) by a kinetic chromogenic method using Endosafe PTS endotoxin, Charles river laboratories India, as per USP 23/NF18<85> showed that the scaffolds were non pyrogenic with endotoxin levels less than 0.5EU/ml. Thus having satisfied several

preclinical safety evaluation procedures, these observations indicated that CDS, JDS and UDS are candidate prototypes of skin grafts.

SECTION II

4.2 *In vivo* evaluation of the CDS, JDS, UDS and CSIS for wound healing application

In order to investigate the wound healing potential of the fabricated scaffolds two animal experiments were performed. In experiment I, the CDS along with the reference material was grafted in full thickness rabbit skin wound model, in a pre-clinical setting (Figure 11). The healing reaction of CDS was assessed by histomorphology and compared with those caused by the clinically proven graft reference material CSIS. In experiment II, the wound healing potential of JDS and UDS grafts was compared with OW as the control (Figure 12). The histomorphology observations (Figure 13- 23) were cross verified with histomorphometry data (Figure 24 - 29). The quantitative data on re-epithelialisation (Figure 24), angiogenesis pattern (Figure 25), collagen deposition (Figure 26), cell proliferation (Figure 27), the distribution of vimentin positive mesenchymal cells (Figure 28) and the distribution of ASMA-positive myofibroblasts (Figure 29) provided objective evidence on the differential healing ability of the prototypes of skin grafts. The selection of animal models and parameters for *in vivo* evaluation of progress of wound healing were based on two pilot studies conducted in rabbit model using chitosan scaffolds (Appendix I Preliminary studies).

Experiment I provided objective data about the suitability of CDS as skin grafts. Significantly, the proliferation of epidermal cells were higher in the epidermis in the CDS treated wound compared to CSIS treated wound in the proliferation phase (3 days)

and early remodelling phase (14 days). But, at the end of the healing process (30 days), as desired, there was no significant difference in re-epithelialisation, collagen deposition, angiogenesis pattern, mesenchymal infiltration and myofibroblast response. The abundance of proliferating cells in dermis was evaluated by IHC for PCNA. Higher rates of proliferation and cell turnover were observed in CDS treated wounds compared to CSIS treated wounds during the initial (3^{rd} day) phase of healing and this suggested that CDS stimulated regeneration of cells presumably those cells involved in better wound healing (Figure 18). Similarly, the cell turnover at the later remodelling phases of wound healing (14^{th} day) was also higher in the CDS-grafted wound suggesting their active participation in the remodelling process. The contributory roles of some of the important cell types especially epithelial (keratinocyte) and mesenchymal (fibroblast) was apparent *(Li et al., 2007)* when studied objectively by quantitative methods based on IHC *(Braiman-Wiksman et al., 2007).*

During the initial stages of the wound healing, fibroblasts from the surrounding healthy tissue are known to migrate and proliferate in to the wound site and within 3 - 4 days get converted to myofibroblasts *(Mutschler, 2012).* The main function of myofibroblasts in a healing wound is tissue contraction by synthesising of ECM proteins notably collagen types I-VI and XVIII, laminin, thrombospondin, glycoproteins, and proteoglycans for the dermal repair. The myofibroblasts usually goes on increasing from the inflammatory stage (3^{rd} to 4^{th} day) till the end of proliferation phase (14-15 days) and by the remodelling phase (around 21-30 days) these

myofibroblasts undergo apoptosis *(Klingberg et al., 2013)* and ASMA in fibroblasts regulate the proteins responsible for motility and contractility *(Li and Wang, 2011).*

To know the nature of this regulation, the extent of ASMA immunoreactivity in tissue section (Figure 29) was quantified and the nature of wound contraction was predicted (Figure 22 and 23). The presence of ASMA was highest during 14^{th} day in both the groups then decreased thereafter which were in accordance with previous literature *(Klingberg et al., 2013).* However, there was significant increase in the ASMA-positivity during the initial inflammatory stage of healing in CDS scaffold compared to CSIS (Figure 22). This suggested that CDS scaffold can bring about more organized healing through better wound contraction and deposition of ECM. It is remarkable to note that there has not been any excess collagen deposition at any stage and the remodelling induced by CDS and SIS was similar at 14 and 30 days.

The experiment II collected objective evidence on the nature of wound healing caused by JDS and UDS compared to an open unassisted wound on full thickness rabbit excision wound model. The extent of cell proliferation (Figure 19) in JDS and UDS was higher during 3^{rd} day compared to OW. This observation indicates quicker initiation of healing reaction in the graft-assisted healing wounds. This is because of presence of the graft that provided a platform for the cells to migrate and proliferate whereas, for OW, it was delayed. The higher proliferation rate was maintained in JDS but, in UDS it decreased by 7 days. The important cells proliferating in a granulation tissue are endothelial cells and the dermal fibroblasts which enhance angiogenesis and deposition of ECM during healing *(Demidova-Rice et al., 2012).* Thus, it may be concluded that

the graft-assisted healing caused accelerated healing than the OW and among the two scaffolds evaluated; JDS induced quicker initiation of the healing reaction than UDS. The results of PCNA IHC corroborated the notion that graft assisted healing initiated quicker healing reaction than the OW and also the process of complete healing was faster in JDS and UDS treated wounds (Figure 24) compared to OW. First, the re-epithelialisation (Figure 13 and 14) assessed in low power H and E stained slides were complete in more number of the graft assisted wounds compared to OWs by the 14th day. The process of re-epithelialisation that aids in epidermal formation (Figure 14) is important for creating physical separation between the underlying granulation tissue and the exterior *(Hanel et al., 2013).* Second, the extent of angiogenesis (Figure 15) in JDS grafted wound was initially much higher compared to UDS grafted wound (Figure 25). Rapid re-establishment of microvasculature provides better nourishment and oxygen to the hypoxic damaged tissue and hence, is a critical component in enhancing wound healing process *(Demidova-Rice et al., 2012).* Increase in angiogenesis also brings about inflammatory cells such as neutrophils and macrophages to the site which secrete various chemokines that further attract fibroblasts into the repair site. The fibroblast can secrete essential components of ECM like elastin, GAG, fibronectin *etc*, which can speed up the healing of wound. Third, vimentin immunopositive cells in JDS-treated wounds were higher, indicative of the nature of mesenchymal cell repopulation, compared to the UDS treated wound (Figure 21). The migration and stability of fibroblast are known to decrease in the absence of vimentin *(Eckes et al., 1998)* which subsequently impairs wound healing efficiency as demonstrated in vimentin null mice

(Eckes et al., 2000). Moreover, during an injury, the fibroblasts at the wound edge or/and the progenitor cells are activated which undergo expansion in number and gets converted to a migratory phenotype to help in repair function. A defining feature of such cells is their high expression of vimentin intermediate filament *(Menko et al., 2014).* Thus, expression of high vimentin in the wound bed during the initial healing phases causes better healing. In the present study, JDS showed higher mesenchymal cell re-population ability (Figure 21) compared to the UDS grafted wound. Again, these observations indicated the superior ability of JDS to promote accelerated healing reaction compared to the UDS. However, in the OW the mesenchymal cell re-population persisted even after 14 days compared to graft assisted healing, probably to make up the deficiency of cell proliferation that was evident during the initial first few days of healing in OW. This observation suggests that the fibroblast proliferation and activation have been delayed during unassisted OW healing compared to graft assisted healing responses.

The transition of fibroblast to myofibroblast is a critical event that happens in wound healing and tissue repair reactions. Myofibroblast responses are characterized by the presence of ASMA and excessive secretion of ECM component including collagen as well as matrix metalloproteases. Furthermore, these cells generate high contractile force and speed up wound healing by contracting the edge of wounds *(El Kahi et al., 2009).* Although myofibroblast reaction is desirable at early phases of healing, their persistence in the tissue induces a fibrotic response which is indicative of hypertrophic

scarring. In fact, during uneventful secondary healing responses, the myofibroblasts are supposed to undergo apoptosis and only minimal numbers persist in the tissue by the end of the healing reaction. In other words, prolonged or persistent myofibroblast reaction is deemed as an undesirable healing reaction *(Darby and Hewitson, 2007).* In the present study, the myofibroblast response peaked during 7^{th} day in JDS and declined by 14^{th} day and 30^{th} day (Figure 23). This can contribute to more wound contraction initially leading to quicker healing *(Van De Water et al., 2013).* The UDS grafts caused a weak myofibroblast response. The OW showed highest number of myofibroblast during the 14^{th} day, suggesting delayed reaction compared the JDS. Even though the myofibroblast response declined by 30 days in OW, its late persistence may also be interpreted as a tendency for scarring *(O'Leary et al., 2003).* Regulated fibroblast and myofibroblast reactions are crucial factors that determine the outcome of a wound healing reaction. Hence, JDS graft can cause faster healing compared to the UDS graft or OW with optimal myofibroblast response.

In the present study, with rabbit full thickness excision wound models, significant differences were not observed with respect to the nature of re-epithelisation (Figure 24) and collagen deposition (Figure 16 and 17) in different scaffolds. But, the ECM scaffold isolated from cholecyst, evaluated *in vivo* for use as skin-graft has the potential to act as an excellent skin-graft for wound healing applications. The JDS and UDS did not cause any differential ability for scar formation; more specifically they induced no more scarring than that of an uncomplicated second degree wound *(Demidova-Rice et al.,*

2012). The extent of collagen deposition in JDS and UDS treated wounds were also adequate (Figure 26). This observation is in consistence with the nature of the vimentin immunoreactivity (Figure 20 and 21), representing mesenchymal or fibroblast response (Figure 28) and ASMA-immunoreactivity (Figure 22 and 23) representing myofibroblast response (Figure 29). Thus, the JDS and UDS prepared by the non-detergent/non-enzymatic method was found to cause accelerated healing of rabbit full thickness skin wounds compared to unassisted wound healing reaction.

However, the CDS promoted a prominent healing reaction with enhanced cell proliferation and adequate collagen deposition. Even though, the healing potential of CDS was not compared directly with the healing ability of UDS and JDS, the quantitative histomorphometry data of the scaffolds suggest that CDS has higher proliferation potential compared to the other grafts. The CDS also has higher elastin and GAG content and it also has ability to retain moisture and provide a better healing environment that the other grafts. The CDS scaffolds thus can be argued to have superior wound healing ability because of these three main reasons when compared to the other scaffolds as skin grafts.

SECTION III

4.3 Fabrication of prototypes of cell loaded ECM scaffolds

This part of the thesis examines if the scaffolds prepared by non-enzymatic/non-detergent method *(Anilkumar et al., 2014)* is suitable for fabricating bioartificial skin grafts. In order to fabricate prototypes of bioartificial skin grafts, a screening study was conducted on CDS, JDS and UDS by seeding HaCaT cells and dermal fibroblasts. The rationale behind this was straight forward from the results of *in vitro* cytotoxicity assay conducted as part of preclinical evaluation of the potential grafts. It provided the clue that cells like L929 can grow on ECM scaffolds in tissue culture system without any toxic effect. Hence, the ECM scaffolds were seeded with two different types of skin cells.

Keratinocytes, the cells of epidermis are in direct contact with the environment *(Wysocki, 1999).* The processes of proliferation, migration and attachment of keratinocyte are some of the factors that play a vital role in the repair and regeneration of any epidermal lined organ during injury. The proliferation and differentiation of epidermal cells are primarily dependent on various clues and signals provided by the ECM of the healing wound bed *(Schultz and Wysocki, 2009).* Primarily isolated keratinocytes from skin are difficult to isolate and maintain in tissue culture without feeder layers. On the other hand, HaCaT cells are immortalized human keratinocyte which maintain full differentiation capacity with nearly regular architecture as that of the keratinocyte in the epidermis *(Schoop et al., 1999).* Therefore, HaCaT cells are

exploited for *in vitro* studies on keratinocytes. Indeed, they have all characteristics of rapidly proliferating keratinocytes in the skin. They are also easier to grow and subculture when compared to primarily isolated keratinocytes from skin *(Deyrieux and Wilson, 2007).* The various advantages of using HaCaT cells for fabrication of skin construct are that they have stable genetic character without showing tumorigencity and invasiveness with differentiation exactly similar to human keratinocytes. They are used in *in vitro* skin models and to substitute human keratinocytes in experiments. Hence, in this study HaCaT cells were initially used to evaluate the behavior of the epidermal cell on these three ECM scaffolds. There are reports of HaCaT cells seeded on scaffolds made of collagen-chitosan *(Sarkar et al., 2013),* poly (ε-caprolactone) *(Gazzarri et al., 2013)* and urethane *(Sarkar et al., 2006),* that are used for wound healing application. The scaffolds from small intestinal submucosa are known to support the growth of human keratinocytes *(Lindberg and Badylak, 2001).* Epidermal cells when seeded alone in small intestinal submucosa formed well differentiated epithelial like structures on the scaffold but with less organization. These models can be used to understand the regulation mechanisms of epidermal cell adhesion, migration and proliferation during wound healing *(Lindberg and Badylak, 2001).* The scaffold from urinary bladder is also reported to support HaCaT cells for wound healing application *(Brehmer et al., 2007).*

The apparent surface morphology of HaCaT cells after H and E staining and immunofluorescence seemed similar in all the three ECM scaffolds. The HaCaT cells showed their typical cobblestone appearance in culture conditions (Figure 30). After direct immunofluorescence staining using phalloidin antibodies, the HaCaT cells were

seen to grow as layer over the ECM scaffolds with surface attachment and cell spreading (Figure 32). The HaCaT cells showed layer formation over the three scaffolds in H and E stained sections (Figure 33). MTT assay showed steady spread of cells evidenced by increase in the viability of cells over time in all three scaffolds (Figure 31). HaCaT cells were seen proliferating on the ECM scaffold as confirmed by immunohistochemistry with PCNA antibodies (Figure 34). Immunohistochemistry using involucrin showed that HaCaT cells were in a highly differentiated state and actively involved in barrier function (Figure 35). Involucrin is the marker for terminal differentiation. They are present in the keratohyalin granules of stratum granulosum. Involucrin are precursor proteins involved in the crosslinkage of the envelopes in the outermost stratum corneum of skin in later stages in the life cycle of the keratinocyte. The HaCaT cells also expressed Vitamin D receptors as demonstrated by IHC (Figure 36). Both Vitamin D receptors and involucrin positivity by HaCaT cells in the culture confirmed that cells are functionally active.

HaCaT cells are known to form multilayer on exposure to air providing excellent opportunity for skin tissue engineering applications *(Boelsma et al., 1999).* At specific regions on the gall bladder and UDS, the HaCaT cells apparently showed formation of bilayer (Figure 33). The presence of calcium concentration is known to have specific role in the stratification of HaCaT cells *(Micallef et al., 2009)*. The chance of presence of extraneous calcium level is higher in gall bladder and urinary bladder compared to small intestine as the former are organs involved with the function of storage of secretion (bile) and excretion (urine) fluids which could be rich in ions

including calcium. This perhaps might have caused multiple layer formation of HaCaT cells on these scaffolds (Figure 33). However, collection of further evidences is required to conclude on the stratification or multilayering of keratinocytes in the tissue engineered construct.

Human epithelial skin models are excellent alternatives to *in vivo* animal models used for testing of pharmaceutical cosmetics and chemical compounds *(Netzlaff et al., 2005, Welss et al., 2004).* The 2D electronspun polystyrene matrix used to demonstrate the role of fibroblasts in the organization and differentiation of keratinocytes in dermis do not have any of the specialized 3 D structural organization of the different types of collagen present in the native dermis that is more suited for show the true physiological response to cytotoxic agents *(Sun et al., 2006).* Hence, ECM scaffold having basement membrane proteins similar to skin may be a better scaffold for developing an *in vitro* skin model for studying the interplay between skin keratinocytes and fibroblasts. *In vitro* keratinocytes skin model is also extensively used to study the interaction between tumor and healthy skin cells and mechanisms of inflammations. The interaction between the tumor cell and adjacent skin cell determine the invasion of tumor cells to undamaged area *(Eves et al., 2000).* The *in vitro* skin model can also used in studying skin diseases such as psoriasis *(Barker et al., 2004),* human epidermal bullosa and also in gene therapy application *(Ferrari et al., 2006).* Hence, the HaCaT cell loaded ECM tissue engineered construct has another dimension as a potential viable *in vitro* model to *in vivo* animal testing.

The second cell type chosen for evidence was dermal fibroblasts. The rationale was based on the following. Human dermal fibroblast cultured on small intestine submucosa seeded with dermal fibroblasts along with ascorbic acid or fibronectin enhanced deposition of type I collagen and increased in thickness in ultra structure morphology. The small intestine submucosa acts as a template for neo-tissue formation rather than a scaffold as there was minimal tissue invasion by the dermal fibroblasts *(Cimini et al., 2005).* In the present study, all the three scaffolds CDS, JDS and UDS supported the growth of dermal fibroblasts from rabbit. MTT assay revealed above 100% viability (Figure 40) of rabbit dermal fibroblasts on ECM scaffolds and scanning electron microscopy analysis showed spreading and attachment of rabbit fibroblasts on all the ECM scaffolds (Figure 41). However, only the fibroblasts loaded CDS (Figure 42) was used for subsequent animal experiment. The CDS scaffolds had higher biomolecules such as elastin and GAG compared to the other scaffolds. The CDS was found to be less immunogenic and they had a fewer residual nuclei compared to the other scaffolds. The CDS also had low WVTR capable of providing a moist healing environment. Hence, the formulated tissue construct containing CDS loaded with homologous dermal fibroblast was used to treat cutaneous burn wounds induced in rabbit.

SECTION IV

4.4 *In vivo* evaluation of wound healing by HFCDS scaffold in full thickness burn model

The most common reason for skin loss is due to trauma especially burns. An estimate of 265 000 deaths/year occur due to burns worldwide. Nearly, half of them are occurring in South East Asia. In India alone, over 1000000 burn cases are reported every year (WHO fact sheets on burn, 2014). The seriousness of burn wounds depends on its extent and depth. Full thickness burns are complicated wounds with significant loss of tissue and cells compared to first degree burn (involving only epidermis) wounds or second degree burn (involving epidermis and some portion of dermis) wounds. The full thickness burns may also reach into the subcutaneous fat or deeper. There is charring and wound looks black or white without any pain or sensations. The healing burn wounds having three distinct zones are – Zone of coagulation is the area where there is the coagulation of tissue and blood vessel which causes a region of irreversible death. Surrounding such a zone is the area of restricted blood flow coagulation called the zone of stasis. The region forming the interface between the wound and the undamaged tissue at the edge of the uninjured area is the zone of hyperemia *(Shakespeare, 2001).*

The healing pattern in a burn wound is extensively different and more problematic than the healing pattern seen in the excision wounds. There is significant loss and destruction of tissue primarily due to necrosis leading to deficiency of growth factors. In addition, there is higher susceptibility to infection *(Church et al., 2006)* due to lack of

barrier function and immune-compromised condition of the patient. Hence, the main issue is the lack of availability of cells and matrix. Tissue engineering approach in treating burn wounds addresses both these deficiencies. The matrix is expected to provide protection from infection and act as a barrier. CDS is known to aid speedy healing of full thickness excision wound in alpine model (as described in experiment I). Hence, CDS loaded with autologous fibroblasts is expected to supply both cells in the form of fibroblast and protective matrix. The CDS has various growth factors which contribute to building up of tissues in burn wound while the deficiency of cells in burn wounds can be compensated with the addition of viable cells. The main advantage of using allogeneic fibroblast is that it saves a lot of time, as pre-fabricated off shelves products can be made available for the immediate treatment of burn treatment. Yet, the golden standard still remains the use of autologous cultured cells to fabricate wound healing substitutes for burn wounds *(Andreassi et al., 2005).* Biopsies from skin can be used as a source of explants to isolate fibroblasts for the fabrication of a tissue construct on suitable scaffold in shortest possible time.

The healing potential of the homologous dermal fibroblast loaded CDS in an animal model was compared with the non cell loaded CDS scaffolds using histomorphometry techniques. For this purpose, the first challenge was to create uniform full thickness burn wounds in every rabbit involved in the experiment without other peril-operative complications. Therefore, a device (Figure 43) was fabricated to induce uniform burns in rabbit model. This was achieved by removing the nozzle of a soldiering station having a proper temperature control and attaching a brass template of

1cm x 1cm size by replacing the nozzle in the soldiering station. This helped to have perfect control the over the temperature on the brass template which is pressed over the rabbit skin with uniform pressure for 45 seconds to make burn wounds. Using this modified technique, third degree burns of uniform size and thickness were made on rabbit dorsum *(Tajik and Jalali, 2007).* A pilot study was conducted to study the normal histology and histopathology of burn wounds induced by this fabricated device in rabbit models. Histology of burn wounds created as a part of the study gave confidence on the uniformity of the wounds created by the fabricated device. The details of pilot study are recorded in Appendix II.

The progression of wound healing was successfully evaluated using histomorphometry techniques which quantified various wound healing parameters in four independent *in vivo* experiments with rabbit full thickness excision wound model. Two of the studies involved comparative evaluation of acellular bioartificial graft fabricated using CDS and CSIS and JDS, UDS and OW which is discussed in detail in chapter 4, in the session 2 - '*In vivo* evaluation of the CDS, JDS, UDS and CSIS for wound healing application as experiment I and experiment II. The other two experiments (abstracts given in Appendix II) involved comparative evaluation of cell loaded chitosan based bioartificial skin grafts. In the first experiment, the wound healing potential of homologous fibroblast loaded on to chitosan sponge (HFLC) was compared with non cell loaded chitosan sponge (NCC) *(Revi et al., 2013).* It was observed that the HFLC showed a significant rise in angiogenesis epidermal thickness and percentage proliferation of cells in both dermis and epidermis clearly indicating

differential healing pattern of cell loaded chitosan skin graft with advance of time. Significantly, the abundance of cell population noticed was at the expense of decreased collagen deposition in the HFLC graft a desirable wound healing property. In Experiment II co-cultured fibroblast and keratinocyte were seeded on to the chitosan scaffold and its wound healing potential was evaluated *(Revi et al., 2014).* The observations in the paper suggested that the cell loaded chitosan grafts aided differential pattern of healing with lower scarring tendency.

In the present study, HFCDS induced differential wound healing reaction compared to non cell loaded CDS in full thickness burn wound. As observed by histomorphometry analysis of the healing wound, fibroblast loaded CDS induced thicker epidermis, higher cell proliferation and initial high myofibroblast response compared to CDS grafted alone. Thicker epidermis in the initial stages of healing provides a higher barrier protective function from the environment as well as infection *(Denda et al., 1998).* The addition of fibroblast is known to induce the proliferation of keratinocytes through secretion of various growth factors with increase in the proliferation and survival potential of keratinocytes *(Wang et al., 2012).* In the HFCDS graft treated burns, this might explain the reason for thicker epidermis (Figure 52). The growth factors secreted by the loaded fibroblasts are known to increase the overall proliferation of cells by secretion of various growth factors *(Darby and Hewitson, 2007).* In the HFCDS graft treated burns, this was evidenced by the increase in the higher cell proliferation during 14^{th} day (Figure 57). Hence, the *in vitro* loading of fibroblast in CDS has many added

advantages favorable for healing burn wounds compared to bare CDS treated burn wounds.

The homologous fibroblasts loaded on to CDS, tagged with the PKH26 dye, which a commonly used dye to track cells in experiments *(Strauss et al., 2011),* were detected in the healing dermis, during the *in vivo* experiment. It was found the labeled homologous fibroblasts were present in the healing dermis up to 14 days during the *in vivo* wound healing experiment. Fibroblast sprayed or transplanted on to the wound was known to survive till 7^{th} day in rabbit excision wound model in an earlier study *(Sandulache et al., 2003).* In prior wound healing experiments using porcine model also the fibroblast survived in the healing wound up to at least for 7 days *(Price et al., 2004).* But, fibroblast attached on to a matrix may have longer ability to survive compared to fibroblast provided alone without the presence of a matrix. This might probably be due to the fact that the scaffold/matrix provided a platform for attachment and growth, hence have higher survival rate unlike the sprayed free fibroblasts that needs to home a suitable niche to attach in the hostile wound healing environment containing inflammatory and immune cells. In another experiment similar to this study, using guinea pigs treated with PKH26 tagged allogeneic as well as autologous fibroblasts loaded ECM matrix, it was found that the fibroblasts were viable up to three weeks irrespective of allogencity or autogencity of the cells *(Morimoto et al., 2005).* However, in that study, the re-epithelialization was faster in autologous loaded fibroblast ECM compared to allogeneic loaded fibroblast ECM. In real clinical condition, there are

reports on longer survival of allogeneic fibroblasts. For example, fetal fibroblast alone with keratinocytes on collagen type I matrix, the cells were found to be viable up to 6 weeks in immune-competent human subjects *(Griffiths et al., 2004).* In yet another example of clinical conditions, new born fibroblast (allogeneic) along cultured on porcine collagen coated nylon mesh *(Kumar et al., 2004)* was found also to be effective for burns *(Juhasz et al., 2010).* The present study demonstrated that homologous fibroblasts loaded on porcine cholecyst derived matrix are viable up to 14 days and improved the healing of burn wounds in rabbit model. This also has implications that the CDS is a less immunogenic matrix (*Muhamed et al., 2014*) and can act a carrier to deliver fibroblasts in case of skin tissue damage and deficiency such as in burn wounds. However, further research is needed to explore the potential and modulatory effect of CDS in the application of delivering cells like keratinocytes, growth factors and cytokines into wound healing region of skin tissue damage.

Chapter 6

Summary and Conclusion

6.1 Summary

- Scaffolds can be fabricated from porcine small intestine, urinary bladder and cholecyst without using any enzymes or detergent. Such scaffolds have wound healing potential similar to commercial products developed from porcine small intestine submucosa and currently used in clinical wound healing application.
- The cholecyst derived scaffold has the capacity to produce a moist environment during graft assisted repair which is important for speedy progression of wound healing because of its low water vapor transmission rate and increased fluid uptake by weight.
- The jejunum derived scaffold and urinary bladder derived scaffold prepared by the non enzymatic/non detergent method have similar water vapor transmission rate and fluid uptake to the commercially available products.
- The cholecyst derived scaffold, jejunum derived scaffold and urinary bladder derived scaffold prepared by this method had sufficient suture retention strength and flexural rigidity and hence, can be used in soft tissue engineering application.
- The cholecyst derived scaffold, jejunum derived scaffold and urinary bladder derived scaffold prepared by this method preserved various biomolecules in the

scaffold such as laminin, collagen VI, collagen VII, collagen elastin and glucosaminoglycans. However, the cholecyst derived scaffold showed higher elastin and glucosaminoglycans content compared to the reference material which implies potential for better wound healing compared to other biosaffolds.

- The jejunum derived scaffold and urinary bladder derived scaffold prepared by this method had similar DNA content, but the cholecyst derived scaffold had lower DNA content compared to the reference material.
- The cholecyst derived scaffold, jejunum derived scaffold and urinary bladder derived scaffold had the potential to act as acellular bioartificial grafts for cutaneous wound healing. When used as grafts all the three scaffolds induced faster healing of full thickness excision skin wounds in rabbit models.
- The cholecyst derived scaffold, jejunum derived scaffold, urinary bladder derived scaffold and the reference scaffold, showed similarity in their ability to induce re-epithelialization and collagen deposition during healing of full thickness skin wound in rabbit. Among the scaffolds evaluated, cholecyst derived scaffold had higher cell proliferation during the initial stages of healing compared to the commercial product as shown by IHC to proliferating cell nuclear antigen antibodies.
- The cholecyst derived scaffold also showed similar percentage of mesenchymal cell infiltration compared to the reference material. However, the initial percentage of myofibroblast response was higher in cholecyst derived scaffold

treated wound compared to the reference material. This observation indicated faster wound healing response by the scaffold.

- All the three scaffolds had porous fibrous surface topography capable of supporting cell attachment, proliferation and differentiation.
- All the three scaffolds could act as matrix for the growth of skin cells of both epidermal and dermal origin.
- The epidermal cells of the skin, HaCaT, grew as layers over the cholecyst derived scaffold, jejunum derived scaffold and urinary bladder derived scaffold and assumed cobblestone morphology.
- The lapine dermal fibroblasts adhered and grew on the cholecyst derived scaffold, jejunum derived scaffold and urinary bladder derived scaffold. The lapine fibroblast loaded cholecyst derived scaffold was selected to treat full thickness burn wound in rabbit model.
- The homologous fibroblasts loaded cholecyst derived scaffold, when used as skin grafts for treating full thickness burn wound healed them in 28 days.
- The loaded homologous fibroblasts in the skin grafts were trackable in the healing dermis up to 14 days *in vivo*. Indicated that the cells survived at least for 14 days in healing region of burn wound.
- The homologous cell loaded cholecyst derived scaffold showed thicker epidermis and faster re-epithelialization and higher collagen deposition compared non cell loaded cholecyst derived scaffold while healing full thickness burn wounds in rabbit model.

- The homologous cell loaded cholecyst derived scaffold also induced higher cell proliferation and myofibroblasts response compared non cell loaded cholecyst derived scaffold in full thickness burn wounds in rabbit model as revealed by immunohistochemistry to proliferating cell nuclear antigen and alpha smooth muscle actin.
- This loading of homologous fibroblasts over cholecyst derived scaffold caused faster healing of burn wounds in rabbit compared to cholecyst derived scaffold alone as grafts.

- Use of specific histology markers to quantify parameters such as re-epithelialization, epidermal thickness, collagen deposition, collagen remodeling, cell proliferation, mesenchymal infiltration and myofibroblasts response and subsequent image analysis are good strategies for quantification of histomorphological observations.

- Quantification of histomorphological findings during *in vivo* wound healing studies may substantially assist in interpretation of data and possibly predict the progress of the healing reaction.

6.2 Conclusion

- The cholecyst derived scaffold, jejunum derived scaffold and urinary bladder derived scaffold prepared by non enzymatic/non detergent method have desirable physical and mechanical properties for skin graft application.

    - Cholecyst derived scaffold retained biomolecules such as elastin and sulphated glucosaminoglycans with low DNA content.
- When used as grafts, the cholecyst derived scaffold, jejunum derived scaffold and urinary bladder derived scaffold prepared by non detergent/non enzymatic method healed full thickness excision wound in rabbit model.
    - Cholecyst derived scaffold induced faster healing response.
- The cholecyst derived scaffold, jejunum derived scaffold and urinary bladder derived scaffold can be used for fabricating cell loaded bioartificial skin grafts
    - Cholecyst derived scaffold supported the growth of epidermal cells and dermal fibroblasts.
- Cholecyst derived scaffold and homologous lapine fibroblast loaded cholecyst derived scaffold healed full thickness burn wounds induced on rabbit dorsal skin.
    - The homologous fibroblast loaded cholecyst derived scaffold induced faster healing of burn wounds in rabbit compared to cholecyst derived scaffold alone.
- Quantitative histomorphology is probably potential tool for evaluating wound healing progression during animal experiments.

6.3 Limitations and future prospectus

- The present study did not involve *in vitro* characterization of human keratinocytes and human fibroblasts in the ECM scaffold. For fabrication of

complete skin, cells of both epidermis and dermis such as melanocytes, endothelial cells, dendritic cells alone with keratinocytes and fibroblast should also be included in the culture system. Hence, future study involving co-culture systems containing different types of skin cells on the ECM scaffolds and it' s *in vitro* evaluation is envisaged.

- The present study only evaluated the healing potential of extracellular matrix scaffolds as acellular skin grafts on 1 x 1 cm full thickness excision and healing potential of homologous fibroblast loaded cholecyst derived scaffolds as cell loaded skin grafts on 1 x 1 cm burn wounds. The potential of extracellular matrix scaffolds to heal diabetic ulcers and very large size wounds in higher species similar to human beings like pig and monkey has to be studied.
- The study does not involve seeding of any stem cells on the ECM scaffolds and the *in vitro* characterization of the construct. The present study also does not use the ECM scaffolds as a vehicle for delivery of growth factors into the healing wounds. Hence, the study on behavior of stem cells on ECM scaffolds and use of ECM scaffolds for gene delivery applications also needs to be studied in detail.

Reference

Achora S, Muliira JK, Thanka AN (2014) Strategies to promote healing of split thickness skin grafts: an integrative review. *J Wound Ostomy Continence Nurs* 41**:**335-9; quiz E1-2.

Adams DC, Ramsey ML (2005) Grafts in dermatologic surgery: review and update on full- and split-thickness skin grafts, free cartilage grafts, and composite grafts. *Dermatologic Surgery* 31**:**1055-67.

Alrubaiy L, Al-Rubaiy KK (2009) Skin substitutes: a brief review of types and clinical applications. *Oman Med J* 24**:**4-6.

Andreassi A, Bilenchi R, Biagioli M, D'Aniello C (2005) Classification and pathophysiology of skin grafts. *Clin Dermatol* 23**:**332-7.

Anilkumar TV, Vineetha VP, Revi D, Muhamed J, Rajan A (2014) Biomaterial properties of cholecyst-derived scaffold recovered by a non-detergent/enzymatic method. *J Biomed Mater Res B Appl Biomater* 102**:**1506-16.

Ansaloni L, Catena F, Coccolini F, Gazzotti F, D'Alessandro L, Pinna AD (2009) Inguinal hernia repair with porcine small intestine submucosa: 3-year follow-up results of a randomized controlled trial of Lichtenstein's repair with polypropylene mesh versus Surgisis Inguinal Hernia Matrix. *American Journal of Surgery* 198**:**303-12.

Aumailley M, Smyth N (1998) The role of laminins in basement membrane function. *Journal of Anatomy* 193**:**1-21.

Badylak SE, Gilbert TW (2008) Immune response to biologic scaffold materials. *Seminars in Immunology* 20**:**109-116.

Badylak SF (2007) The extracellular matrix as a biologic scaffold material. *Biomaterials* 28**:**3587-93.

Badylak SF, Freytes DO, Gilbert TW (2009) Extracellular matrix as a biological scaffold material: Structure and function. *Acta Biomaterialia* 5**:**1-13.

Barker CL, McHale MT, Gillies AK, Waller J, Pearce DM, Osborne J, Hutchinson PE, Smith GM, Pringle JH (2004) The development and characterization of an *in vitro* model of psoriasis. *J Invest Dermatol* 123**:**892-901.

Bibbo C (2010) The porcine small intestinal submucosa (SIS) patch in foot and ankle reconstruction. *J Foot Ankle Surg* 49**:**123-7.

Blais M, Parenteau-Bareil R, Cadau S, Berthod F (2013) Concise review: tissue-engineered skin and nerve regeneration in burn treatment. *Stem Cells Transl Med* 2**:**545-51.

Boelsma E, Verhoeven MCH, Ponec M (1999) Reconstruction of a human skin equivalent using a spontaneously transformed keratinocyte cell line (HaCaT). *Journal of Investigative Dermatology* 112**:**489-498.

Braiman-Wiksman L, Solomonik I, Spira R, Tennenbaum T (2007) Novel insights into wound healing sequence of events. *Toxicologic Pathology* 35**:**767-779.

Brehmer B, Rohrmann D, Becker C, Rau G, Jakse G (2007) Different types of scaffolds for reconstruction of the urinary tract by tissue engineering. *Urol Int* 78**:**23-9.

Breyer BN, Brant WO, Garcia MM, Bella AJ, Lue TF (2007) Complications of porcine small intestine submucosa graft for Peyronie's disease. *J Urol* 177**:**589-91.

Bryan J (2004) Moist wound healing: a concept that changed our practice. *J Wound Care* 13**:**227-8.

Burgeson RE (1993) Type-Vii Collagen, Anchoring Fibrils, and Epidermolysis-Bullosa. *Journal of Investigative Dermatology* 101**:**252-255.

Burugapalli K, Chan JC, Kelly JL, Pandit A (2008) Buttressing staples with cholecyst-derived extracellular matrix (CEM) reinforces staple lines in an ex vivo peristaltic inflation model. *Obes Surg* 18**:**1418-23.

Burugapalli K, Chan JC, Naik H, Kelly JL, Pandit A (2009) Tailoring the properties of cholecyst-derived extracellular matrix using carbodiimide cross-linking. *J Biomater Sci Polym Ed* 20**:**1049-63.

Burugapalli K, Pandit A (2007) Characterization of tissue response and in vivo degradation of cholecyst-derived extracellular matrix. *Biomacromolecules* 8**:**3439-51.

Burugapalli K, Thapasimuttu A, Chan JC, Yao L, Brody S, Kelly JL, Pandit A (2007) Scaffold with a natural mesh-like architecture: isolation, structural, and *in vitro* characterization. *Biomacromolecules* 8**:**928-36.

Callanan A, Davis NF, Walsh MT, McGloughlin TM (2012) Mechanical characterisation of unidirectional and cross-directional multilayered urinary bladder matrix (UBM) scaffolds. *Med Eng Phys* 34**:**1368-74.

Chan BP, Leong KW (2008) Scaffolding in tissue engineering: general approaches and tissue-specific considerations. *Eur Spine J* 17 Suppl 4**:**467-79.

Chan JC, Burugapalli K, Naik H, Kelly JL, Pandit A (2008) Amine functionalization of cholecyst-derived extracellular matrix with generation 1 PAMAM dendrimer. *Biomacromolecules* 9**:**528-36.

Chang H, Wind S, Kerstein MD (1996) Moist wound healing. *Dermatol Nurs* 8**:**174-6, 204.

Church D, Elsayed S, Reid O, Winston B, Lindsay R (2006) Burn wound infections. *Clin Microbiol Rev* 19**:**403-34.

Cimini M, Boughner DR, Ronald JA, Johnston DE, Rogers KA (2005) Dermal fibroblasts cultured on small intestinal submucosa: Conditions for the formation of a neotissue. *Journal of Biomedical Materials Research Part A* 75**:**895-906.

Cintron JR, Abcarian H, Chaudhry V, Singer M, Hunt S, Birnbaum E, Mutch MG, Fleshman J (2012) Treatment of fistula-in-ano using a porcine small intestinal submucosa anal fistula plug. *Tech Coloproctol*

Coburn JC, Brody S, Billiar KL, Pandit A (2007) Biaxial mechanical evaluation of cholecyst-derived extracellular matrix: a weakly anisotropic potential tissue engineered biomaterial. *J Biomed Mater Res A* 81**:**250-6.

Coombe DR (2008) Biological implications of glycosaminoglycan interactions with haemopoietic cytokines. *Immunol Cell Biol* 86**:**598-607.

Currie LJ, Sharpe JR, Martin R (2001) The use of fibrin glue in skin grafts and tissue-engineered skin replacements: a review. *Plast Reconstr Surg* 108**:**1713-26.

Darby IA, Hewitson TD (2007) Fibroblast differentiation in wound healing and fibrosis. *Int Rev Cytol* 257**:**143-79.

Darwish A (2011) *Indications of Skin Graft*,INTECH Open Access Publisher,

Demidova-Rice TN, Durham JT, Herman IM (2012) Wound Healing Angiogenesis: Innovations and Challenges in Acute and Chronic Wound Healing. *Adv Wound Care (New Rochelle)* 1**:**17-22.

Denda M, Sato J, Masuda Y, Tsuchiya T, Koyama J, Kuramoto M, Elias PM, Feingold KR (1998) Exposure to a dry environment enhances epidermal permeability barrier function. *J Invest Dermatol* 111**:**858-63.

Deyrieux AF, Wilson VG (2007) *In vitro* culture conditions to study keratinocyte differentiation using the HaCaT cell line. *Cytotechnology* 54**:**77-83.

Diegelmann RF, Evans MC (2004) Wound healing: an overview of acute, fibrotic and delayed healing. *Front Biosci* 9**:**283-9.

Dreno B (2009) [Anatomy and physiology of skin and cutaneous annexes]. *Ann Dermatol Venereol* 136 Suppl 6**:**S247-51.

Eckes B, Colucci-Guyon E, Smola H, Nodder S, Babinet C, Krieg T, Martin P (2000) Impaired wound healing in embryonic and adult mice lacking vimentin. *J Cell Sci* 113 (Pt 13)**:**2455-62.

Eckes B, Dogic D, Colucci-Guyon E, Wang N, Maniotis A, Ingber D, Merckling A, Langa F, Aumailley M, Delouvee A, Koteliansky V, Babinet C, Krieg T (1998) Impaired mechanical stability, migration and contractile capacity in vimentin-deficient fibroblasts. *J Cell Sci* 111 (Pt 13)**:**1897-907.

El Kahi CG, Atiyeh BS, Abdallah Hajj Hussein I, Jurjus R, Dibo SA, Jurjus A (2009) Modulation of wound contracture alpha-smooth muscle actin and multispecific vitronectin receptor integrin alphavbeta3 in the rabbit's experimental model. *Int Wound J* 6**:**214-24.

Eves P, Layton C, Hedley S, Dawson RA, Wagner M, Morandini R, Ghanem G, Mac Neil S (2000) Characterization of an *in vitro* model of human melanoma invasion based on reconstructed human skin. *Br J Dermatol* 142**:**210-22.

Faulk DM, Carruthers CA, Warner HJ, Kramer CR, Reing JE, Zhang L, D'Amore A, Badylak SF (2014) The effect of detergents on the basement membrane complex of a biologic scaffold material. *Acta Biomaterialia* 10**:**183-93.

Felder JM, 3rd, Goyal SS, Attinger CE (2012) A systematic review of skin substitutes for foot ulcers. *Plast Reconstr Surg* 130**:**145-64.

Ferrari S, Pellegrini G, Matsui T, Mavilio F, De Luca M (2006) Gene therapy in combination with tissue engineering to treat epidermolysis bullosa. *Expert Opin Biol Ther* 6**:**367-78.

Fleming ME, O'Daniel A, Bharmal H, Valerio I (2014) Application of the Orthoplastic Reconstructive Ladder to Preserve Lower Extremity Amputation Length. *Annals of Plastic Surgery* 73**:**183-189 10.1097/SAP.0b013e3182a638d8.

Fohn M, Bannasch H (2007) Artificial skin. *Methods Mol Med* 140**:**167-82.

Francesko A, Tzanov T (2011) Chitin, chitosan and derivatives for wound healing and tissue engineering. *Adv Biochem Eng Biotechnol* 125**:**1-27.

Gallico GG, 3rd, O'Connor NE, Compton CC, Kehinde O, Green H (1984) Permanent coverage of large burn wounds with autologous cultured human epithelium. *N Engl J Med* 311**:**448-51.

Gazzarri M, Bartoli C, Mota C, Puppi D, Dinucci D, Volpi S, Chiellini F (2013) Fibrous star poly(ε-caprolactone) melt-electrospun scaffolds for wound healing applications. *Journal of Bioactive and Compatible Polymers*

Geoffrion R, Murphy M, Robert M, Birch C, Ross S, Tang S, Milne J (2011) Vaginal paravaginal repair with porcine small intestine submucosa: midterm outcomes. *Female Pelvic Med Reconstr Surg* 17**:**174-9.

Glim JE, Everts V, Niessen FB, Ulrich MM, Beelen RH (2014) Extracellular matrix components of oral mucosa differ from skin and resemble that of foetal skin. *Arch Oral Biol* 59**:**1048-55.

Griffiths M, Livingstone R, Price R, Navsaria H (2004) Survival of Apligraf in acute human wounds. *Tissue Engineering* 10**:**1180-1195.

Halim AS, Khoo TL, Mohd Yussof SJ (2010) Biologic and synthetic skin substitutes: An overview. *Indian J Plast Surg* 43**:**S23-8.

Han SK, Yoon TH, Kim JB, Kim WK (2007) Dermis graft for wound coverage. *Plast Reconstr Surg* 120**:**166-72.

Hanel KH, Cornelissen C, Luscher B, Baron JM (2013) Cytokines and the skin barrier. *Int J Mol Sci* 14**:**6720-45.

Hauser S, Bastian PJ, Fechner G, Muller SC (2006) Small intestine submucosa in urethral stricture repair in a consecutive series. *Urology* 68**:**263-6.

Hayn MH, Bellinger MF, Schneck FX (2009) Small intestine submucosa as a corporal body graft in the repair of severe chordee. *Urology* 73**:**277-9.

He G, Lin XH, Zhong Q (2003) [Clinical application of meshed porcine acellular dermis xenograft with split-thickness skin autograft]. *Di Yi Jun Yi Da Xue Xue Bao* 23**:**977-8.

Heisenberg CP, Fassler R (2012) Cell-cell adhesion and extracellular matrix: diversity counts. *Curr Opin Cell Biol* 24**:**559-61.

Heng MC (2011) Wound healing in adult skin: aiming for perfect regeneration. *Int J Dermatol* 50**:**1058-66.

Hitzig G (2012) Use of Urinary Bladder Matrix, a Bioactive, Acellular Scaffold, in Transplant Donor Scars and Androgenetic Alopecia: Initial Clinical Experience. *American Journal of Cosmetic Surgery* 29**:**11-18.

Hodde JP, Allam R (2007) Small intestinal submucosa wound matrix for chronic wound healing. *Wounds-a Compendium of Clinical Research and Practice* 19**:**157-162.

Horch RE, Kopp J, Kneser U, Beier J, Bach AD (2005) Tissue engineering of cultured skin substitutes. *J Cell Mol Med* 9**:**592-608.

Howard D, Buttery LD, Shakesheff KM, Roberts SJ (2008) Tissue engineering: strategies, stem cells and scaffolds. *J Anat* 213**:**66-72.

Ireton JE, Unger JG, Rohrich RJ (2013) The role of wound healing and its everyday application in plastic surgery: a practical perspective and systematic review. *Plast Reconstr Surg Glob Open* 1**:**

Jacyna MR (1990) Interactions between Gall-Bladder Bile and Mucosa - Relevance to Gall Stone Formation. *Gut* 31**:**568-570.

John TT, Aggarwal N, Singla AK, Santucci RA (2008) Intense inflammatory reaction with porcine small intestine submucosa pubovaginal sling or tape for stress urinary incontinence. *Urology* 72**:**1036-9.

Jones J (2005) Winter's concept of moist wound healing: a review of the evidence and impact on clinical practice. *J Wound Care* 14**:**273-6.

Juhasz I, Kiss B, Lukacs L, Erdei I, Peter Z, Remenyik E (2010) Long-term followup of dermal substitution with acellular dermal implant in burns and postburn scar corrections. *Dermatol Res Pract* 2010**:**210150.

Junker JP, Kamel RA, Caterson EJ, Eriksson E (2013) Clinical Impact Upon Wound Healing and Inflammation in Moist, Wet, and Dry Environments. *Adv Wound Care (New Rochelle)* 2**:**348-356.

Kamel RA, Ong JF, Eriksson E, Junker JP, Caterson EJ (2013) Tissue engineering of skin. *J Am Coll Surg* 217**:**533-55.

Kim JH, Cho YP, Kwon TW, Kim H, Kim GE (2012) Ten-year comparative analysis of bovine pericardium and autogenous vein for patch angioplasty in patients undergoing carotid endarterectomy. *Ann Vasc Surg* 26**:**353-8.

Kim MS, Hong KD, Shin HW, Kim SH, Kim SH, Lee MS, Jang WY, Khang G, Lee HB (2005) Preparation of porcine small intestinal submucosa sponge and their application as a wound dressing in full-thickness skin defect of rat. *International Journal of Biological Macromolecules* 36**:**54-60.

Kirker KR, Luo Y, Nielson JH, Shelby J, Prestwich GD (2002) Glycosaminoglycan hydrogel films as bio-interactive dressings for wound healing. *Biomaterials* 23**:**3661-3671.

Kleinman HK, Philp D, Hoffman MP (2003) Role of the extracellular matrix in morphogenesis. *Current Opinion in Biotechnology* 14**:**526-532.

Klingberg F, Hinz B, White ES (2013) The myofibroblast matrix: implications for tissue repair and fibrosis. *Journal of Pathology* 229**:**298-309.

Kumar RJ, Kimble RM, Boots R, Pegg SP (2004) Treatment of partial-thickness burns: A prospective, randomized trial using Transcyte (TM). *Anz Journal of Surgery* 74**:**622-626.

Laster L, Ingelfinger FJ (1961) Intestinal absorption--aspects of structure, function and disease of the small-intestine mucosa. *N Engl J Med* 264**:**1246-53 concl.

Lawton S (2006a) Anatomy and function of the skin, part 1. *Nurs Times* 102**:**26-7.

Lawton S (2006b) Anatomy and function of the skin. Part 2--The epidermis. *Nurs Times* 102**:**28-9.

Lawton S (2006c) Anatomy and function of the skin. Part 3--dermis and adjacent structures. *Nurs Times* 102**:**26-7.

Lawton S (2006d) Anatomy and function of the skin. Part 4--Appendages. *Nurs Times* 102**:**26-7.
Li B, Wang JHC (2011) Fibroblasts and myofibroblasts in wound healing: Force generation and measurement. *Journal of Tissue Viability* 20**:**108-120.
Li J, Chen J, Kirsner R (2007) Pathophysiology of acute wound healing. *Clinics in Dermatology* 25**:**9-18.
Liang R, Woo SL, Takakura Y, Moon DK, Jia F, Abramowitch SD (2006) Long-term effects of porcine small intestine submucosa on the healing of medial collateral ligament: a functional tissue engineering study. *J Orthop Res* 24**:**811-9.
Lindberg K, Badylak SF (2001) Porcine small intestinal submucosa (SIS): a bioscaffold supporting *in vitro* primary human epidermal cell differentiation and synthesis of basement membrane proteins. *Burns* 27**:**254-266.
Lindblad WJ (2002) Wound healing, regenerative medicine and tissue engineering: a continuum. *Wound Repair Regen* 10**:**345.
Long MM, King VJ, Prasad KU, Freeman BA, Urry DW (1989) Elastin repeat peptides as chemoattractants for bovine aortic endothelial cells. *Journal of Cellular Physiology* 140**:**512-518.
McLafferty E, Hendry C, Alistair F (2012) The integumentary system: anatomy, physiology and function of skin. *Nurs Stand* 27**:**35-42.
Menko AS, Bleaken BM, Libowitz AA, Zhang L, Stepp MA, Walker JL (2014) A central role for vimentin in regulating repair function during healing of the lens epithelium. *Mol Biol Cell* 25**:**776-90.
Merguerian PA, Reddy PP, Barrieras DJ, Wilson GJ, Woodhouse K, Bagli DJ, McLorie GA, Khoury AE (2000) Acellular bladder matrix allografts in the regeneration of functional bladders: evaluation of large-segment (> 24 cm) substitution in a porcine model. *BJU Int* 85**:**894-8.
Metcalfe AD, Ferguson MW (2007) Tissue engineering of replacement skin: the crossroads of biomaterials, wound healing, embryonic development, stem cells and regeneration. *J R Soc Interface* 4**:**413-37.
Mi FL, Shyu SS, Wu YB, Lee ST, Shyong JY, Huang RN (2001) Fabrication and characterization of a sponge-like asymmetric chitosan membrane as a wound dressing. *Biomaterials* 22**:**165-73.
Micallef L, Belaubre F, Pinon A, Jayat-Vignoles C, Delage C, Charveron M, Simon A (2009) Effects of extracellular calcium on the growth-differentiation switch in immortalized keratinocyte HaCaT cells compared with normal human keratinocytes. *Experimental Dermatology* 18**:**143-151.
Mitchell KB, Gallagher JJ (2012) Porcine bladder extracellular matrix for closure of a large defect in a burn contracture release. *J Wound Care* 21**:**454-6.
Mittal A, Kumar N (2012) Drug-loaded polymeric composite skin graft for infection-free wound healing: fabrication, characterization, cell proliferation, migration, and antimicrobial activity. *Pharm Res* 29**:**3110-21.

Morimoto N, Saso Y, Tomihata K, Taira T, Takahashi Y, Ohta M, Suzuki S (2005) Viability and function of autologous and allogeneic fibroblasts seeded in dermal substitutes after implantation. *Journal of Surgical Research* 125**:**56-67.

Mostow EN, Haraway GD, Dalsing M, Hodde JP, King D (2005) Effectiveness of an extracellular matrix graft (OASIS Wound Matrix) in the treatment of chronic leg ulcers: a randomized clinical trial. *J Vasc Surg* 41**:**837-43.

Muhamed J, Revi D, Rajan A, Geetha S, Anilkumar TV (2014) Biocompatibility and Immunophenotypic Characterization of a Porcine Cholecyst–derived Scaffold Implanted in Rats. *Toxicologic Pathology*

Mutschler W (2012) Physiology and pathophysiology of wound healing of wound defects. *Unfallchirurg* 115**:**767-773.

Namazi H (2014) Donor-Site morbidity of the radial forearm free flap versus the ulnar forearm free flap. *Plast Reconstr Surg* 133**:**224e-5e.

Netzlaff F, Lehr CM, Wertz PW, Schaefer UF (2005) The human epidermis models EpiSkin, SkinEthic and EpiDerm: an evaluation of morphology and their suitability for testing phototoxicity, irritancy, corrosivity, and substance transport. *Eur J Pharm Biopharm* 60**:**167-78.

Newman MI (2010) Comparison of Surgisis, AlloDerm, and Vicryl Woven Mesh grafts for abdominal wall defect repair in an animal model. *Aesthetic Plast Surg* 34**:**297-8.

Nicol NH (2005) Anatomy and physiology of the skin. *Dermatol Nurs* 17**:**62.

Nieponice A, Ciotola FF, Nachman F, Jobe BA, Hoppo T, Londono R, Badylak S, Badaloni AE (2014) Patch Esophagoplasty: Esophageal Reconstruction Using Biologic Scaffolds. *The Annals of Thoracic Surgery* 97**:**283-288.

Nordback PH, Miettinen S, Kaariainen M, Pelto-Huikko M, Kuokkanen H, Suuronen R (2012) Amniotic membrane reduces wound size in early stages of the healing process. *J Wound Care* 21**:**190, 192-4, 196-7.

O'Leary R, Ponnambalam S, Wood EJ (2003) Pioglitazone-induced myofibroblast cell death: implications for cutaneous scarring. *Br J Dermatol* 149**:**665-7.

Osonoi M, Iwanuma O, Kikuchi A, Abe S (2011) Fibroblasts have plasticity and potential utility for cell therapy. *Human Cell* 24**:**30-34.

Pajardi G, Rapisarda V, Somalvico F, Scotti A, Russo GL, Ciancio F, Sgro A, Nebuloni M, Allevi R, Torre ML, Trabucchi E, Marazzi M (2014) Skin substitutes based on allogenic fibroblasts or keratinocytes for chronic wounds not responding to conventional therapy: a retrospective observational study. *Int Wound J*

Pham C, Greenwood J, Cleland H, Woodruff P, Maddern G (2007) Bioengineered skin substitutes for the management of burns: a systematic review. *Burns* 33**:**946-57.

Phipatanakul WP, Petersen SA (2009) Porcine small intestine submucosa xenograft augmentation in repair of massive rotator cuff tears. *Am J Orthop (Belle Mead NJ)* 38**:**572-5.

Poschl E, Schlotzer-Schrehardt U, Brachvogel B, Saito K, Ninomiya Y, Mayer U (2004) Collagen IV is essential for basement membrane stability but dispensable

for initiation of its assembly during early development. *Development* 131**:**1619-1628.

Price RD, Das-Gupta V, Harris PA, Leigh IM, Navsaria HA (2004) The role of allogenic fibroblasts in an acute wound healing model. *Plastic and Reconstructive Surgery* 113**:**1719-1729.

Priya SG, Jungvid H, Kumar A (2008) Skin tissue engineering for tissue repair and regeneration. *Tissue Eng Part B Rev* 14**:**105-18.

Puglisi F, Capuano P, Iambrenghi OC, Armenise N, Carlucci F, Memeo M, Memeo R, Martines G (2009) Laparoscopic repair of Morgagni hernia in an adult: use of a porcine small intestine submucosa biocompatible prosthesis. *Chir Ital* 61**:**351-6.

Raines EW (2000) The extracellular matrix can regulate vascular cell migration, proliferation, and survival: relationships to vascular disease. *International Journal of Experimental Pathology* 81**:**173-182.

Ratner D (1998) SKIN GRAFTING: From Here to There* * Portions of this article were previously published in Johnson TM, Ratner D, Nelson BR: Soft tissue reconstruction with skin grafting. J Am Acad Dermatol 27:151, 1992, and Ratner D, Skouge JW: Surgical pearl: The use of free cartilage grafts in nasal alar reconstruction. J Am Acad Dermatol 36:622, 1997; with permission. *Dermatologic Clinics* 16**:**75-90.

Reing JE, Zhang L, Myers-Irvin J, Cordero KE, Freytes DO, Heber-Katz E, Bedelbaeva K, McIntosh D, Dewilde A, Braunhut SJ, Badylak SF (2009) Degradation Products of Extracellular Matrix Affect Cell Migration and Proliferation. *Tissue Engineering Part A* 15**:**605-614.

Revi D, Paul W, Anilkumar TV, Sharma CP (2013) Differential Healing of Full Thickness Rabbit Skin Wound by Fibroblast Loaded Chitosan Sponge. *Journal of Biomaterials and Tissue Engineering* 3**:**261-272.

Revi D, Paul W, Anilkumar TV, Sharma CP (2014) Chitosan scaffold co-cultured with keratinocyte and fibroblast heals full thickness skin wounds in rabbit. *J Biomed Mater Res A* 102**:**3273-81.

Ridha H, Crerar-Gilbert A, Fleming A (2008) The use of Tegaderm for finger buddy-strapping: a dressing with many advantages. *Ann R Coll Surg Engl* 90**:**525.

Ringe J, Sittinger M (2014) Regenerative medicine: Selecting the right biological scaffold for tissue engineering. *Nat Rev Rheumatol* 10**:**388-9.

Rinker B, Vyas KS (2014) Clinical applications of autografts, conduits, and allografts in repair of nerve defects in the hand: current guidelines. *Clin Plast Surg* 41**:**533-50.

Rnjak J, Li Z, Maitz PKM, Wise SG, Weiss AS (2009) Primary human dermal fibroblast interactions with open weave three-dimensional scaffolds prepared from synthetic human elastin. *Biomaterials* 30**:**6469-6477.

Robinet A, Fahem A, Cauchard JH, Huet E, Vincent L, Lorimier S, Antonicelli F, Soria C, Crepin M, Hornebeck W, Bellon G (2005) Elastin-derived peptides enhance angiogenesis by promoting endothelial cell migration and tubulogenesis through upregulation of MT1-MMP. *J Cell Sci* 118**:**343-56.

Roh HW, Song MJ, Han DK, Lee DS, Ahn JH, Kim SC (1999) Effect of cross-link density and hydrophilicity of PU on blood compatibility of hydrophobic PS/hydrophilic PU IPNs. *J Biomater Sci Polym Ed* 10**:**123-43.

Romanelli M, Dini V, Bertone MS (2010) Randomized comparison of OASIS wound matrix versus moist wound dressing in the treatment of difficult-to-heal wounds of mixed arterial/venous etiology. *Advances in Skin & Wound Care* 23**:**34-8.

Sandulache VC, Zhou Z, Sherman A, Dohar JE, Hebda PA (2003) Impact of transplanted fibroblasts on rabbit skin wounds. *Arch Otolaryngol Head Neck Surg* 129**:**345-50.

Sarkar S, Chourasia A, Maji S, Sadhukhan S, Kumar S, Adhikari B (2006) Synthesis and characterization of gelatin based polyester urethane scaffold. *Bulletin of Materials Science* 29**:**475-484.

Sarkar SD, Farrugia BL, Dargaville TR, Dhara S (2013) Chitosan-collagen scaffolds with nano/microfibrous architecture for skin tissue engineering. *Journal of Biomedical Materials Research Part A* 101**:**3482-92.

Sasse KC, Brandt J, Lim DC, Ackerman E (2013) Accelerated healing of complex open pilonidal wounds using MatriStem extracellular matrix xenograft: nine cases. *J Surg Case Rep* 2013**:**

Sassolas B (2010) [Anatomy of normal skin]. *Soins* 28.

Schallberger SP, Stanley BJ, Hauptman JG, Steficek BA (2008) Effect of porcine small intestinal submucosa on acute full-thickness wounds in dogs. *Vet Surg* 37**:**515-24.

Schnoeller TJ, de Petriconi R, Hefty R, Jentzmik F, Waalkes S, Zengerling F, Schrader M, Schrader AJ (2011) Partial nephrectomy using porcine small intestinal submucosa. *World J Surg Oncol* 9**:**126.

Schoop VM, Mirancea N, Fusenig NE (1999) Epidermal organization and differentiation of HaCaT keratinocytes in organotypic coculture with human dermal fibroblasts. *Journal of Investigative Dermatology* 112**:**343-53.

Schultz GS, Wysocki A (2009) Interactions between extracellular matrix and growth factors in wound healing. *Wound Repair and Regeneration* 17**:**153-162.

Seymour PE, Leventhal DD, Pribitkin EA (2008) Lip augmentation with porcine small intestinal submucosa. *Arch Facial Plast Surg* 10**:**30-3.

Shah JM, Omar E, Pai DR, Sood S (2012) Cellular events and biomarkers of wound healing. *Indian J Plast Surg* 45**:**220-8.

Shakespeare P (2001) Burn wound healing and skin substitutes. *Burns* 27**:**517-522.

Shevchenko RV, James SL, James SE (2010) A review of tissue-engineered skin bioconstructs available for skin reconstruction. *J R Soc Interface* 7**:**229-58.

Shipp EL, Hsieh-Wilson LC (2007) Profiling the sulfation specificities of glycosaminoglycan interactions with growth factors and chemotactic proteins using microarrays. *Chem Biol* 14**:**195-208.

Shores JT, Gabriel A, Gupta S (2007) Skin substitutes and alternatives: a review. *Advances in Skin & Wound Care* 20**:**493-508; quiz 509-10.

Sicari BM, Rubin JP, Dearth CL, Wolf MT, Ambrosio F, Boninger M, Turner NJ, Weber DJ, Simpson TW, Wyse A, Brown EHP, Dziki JL, Fisher LE, Brown S, Badylak SF (2014) An Acellular Biologic Scaffold Promotes Skeletal Muscle Formation in Mice and Humans with Volumetric Muscle Loss. *Science Translational Medicine* 6**:**234ra58.

Silva JM, Georgi N, Costa R, Sher P, Reis RL, Van Blitterswijk CA, Karperien M, Mano JF (2013) Nanostructured 3D constructs based on chitosan and chondroitin sulphate multilayers for cartilage tissue engineering. *PLoS One* 8**:**e55451.

Sindrilaru A, Scharffetter-Kochanek K (2013) Disclosure of the Culprits: Macrophages-Versatile Regulators of Wound Healing. *Adv Wound Care (New Rochelle)* 2**:**357-368.

Smith RM, Wiedl C, Chubb P, Greene CH (2004) Role of small intestine submucosa (SIS) as a nerve conduit: preliminary report. *J Invest Surg* 17**:**339-44.

Strauss R, Li ZY, Liu Y, Beyer I, Persson J, Sova P, Moller T, Pesonen S, Hemminki A, Hamerlik P, Drescher C, Urban N, Bartek J, Lieber A (2011) Analysis of epithelial and mesenchymal markers in ovarian cancer reveals phenotypic heterogeneity and plasticity. *Plos One* 6**:**e16186.

Subramanyan K, Misra M, Mukherjee S, Ananthapadmanabhan K (2007) Advances in the materials science of skin: A composite structure with multiple functions. *Mrs Bulletin* 32**:**770-778.

Sun T, Jackson S, Haycock JW, MacNeil S (2006) Culture of skin cells in 3D rather than 2D improves their ability to survive exposure to cytotoxic agents. *Journal of Biotechnology* 122**:**372-81.

Supp DM, Boyce ST (2005) Engineered skin substitutes: practices and potentials. *Clin Dermatol* 23**:**403-12.

Tajik H, Jalali FSS (2007) Influence of aqueous extract of yarrow on healing process of experimental burn wound in rabbit: Clinical and microbiological study. *Journal of Animal and Veterinary Advances* 6**:**1464-1468.

Thione A, Cavadas PC, Landin L, Ibanez J (2011) Microvascular pedicle coverage with split thickness skin graft: Indications and surgical tips. *Indian J Plast Surg* 44**:**528-9.

Tran RT, Thevenot P, Zhang Y, Gyawali D, Tang L, Yang J (2010) Scaffold Sheet Design Strategy for Soft Tissue Engineering. *Nat Mater* 3**:**1375-1389.

Van De Water L, Varney S, Tomasek JJ (2013) Mechanoregulation of the Myofibroblast in Wound Contraction, Scarring, and Fibrosis: Opportunities for New Therapeutic Intervention. *Adv Wound Care (New Rochelle)* 2**:**122-141.

Wang Y, Liu L, Li Y, Xu J, Huo R, Li Q, Li S (2006) [Biocompatibility of acellular urinary bladder submucosa]. *Zhongguo Xiu Fu Chong Jian Wai Ke Za Zhi* 20**:**210-2.

Wang Z, Wang Y, Farhangfar F, Zimmer M, Zhang Y (2012) Enhanced keratinocyte proliferation and migration in co-culture with fibroblasts. *Plos One* 7**:**e40951.

Weigel T, Schinkel G, Lendlein A (2006) Design and preparation of polymeric scaffolds for tissue engineering. *Expert Rev Med Devices* 3**:**835-51.

Welss T, Basketter DA, Schroder KR (2004) *In vitro* skin irritation: facts and future. State of the art review of mechanisms and models. *Toxicol In Vitro* 18**:**231-43.

Whitaker IS, Prowse S, Potokar TS (2008) A Critical Evaluation of the Use of Biobrane as a Biologic Skin Substitute: A Versatile Tool for the Plastic and Reconstructive Surgeon. *Annals of Plastic Surgery* 60**:**333-337 10.1097/SAP.0b013e31806bf446.

WHO. 2014. Key facts. http://www.who.int/mediacentre/factsheets/fs365/en/

Winkler JT, Swaim SF, Sartin EA, Henderson RA, Welch JA (2002) The effect of a porcine-derived small intestinal submucosa product on wounds with exposed bone in dogs. *Vet Surg* 31**:**541-51.

Wu YG, Li SK, Wang YQ, Xin ZC, Li YQ, Yang MY, Li Q (2007) [The clinical application of acellular urinary bladder submucosa to reconstructive the urethral duct of hypospadias patients]. *Zhonghua Zheng Xing Wai Ke Za Zhi* 23**:**118-20.

Wysocki AB (1999) Skin anatomy, physiology, and pathophysiology. *Nurs Clin North Am* 34**:**777-97.

Yannas IV, Burke JF (1980) Design of an artificial skin. I. Basic design principles. *J Biomed Mater Res* 14**:**65-81.

Yao M, Attalla K, Ren Y, French MA, Driver VR (2013) Ease of use, safety, and efficacy of integra bilayer wound matrix in the treatment of diabetic foot ulcers in an outpatient clinical setting: a prospective pilot study. *J Am Podiatr Med Assoc* 103**:**274-80.

Yim H, Cho YS, Seo CH, Lee BC, Ko JH, Kim D, Hur J, Chun W, Kim JH (2010) The use of AlloDerm on major burn patients: AlloDerm prevents post-burn joint contracture. *Burns* 36**:**322-8.

Zhang F, Zhu C, Oswald T, Lei MP, Lineaweaver WC (2003) Porcine small intestinal submucosa as a carrier for skin flap prefabrication. *Annals of Plastic Surgery* 51**:**488-492.

Zhang Z, Michniak-Kohn BB (2012) Tissue engineered human skin equivalents. *Pharmaceutics* 4**:**26-41.

Zheng MH, Chen J, Kirilak Y, Willers C, Xu J, Wood D (2005) Porcine small intestine submucosa (SIS) is not an acellular collagenous matrix and contains porcine DNA: possible implications in human implantation. *J Biomed Mater Res B Appl Biomater* 73**:**61-7.

Appendix- I

Evaluation of histomorphology has been an efficient tool for assessing the extent of tissue response to injury in animal models. In this study, many techniques were adopted for studying histology, histopathology of induced skin wounds and histomorphology of the healing wounds. Whereas, some of these techniques were routinely followed in the host laboratory, several techniques needed standardization and validation of procedures. The validated procedures were used for studying histology and evaluation of wound healing reactions in chitosan-matrix assisted skin wounds in rabbit.

This appendix documents the preliminary data collected as part of the research for standardization and validation of the above techniques. Remarkably, a substantial part of the data has been communicated in the form of peer-reviewed research publications in reputed journals (*Revi et. al., 2013 and Revi et al., 2014*).

Histology of skin

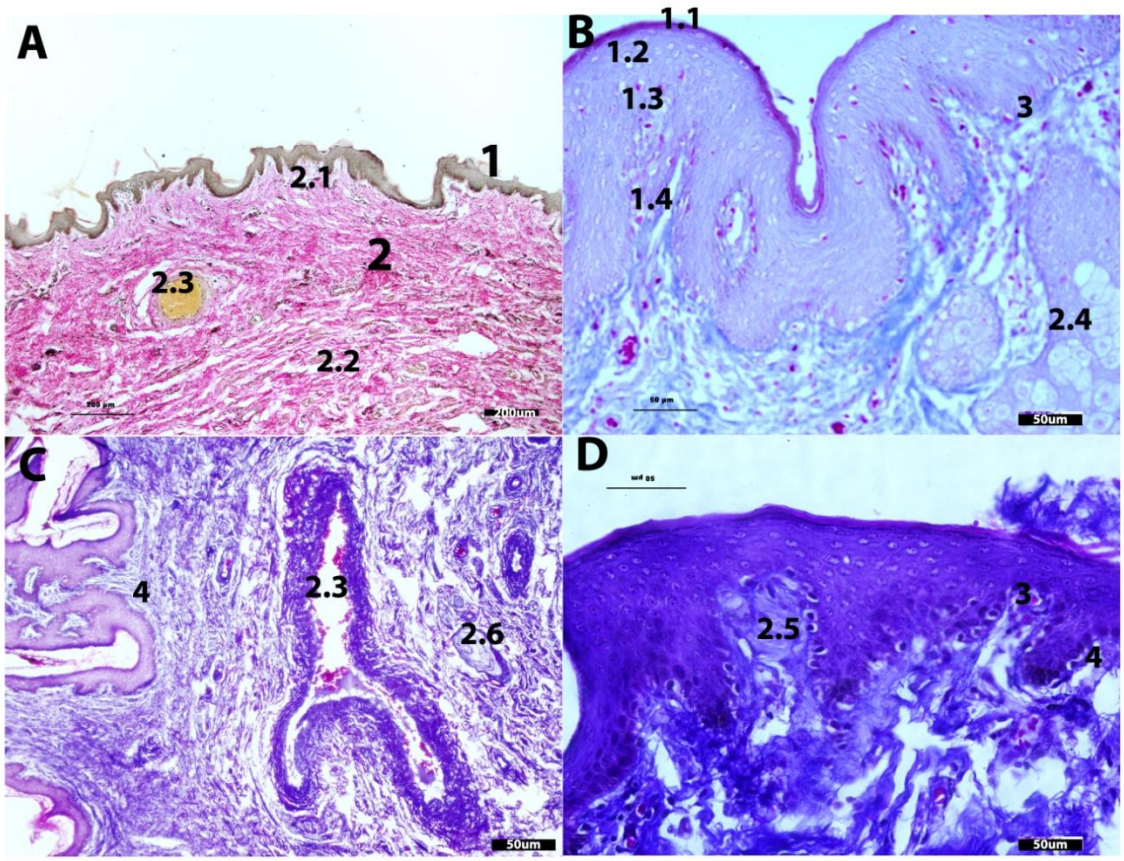

Figure A1: Special staining procedures intended for demonstrating collagen (A, Van Geison staining; B, C and D, Massons Trichrome staining) were used for histology of skin. Components of epidermis (1) and dermis (2) were depicted in these microphotographs. 1.1, Stratum corneum; 1.2, Stratum granulosum; 1.3, Stratum spinosum; 1.4, Stratum basale; 2.1, the papillary dermis; 2.2, the reticular dermis. The dermal structures like blood vessels (2.3), sebaceous gland (2.4), Meseniers corposule (2.5) and Paccinian corposules (2.6) were discernible in these photographs. Basement membrane (3) separated dermis from epidermis as well as rete pegs (4) and rete ridge (5) were also prominently visible.

Histopathology of burn wound healing

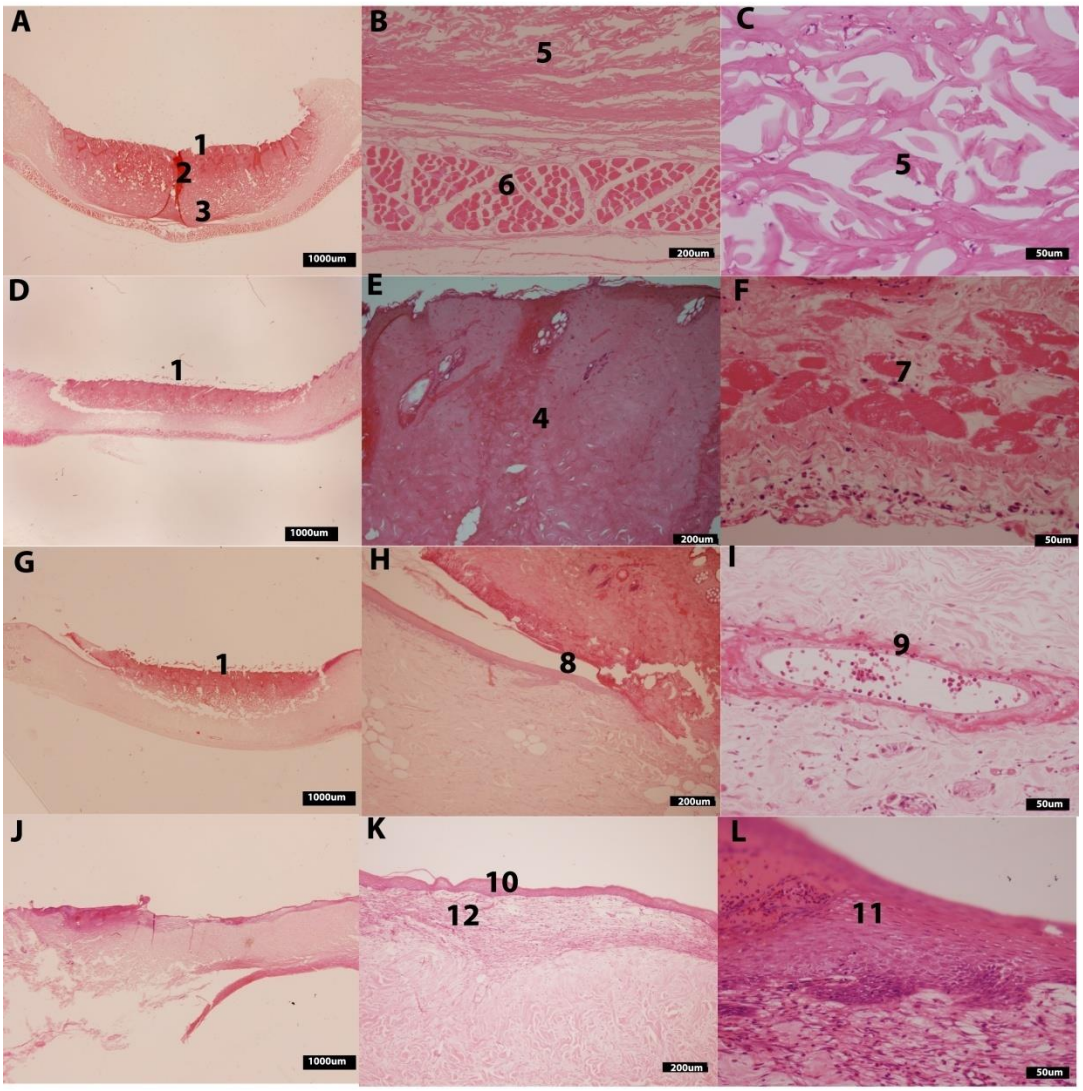

Figure A2: Histomorphology of burn wounds (haematoxilin and eosin) in rabbit model 0 day (A, B and C), 7 day (D, E and F), 14 day and 28 day (J, K and L). Three zones on day 0 (1) Zone of coagulation (2) Zone of stasis and (3) Zone of hyperemia were evident. The Zone of coagulation showed (4) Necrotized epidermis with damaged hair follicle and (5) Necrotized dermis with coagulated collagen fibers above the (6) Muscularis layer. However during 7th day some regenerating were seen characterized by (7) centrally placed nucleus muscle bundles beneath the dermis region. On 14th day partially re-epithelialization has occurred and (8) leading edge of re-epithelialization in epidermis and (9) blood vessels in the zone of stasis were evident. By 28th day (10) Complete re-epithelialization with (11) hypertrophic neo-epidermis and neodermis with (12) disorganized collagen deposition were also observed.

Preliminary studies I- Differential healing of full thickness rabbit skin wound by fibroblast loaded chitosan sponge

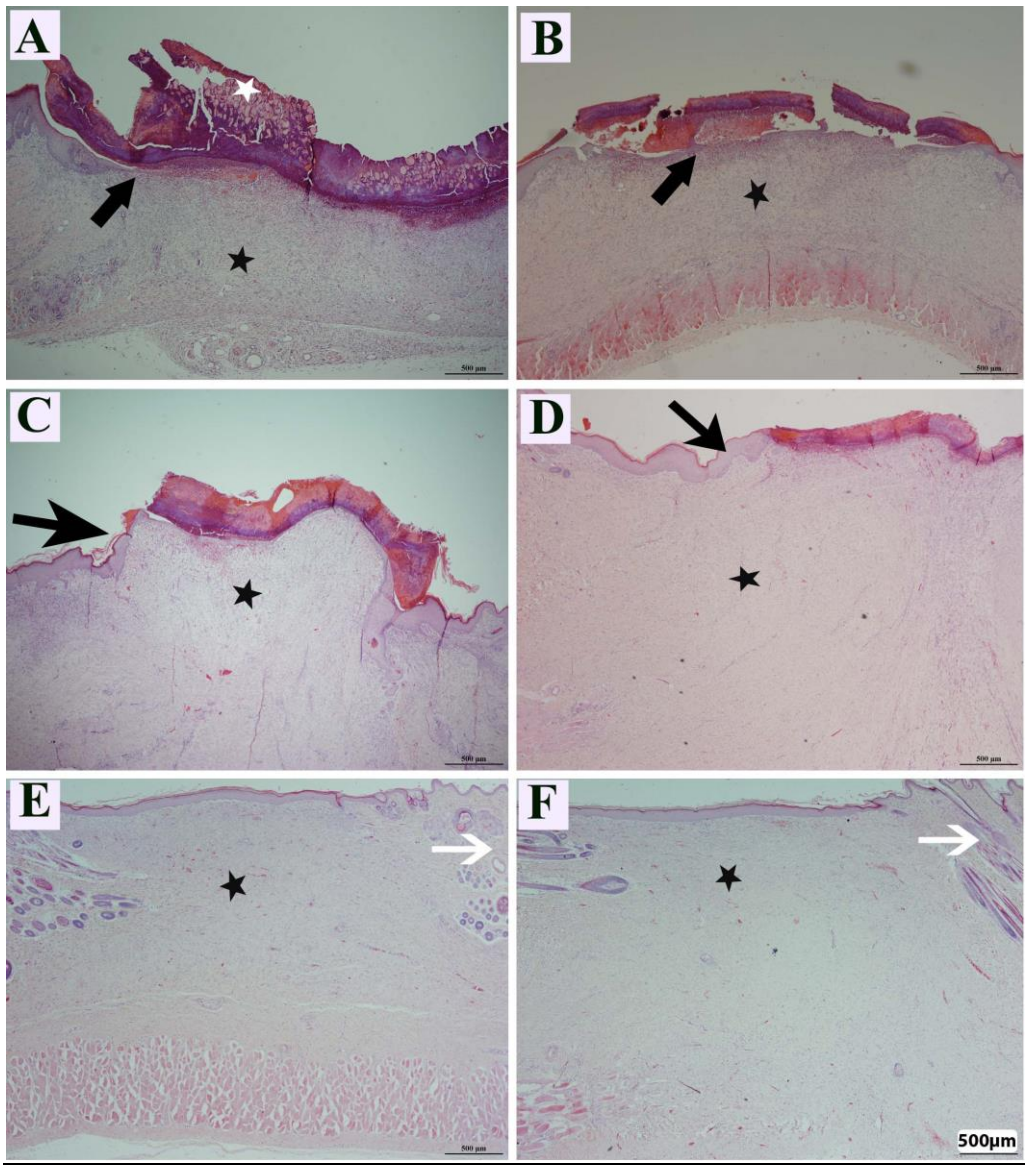

Figure A3 Photomicrograph (HE stains; 4x magnification) of the graft assisted healing full thickness skin wound (cross section; original wound size, 1cm x 1cm) in the rabbit model at 7 days (A and B: showing the leading edge of the neo- epidermis, black arrow and the chitosan sponge white star), 14 days (C and D: where the epidermis became thicker, black arrow) and 21 days (E and F: where the epithelium fully regenerated and the newly formed dermis devoid of hair follicle and sebaceous gland when compared with the normal skin, white arrow). Both the HFLC graft-assisted (A, C and E) and the non-cell loaded graft-assisted (B, D and F) wounds healed by granulation tissue formation (black star).

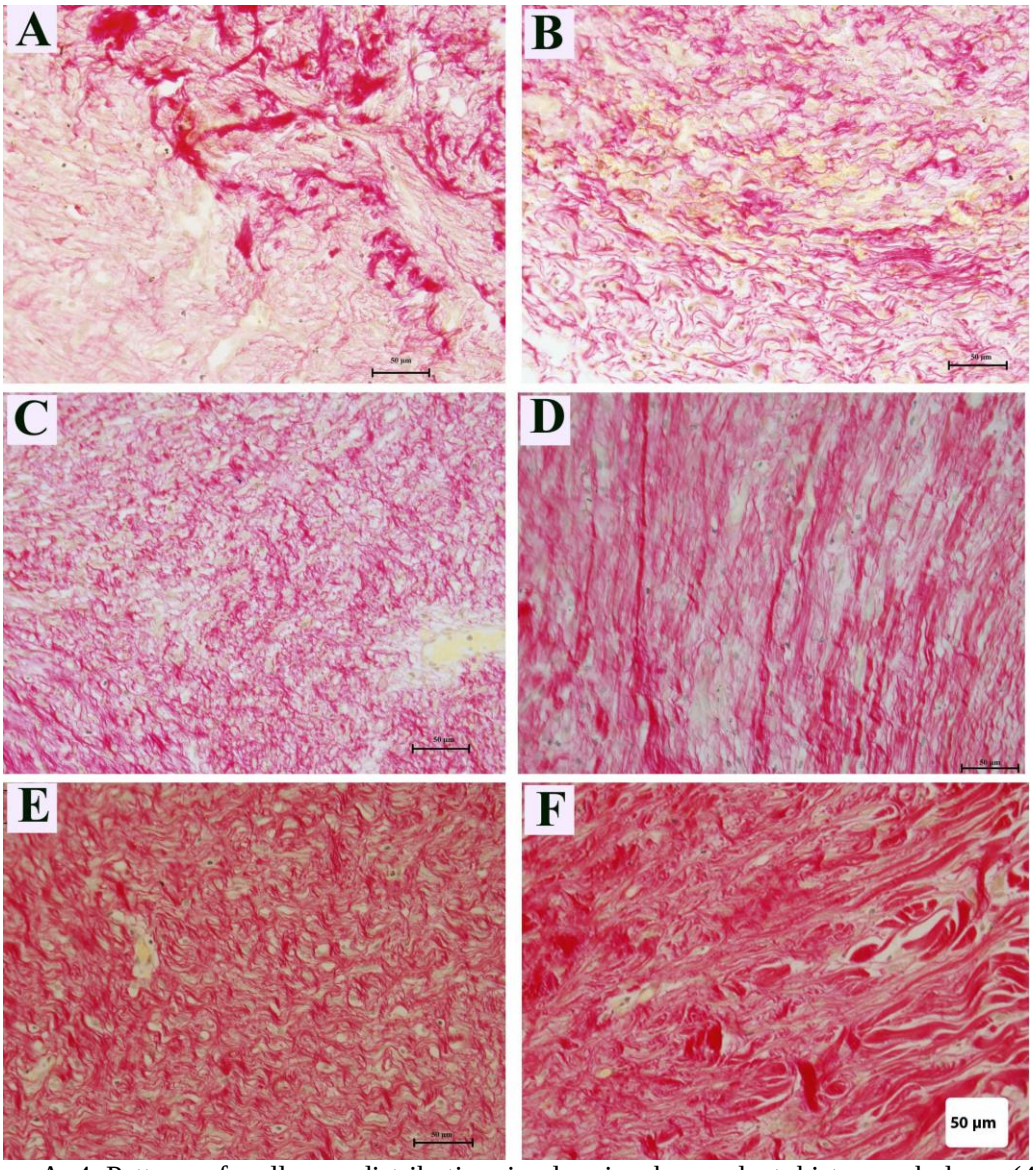

Figure A 4 Pattern of collagen distribution in dermis observed at histomorphology (40 x magnifications) by picro-sirius red staining. On the 7th days (A and B) the pink stained collagen fibers were arranged in a disorganized fashion compared to 14thday samples (C and D) which became further compact by 21 days (E and F). Occasional smooth muscle (yellow) of blood vessels were seen in both (HFLC; A, C, and E and original chitosan; B, D and F) treated wounds.

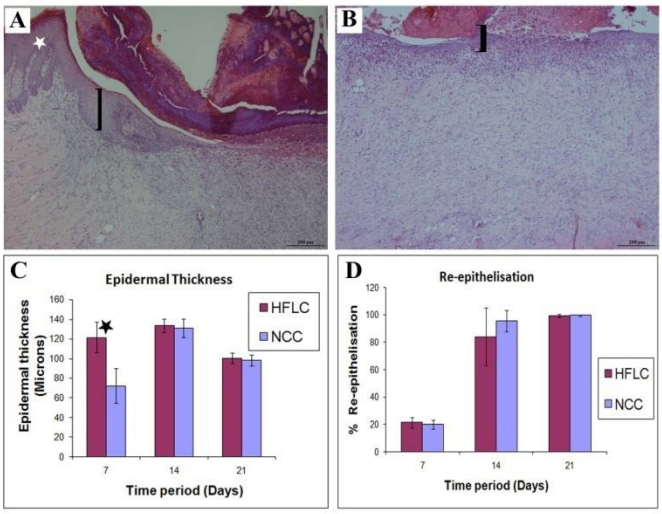

Figure A5 Higher magnification (10x magnification) of the 7thday samples pictured in Fig 1 (A and B) and quantitative histomorphometry (C and D). The relative thickness of the epidermis (black arrow) of the HFLC-treated wound (A and C) was higher compared to non-cell loaded graft (B and C) wound healing reactions but there was complete re-epithelialization by 21 days in both wounds. Note the prominence of rete-pegs and rete-ridges and chitosan sponge (white star) in HFLC-treated wound (A).

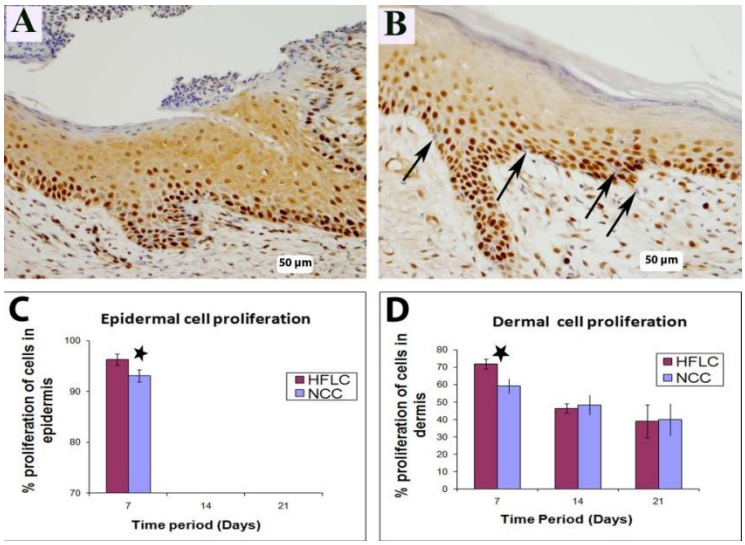

Figure A6 When studied by immunohistochemistry for PCNA, the HFLC- treated wound(A) had a higher density of proliferating cells (brown nucleus) in the stratum basalis compared to the non-modified chitosan-treated wounds (B) where non-proliferating cells in the basal layer of the epidermis (black arrow) were frequent. Quantitative data on the relative distribution of PCNA-positive proliferating cells in the epidermis (C) and dermis (D).

Preliminary studies II - Chitosan Scaffold Co cultured with Keratinocyte and Fibroblast Heals Full Thickness Skin Wounds in Rabbit

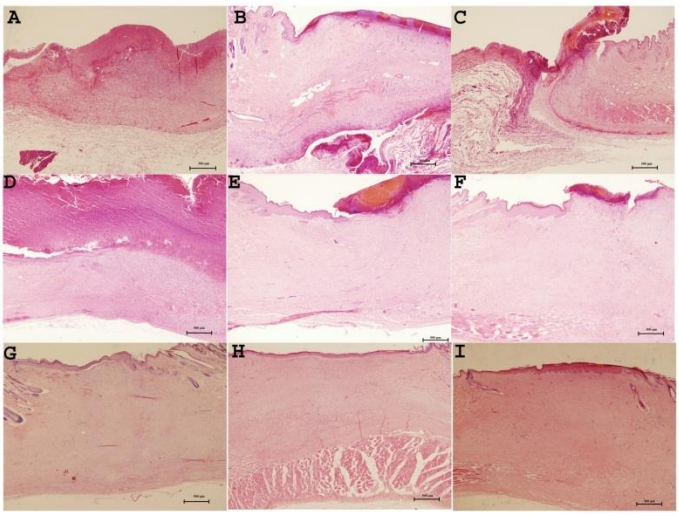

Figure A7 H&E stained sections during 7 day (A,B & C) 14 day (D, E & F) and 21 day (G, H & I)for quantifying re-epithelialization in homologous keratinocyte fibroblast loaded chitosan graft (A, D & E), a non-cellular chitosan graft (B, E & H) and the commercial product (C, F & I) (10X magnification).

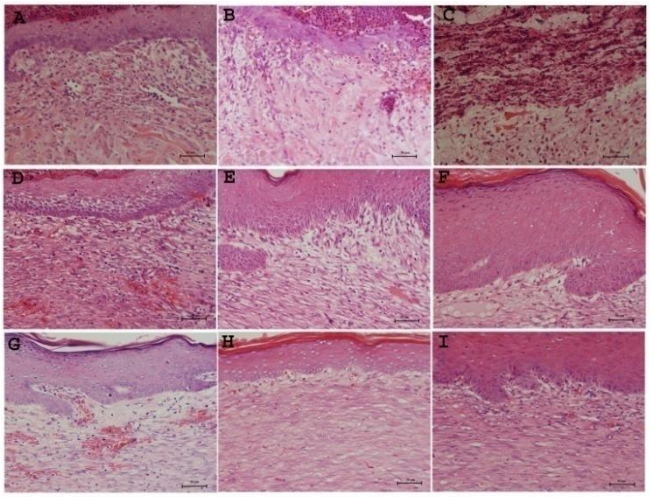

Figure A8 H&E stained sections during 7 day (A,B & C) 14 day (D, E & F) and 21 day (G, H & I) for quantifying percentage angiogenesis in homologous keratinocyte fibroblast loaded chitosan graft (A, D & E), a non-cellular chitosan graft (B, E & H) and the commercial product (C, F & I) (40X magnification)

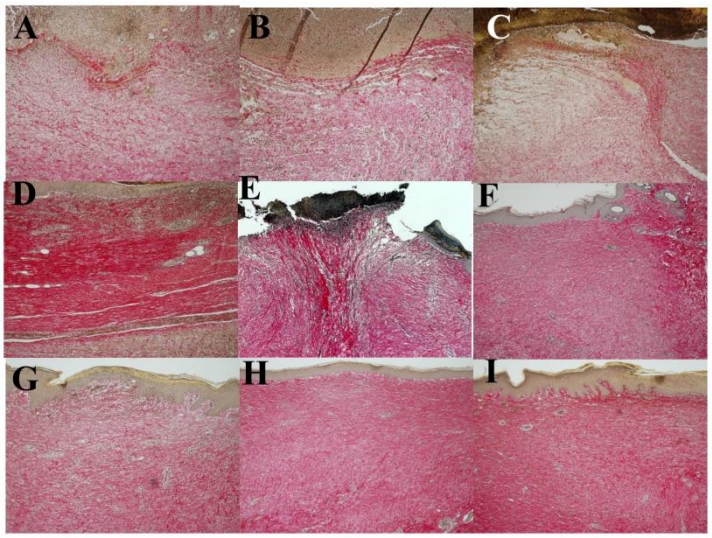

Figure A9 Picrosirius stained sections during 7 day (A,B & C) 14 day (D, E & F) and 21 day (G, H & I)for quantifying collagen in homologous keratinocyte fibroblast loaded chitosan graft (A, D & E), a non-cellular chitosan graft (B, E & H) and the commercial product (C, F & I) (10X magnification).

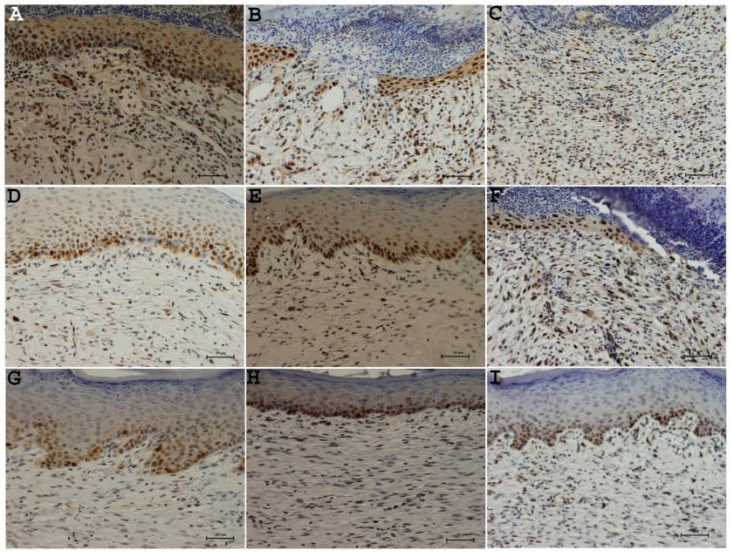

Figure A10 PCNA immunostained sections during 7 day (A,B & C) 14 day (D, E & F) and 21 day (G, H & I) for quantifying cell proliferation in dermis in homologous keratinocyte fibroblast loaded chitosan graft (A, D & E), a non-cellular chitosan graft (B, E & H) and the commercial product (C, F & I) (40X magnification).

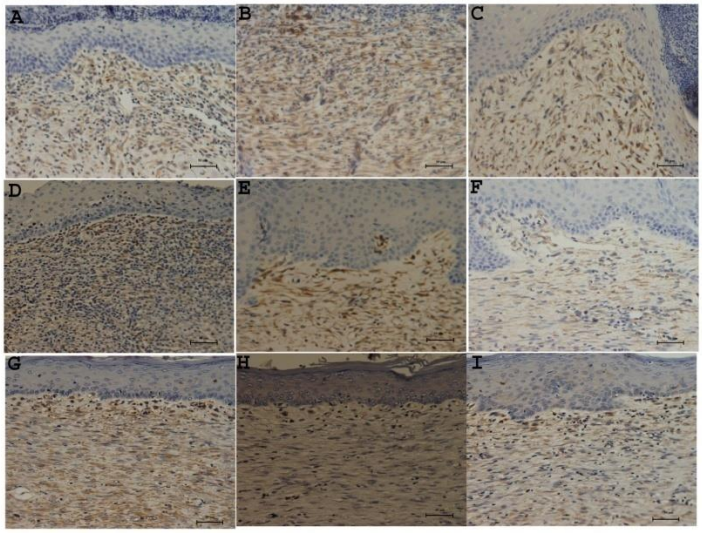

Figure A 11 Vimentin immunostained sections during 7 day (A, B & C) 14 day (D, E & F) and 21 day (G, H & I) for quantifying mesenchymal cells in dermis in homologous keratinocyte fibroblast loaded chitosan graft (A, D & E), a non-cellular chitosan graft (B, E & H) and the commercial product (C, F & I) (40X magnification)

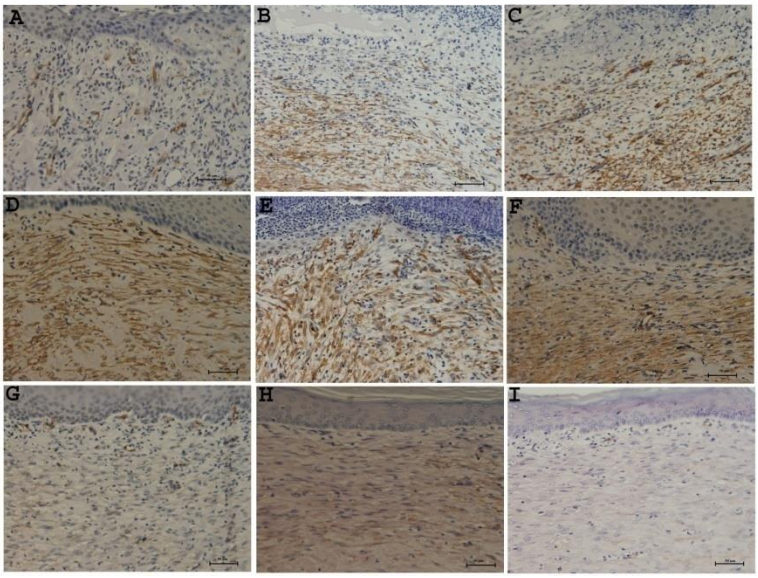

Figure A12 ASMA immunostained sections during 7 day (A,B & C) 14 day (D, E & F) and 21 day (G, H & I) for quantifying myofibroblasts in dermis in homologous keratinocyte fibroblast loaded chitosan graft (A, D & E), a non-cellular chitosan graft (B, E & H) and the commercial product (C, F & I) (40X magnification).

APPENDIX II
List of patents and publications

List of patents

- **Revi Deepa,** Anilkumar. T.V and Jaseer Muhamed CJ (Provisional Patent No2338/CHE/2013): A procedure for fabricating xenograft using mammalian cholecyst-derived extracellular matrix for wound healing applications.

- **Deepa Revi,** Anilkumar. T.V and Anoopkumar T. (Provisional Patent No6194/CHE/2013): A procedure for manufacturing prototype of cell loaded cholecyst extracellular matrix for healing of burn wound.

List of publications

- **Revi D,** Geetha CS, Rajan, A., Anoopkumar T, Anilkumar, TV (2015) Homologous fibroblast loaded cholecyst-derived scaffold heals full thickness burn wounds in rabbit model. *Journal for Biomaterial Application* (accepted for publication).

- **Revi D**, Paul W, Anilkumar TV, Sharma CP (2013) Differential Healing of Full Thickness Rabbit Skin Wound by Fibroblast Loaded Chitosan Sponge. *Journal of Biomaterials and Tissue Engineering* 3**:**261-272.

- **Revi D**, Vineetha VP, Muhamed J, Rajan A , Anilkumar TV (2013) Porcine cholecyst-derived scaffold promotes full-thickness wound healing in rabbit. *J Tissue Eng* 4**:**2041731413518060.

- **Revi D**, Paul W, Anilkumar TV, Sharma CP (2014) Chitosan scaffold co-cultured with keratinocyte and fibroblast heals full thickness skin wounds in rabbit. *J Biomed Mater Res A* 102**:**3273-81.

- **Revi D**, Vineetha VP, Muhamed J, Rajan A, Kumary TV, Anilkumar TV (2014) Wound healing potential of scaffolds prepared from porcine jejunum and urinary bladder by a non-detergent/enzymatic method. *Journal for Biomaterial Application* (accepted for publication).

- Anilkumar TV, Vineetha VP, **Revi D**, Muhamed J, Rajan A (2014) Biomaterial properties of cholecyst-derived scaffold recovered by a non-detergent/enzymatic method. *J Biomed Mater Res B Appl Biomater* 102**:**1506-16.

- Muhamed J, **Revi D**, Rajan A, Geetha S, Anilkumar TV (2014) Biocompatibility and Immunophenotypic Characterization of a Porcine Cholecyst–derived Scaffold Implanted in Rats. *Toxicologic Pathology*

- Muhamed J, **Revi D**, Rajan A, Anilkumar TV (2014) Comparative local immunogenic potential of scaffolds prepared from porcine cholecyst, jejunum, and urinary bladder in rat subcutaneous model. *J Biomed Mater Res B Appl Biomater*

List of conference attended

- **Revi D,** Vineetha VP, Jaseer M and Anilkumar TV; Cholecyst derived extracellular matrix as scaffold for skin tissue engineering. Oral presentation at the International conference on tissue engineering and regenerative medicine on 29th September - 2nd October 2011 at NIT Rourkela.

- **Revi D,** Jaseer M, Akhila R, and Anilkumar TV; Comparative study on behavior of HaCaT cells on ECM matrix. Poster presentation at the International conference on design of biomaterials on December 9-11 2012 at IISc Bangalore.

- **Revi D**, Vineetha VP, Muhamed J, and Anilkumar TV. Development of a potential bioartificial skin graft using cholecyst derived extracellular matrix. Poster Presented at 9th World biomaterial congress, Chengdu, China on 1-5 June 2012. (**Poster award**)

- **Revi D,** Jaseer M, Geetha CS, Akhila R and Anilkumar TV. Healing potential of homologous fibroblast loaded cholecyst derived scaffold for healing full thickness burn wound in rabbit model. Poster Presented at 2nd International conference on Animal and Dairy Science held in Hyderabad on 15-17 September 2014. (**Best poster award**)